Detection, Identification and Quantification of Metallic Nanoparticles in Aquaculture using Electron Microscopy and Surface-enhanced Raman Scattering

Monica Quarato

2023

Universidade Vigo

EIDO
Escola Internacional
de Doutoramento

Universidade Vigo

International Doctoral School

Monica Quarato

PhD Thesis

Detection, identification and quantification of metallic nanoparticles in aquaculture using electron microscopy and Surface-enhanced Raman scattering

Supervised by:

Dr. Laura Rodríguez Lorenzo

Prof. Miguel Ángel Correa Duarte

May, 2023

Universidade Vigo

Universidade Vigo

International Doctoral School

Dr. Laura Rodríguez Lorenzo and Prof. Miguel Ángel Correa Duarte

DECLARE that the present work, entitled "Detection, identification and quantification of metallic nanoparticles in aquaculture using electron microscopy and Surface-enhanced Raman scattering", submitted by Monica Quarato to obtain the title of Doctor, was carried out under their supervision in the PhD programme in “Ciencia e Tecnoloxía de Coloides e Interface”

Vigo, May 2023.

Dr.a Laura Rodríguez Lorenzo Dr. Miguel Ángel Correa Duarte

Alla mia famiglia...

Contents

Thesis Scope

Engineering nanomaterials (ENMs) are chemical substances or materials intentionally synthesized or manufactured to obtain a final size between 1 and 100 nm in at least one dimension. They are precisely designed and tailored to achieve specific properties and improve industrial applications. On the market, this is translated in an exponential inclusion of these materials into commercial products and therefore in an increase of their potential release into the environment during or after disposal.

However, besides the numerous benefits associated to the use of these nanomaterials there is a lack of consolidated information about the potential toxic effect that they may have in waters, organisms, and finally humans.

To bridge the gap, this thesis work takes place in the framework of NANOCULTURE and ACUINANO projects, founded by Interreg Atlantic Area and Interreg España – Portugal program respectively, and with which it shares some of the main objectives, including the advance in knowledge, risk assessment and mitigation of the environmental presence of the most-used metallic nanoparticles (MNPs), such as titanium dioxide (TiO_2), silver (Ag) and antimony tin oxide (ATO) NPs, in market products.

What makes these MNPs attractive for industrial purposes are their peculiar properties, especially if compared to bulk materials. TiO_2 NPs owe their success to the ability to efficiently scatter visible light and filtrate UV-light, finding its main application in painting and coating industries and cosmetics, while Ag NPs market growth includes rise in demand mainly for pharmaceutical and electronics purposes, due to their anti-microbial and high electrical conductivity properties. ATO NPs instead, have attracted significant attention due to their well-known infrared light insulation quality, electrically conducting oxide and optical transparency, being mainly employed as transparent electrodes and thin films for energy storage devices, solar cells applications and heat reflecting coatings. The high market demand is strictly correlated to the impact that these MNPs can have on the

environment, especially on aquatic ecosystems, seen as the most predicted sites where they could end up during their entire life cycle. Therefore, this work focuses on the aquatic ecosystems related to marine aquaculture, a sector of high economic relevance in the European Union, developed in Atlantic Europe.

The main objectives of this thesis involve the study of the current situation about the presence, transformation, and bioaccumulation of TiO_2, Ag and ATO NPs in aquaculture products from Spain and Ireland and the development of sensors for in-situ identification and quantification of the above-mentioned NPs in aquaculture facilities, allowing for decentralized monitoring and rapid implementation of risk mitigation measures.

These main objectives are divided and extensively covered in four chapter of this thesis where, Chapter 1 corresponds to a general introduction section presenting the problematic and an overview of the techniques used for the identification, quantification and localization of selected MNPs in both, living organisms and seawater. The subsequent chapters, including the main research results, are structured as follow.

Chapter 2 focuses on sample preparation and extraction methods of MNPs from complex matrices. To be identified and well characterized, NPs need to be isolated from the organisms they are interacting with in order to avoid matrix interferences and artifacts during analysis. Methodologies differ based on the nature of the particles. Chemical, alkaline, or enzymatic digestions are the most used extraction methods for isolating a wide range of inorganic particles, from those resistant to acids, to those that need to be carefully handled to preserve size and shape.

After sample treatment, one of the techniques used for elemental analysis quantification, as well as their related particulate form is inductively coupled plasma atomic emission spectroscopy (ICP-OES) and single particle inductively coupled plasma mass spectrometry (sp-ICP-MS) where, the presence of any additional particulate matter could be incorrectly counted as analyte and lead to overestimate NPs concentrations, along with incorrect size analysis. Thus, being the sample pre-treatment a crucial step to ensure the success of the technique, this chapter is entirely dedicated to it.

Besides the removal of matrix interferences, additional sample treatments are sometimes required to overcome limitations of the techniques and allow correct sample quantification. One of these is cloud point extraction (CPE), where the presence of a non-ionic surfactant, used under controlled temperature and concentration, allows the NPs sedimentation, concentrating them. In the present study, this technique is investigated as potential pre-treatment prior analytical analysis and as

a possibility to increase NPs concentration prior detection using portable sensors.

Chapter 3 addresses the potential bioaccumulation and biodistribution of Ag and TiO_2 NPs in living organisms. The attention is mainly focused on two different species destined to human consumption and thus widely cultured in aquacultures: clams and seaweeds. Being clams filter-feeding organisms, able to filtrate up to several liters of water per hour, and having seaweeds high sorption capabilities, they prove to be efficient model organisms not only to assess their ability to interact with those MNPs, but also as monitoring systems for the presence of nano-contaminants in coastal waters and oceans.

Here, three different type of electron microscopies are involved to perform the study. Going from the analysis of NPs interactions with the surface of tissues or with subcellular structures, scanning (SEM) and transmission electron microscopy (TEM), respectively, are employed to discriminate between the mere superficial adsorption of the NPs and uptake mechanisms by further investigation of organs and portions of tissue. Then, high-resolution high angle annular dark-field scanning TEM (HR-HAADF-STEM) coupled with energy-dispersive X-ray spectroscopy (EDS), is used to identify particles localized into tissue and perform additional analysis, such as MNPs transformations.

Chapter 4 extensively discusses the development of Surface-enhanced Raman spectroscopy (SERS)-based portable sensor for the detection and quantification of Ag NPs in seawater. After a general overview of the SERS principles (Chapter 1), a proof of concept of the detection strategy is presented, leading to the design and fabrication of a cartridge to improve the performance of the developed SERS method. Synthesis and functionalization of SERS substrate is discussed, as well as the results of kinetic experiments performed to assess the stability of the analyte in different media (ultrapure water, synthetic seawater and seawater containing organic matter). Also, different Ag NPs, in terms of size and aggregation level, are tested for their ability to be detected after surface modification, mimicking processes naturally occurring.

An additional chapter (Chapter 5) elucidates the final conclusion of this work and explores possibilities and impact of future applications.

At the end of the thesis, a general synopsis, in Spanish, of this dissertation is also included, as required by the regulation of Universidade de Vigo.

Chapter 1

General Introduction

With the increase of the production and application of nanomaterials, engineered nanoparticles have been introduced into the environment. Among the metallic NPs listed from the OECD as potentially harmful, TiO_2 and Ag NPs can be found due to their widespread use and commercial importance. In contrast, some others (i.e., ATO NPs), are not yet investigated. What in common, is that when released, they may be taken up and induce effects in several organisms, while the mechanism of interaction seems to be particle specific. Despite the extensive research performed on freshwater species, only few studies involved marine organisms, where NPs properties and behavior are expected to change according to the exposure media. Since the main topic of this thesis is the assessment of NPs bioaccumulation and biodistribution in marine organisms, as well as the development of a portable sensor for the detection of these new emerging classes of nano-contaminants in water, a comprehensive background about the problematic and the main techniques used for the study is presented, to support the work explored in the following chapters.

Chapter 1

1.1. Emerging nanocontaminats and their impact in the aquaculture sector

Emerging nano-contaminants are one of the categories included among the contaminants of emerging concern (CECs), which involve a group of compounds that are becoming a global concern due to their potential toxic effect toward aquatic ecosystems and human health. These compounds can enter the environment from diverse sources, released during production of raw materials, during use or while handling waste disposal of nanoparticles (NPs)-containing products.[1]

When released into the environment, the NPs can interact with a variety of compounds influencing their stability and undergo several transformations processes (i.e., aggregation, dissolution, chemical speciation, surface modification) that will determine their fate and behavior. pH, ionic strength, composition and concentration of natural organic matter (NOM) are the key factors influencing these processes.[2]

While knowledge gaps remain that need to be filled to model their environmental fate, there is a high possibility that these nano-contaminants will end up in seawater, reaching marine species and causing potential health risk. Risk that is real due to the significant role that seafood plays in sustaining the diet of the planet. Furthermore, aquaculture is a key activity to guarantee food production, both in terms of food security and economic impact and, chemical contamination is one of the factors that can have a negative impact on this sector. Aquaculture, in fact, defined as the farming of aquatic organisms including fish, mollusks, crustaceans, and aquatic plants, accounts for about 20% of seafood products in EU, with an annual production growth rate up to 7%. The EU production, with the aim of meeting the increase in demand due to population growth, is mostly concentrated on few species, including mussels, salmon, seabream, rainbow trout, seabass, oysters, and carp, while algae production is increasing over time.[3]

Since contaminants can pose a potential risk to marine species, besides water physical parameters (i.e., pH, water temperature, salinity, dissolved oxygen and turbidity), special attention needs to be given to potential biological and chemical contaminants. Especially when offshore aquacultures activities are practiced, and no control of the water takes place, pollutants can accumulate into aquatic organisms, posing a threat for the whole food webs.[4] Moreover, when nano-contaminants are contemplated, no prevention strategies are employed even at coastal level.

In relation to aquaculture activities, water quality could be affected from several parameters, such as soil compositions and environmental pollution when performed in ponds, while in coastal or open-sea cages, the quality is generally influenced by the natural environment. Being aquatic pollution one of the major threats for aquaculture production, metallic NPs (MNPs) are often employed for water treatments and purification, becoming in turn part of the newly emerging contaminants. To date, silver NPs (Ag NPs), zinc oxide (ZnO NPs) and titanium dioxide NPs (TiO_2 NPs) have been extensively used to inhibit fungal infections, against bacteria proliferation, and to promote surfaces sterilization and disinfection.[5–7]there is few information available on the interaction of colloidal nanosilver with fish pathogens. Hence, the current study investigated the effects of colloidal AgNPs on the in vitro growth of the fish pathogen Saprolegnia sp.. Before the experiments, various important properties of AgNPs were well-characterized. The antifungal activity of AgNPs was then evaluated by determining the minimum inhibitory concentrations (MICs Also, the use of nanomaterials as feed enhancer to promote micronutrient delivery, fish growth and protein content in muscles, as well as to improve fishes reproduction through hormones administrations, has been reported.[8,9] As a result, marine organisms are continuously exposed to the potential hazard of NPs, through direct or indirect routes. Considering the possible human health risks, it is very likely that they are associated with long-term effects produced by the consumption of fishes, which may contain, so far, only a small amount of nanomaterials (NMs).[10] Also, only the edible part of the fishes, like muscle, need to be considered as a potential source for human exposure, removing thus gills or gastrointestinal tract that are considered as the major route for NPs internalization.[11]

However, due to the constant increases of the industry demand for engineered NMs (ENMs) and NPs-containing products, particles bioavailability in oceans and coastal water is only expected to rise to the point where it could undermine the socio-economic development of the whole marine fishery sector. Population to feed, loss of jobs, loss of supremacy in trade, abandonment of the establishments intended for aquaculture, are just

few of the aspects that needs to be faced if the aquaculture sector would be compromised.

On the other side, there is a lack of specific and sensitive analytical methods for NPs detection, especially in situ, making even more difficult to raise awareness against this new concern. Furthermore, being the interactions between NPs and living organisms influenced by a variety of parameters, it is difficult to predict and draw general conclusions about the potential toxic effect they may have.

In the following sections, three of the most used MNPs, TiO_2, Ag and antimony tin oxide (ATO) NPs, as well as three different marine species, mussels, clams and seaweed, are presented in more detail as they are the object of study of the next chapters.

1.1.1. *Titanium Dioxide nanoparticles (TiO_2 NPs)*

TiO_2 NPs, also known as titanium (IV) oxide or titania, are one of the most common MNPs being used in the formulation of several commercially available products, like sunscreens, cosmetics, paints, food and drug colorants, as well as antimicrobial agent or for water and air purification, mostly due to their whitening power and photocatalytic activity.[12] TiO_2 occurs naturally in three crystalline forms: 1) anatase, believed to have the highest photocatalytic activity; 2) rutile, the most common and stable form and 3) brookite, which is not produced by industry or incorporated into commercial products.[13] Initially approved by the European Union authorities as a safe food additive (Annex II of Regulation (EC) No 1333/2008), TiO_2 NPs were then subjected to several charges by the French authority, who classify the chemical substance as carcinogenic.[14] The allegation was confirmed in the following year by the Committee for Risk Assessment (ECHA), recognizing TiO_2 as a category 2 carcinogen by inhalation, in powder form containing 1% or more of particles of a diameter equal to or below 10 μm.[15] On November 23, 2022, the Court of Justice of the European Union issued a press release announcing that it has annulled a previous decision classifying TiO_2 (CAS 13463-67-7) as carcinogenic in powder forms and defining the previous scientific studies not reliable and acceptable.[14]

Besides all the debates, the annual production volume of TiO_2 is predicted to reach 2.5 million tons by 2025.[16] As stated before, the nanomaterials rise in production, is strictly related to their impact onto the environment, where they can interact with marine organisms and enter the food chain. Crustaceans, mollusks and algae are, in fact, only few of the marine living organisms with who these nanoparticles could interact.[17] Being coastal waters and sediments the final sink for most NPs, it is reported that the

surface water concentration of TiO_2 NPs measured in specific area during the peak of a touristic season, shows results in the range of µg/L.[18] However, once in seawater, due to the high ionic strength, TiO_2 NPs tend to aggregate very quickly, promoting sedimentation processes. In this way, these particles become more harmful for benthic and filter-feeding organisms then for organisms living in the water column.[19,20]

Taken note of this, for the experimental part, two different types of TiO_2 NPs have been selected, Degussa (Evonik) P25 NPs of 25 nm and TiO_2 NPs of 5 nm. Degussa P25 TiO_2 NPs are an example of mixed-phase materials, of anatase and rutile, in which the presence of small rutile nanoclusters interwoven with anatase crystallites are responsible for an enhancement of the photocatalytic activity, being thus employed in many applications where the containment of organic contamination is required.[21] TiO_2 NPs of 5 nm instead, present a pure anatase crystal phase and are commercially interesting due to their high refractive index, making them a good candidate as sunscreen component.[22]

1.1.2. Silver nanoparticles (Ag NPs)

Ag NPs are extensively used in several fields due to their unique physicochemical properties that makes them suitable for industrial and medical applications, pharmaceutical and food industry, healthcare-related products, and cosmetics.[23,24] Their nanometer-scale size allows them to have unique optical properties in relation to their counterpart bulk material. One of these optical properties is the localized surface plasmon resonances (LSPRs) which can be defined as the collective oscillation of the surface induced by specific range of the electromagnetic field.[25] LSPRs can be tuned by controlling the NP size, shape, aggregation state and the local refractive index around the NP surface, opening endless possibilities on biomedical and sensing applications. Among other noble metal NPs, Ag NPs are specifically acclaimed for their strong antibacterial and anti-inflammation effects.[26,27] Besides the classic methods for their synthesis, based on physical and chemical approaches, biological methods, employing the use of bacteria, fungi or plants, have been deeply investigated to produce more biologically compatible NPs.[28,29] It is possible in this way to tune their physicochemical properties and obtain NPs with specific properties to fulfill specific applications. As expected, their incorporation into consumer products is only anticipated to increase, reaching ~800 tons by the year 2025.[30] This increase in production may enhance the risk that these NPs are released from consumer products and end up into the environment. Following a probabilistic study on the life cycle of products containing nanomaterials, it has been shown that the accumulation

of Ag NPs in surface waters it is stated to be in the ng/L range.[31] Despite this concentration seems "lower", a risk ranking framework developed by Li & Cummins showed that the exposure via natural water sources contributes to the major health concern of Ag NPs.[32]

To exploit their antibacterial properties, the most recognized mechanism is based on the presence of Ag^+ ions, where Ag NPs can act as a source of dissolved ions. This mechanism can only give an idea about Ag NPs reactivity once released into the environment. For example, it is well-known the Ag reactivity against sulfide, chloride and organic matter, all events that will affect particles transportation, reactivity, and toxicity.[33–35] To minimize the reactivity, many different coatings are used to stabilize Ag NPs against aggregation or dissolution, including polymers, biological macromolecules, polysaccharides and surfactants. The different environmental scenarios, in which natural waters and wastewater treatment plants (WWTPs) are involved, due to the release of these particles mainly from domestic and industrial sources, may also play an important role on the impact that these coatings can have.

In the following thesis work, two different types of commercially available Ag NPs have been selected: polyvinylpyrrolidone (PVP)-coated Ag NPs with a diameter of 15 nm and 100 nm. PVP is selected as stabilizing polymer not only because of its biocompatibility and hydrophilicity as a polymer, but also because it is commonly used as stabilizing agent.[36]

1.1.3. Antimony Tin Oxide nanoparticles (ATO NPs)

Antimony tin oxide nanoparticles (Sb_2O_5/SnO_2, ATO NPs) are a type of MNPs with unique optical properties and excellent electrical conductivity, making them good candidates for optoelectronics and electronics applications. Due to their high transparency in the visible region and strong absorption in the ultraviolet region, they are extensively used as conductive coatings for electronics devices, including touch screens, solar cells, and flat panel displays. Referring to the electrical and conductive properties, they are used as support material for electro catalysis, energy storage devices, gas sensors and photo-electrocatalysis. Due to their infrared light insulation properties, they are also employed in the synthesis of heat reflection coatings.[38–40] Despite their industrial use, there are very scarce studies on ATO NPs toxicity, and nothing about their environmental impact.[41]

Figure 1 shows representative images of the NPs used among this thesis work.

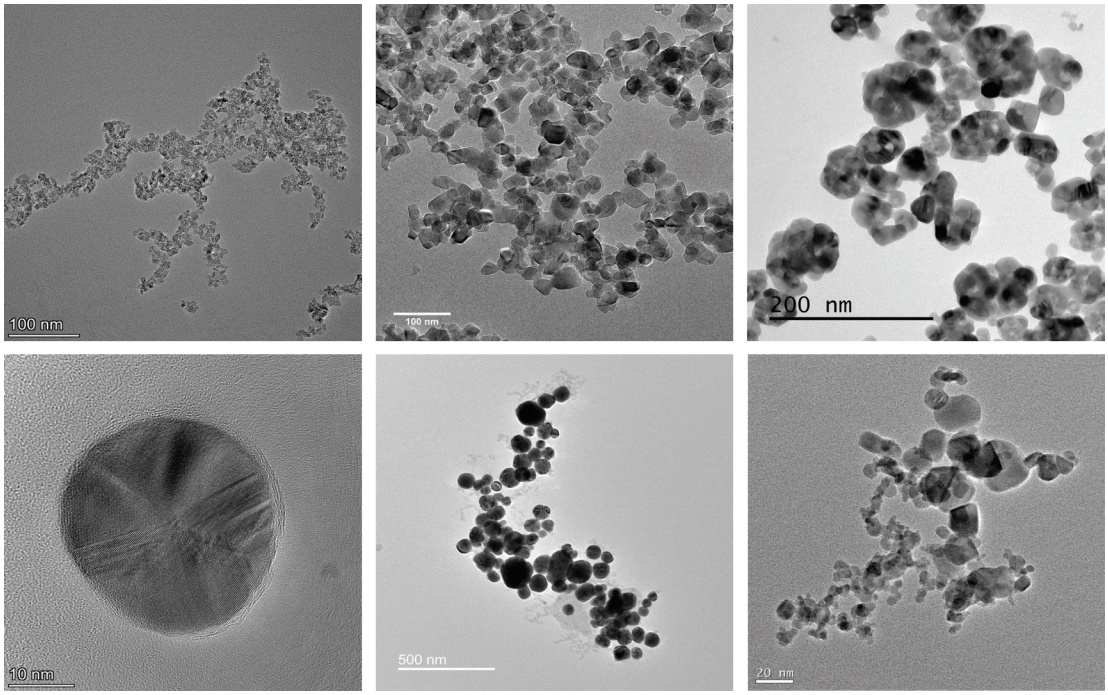

Figure 1. TEM and HRTEM images of the NPs used among this study. Starting from left: citrate-5nm TiO_2 NPs, citrate-25nm TiO_2 NPs, citrate-45nm TiO_2 NPs, PVP-15nm Ag NPs, PVP-100nm Ag NPs and ATO NPs.

1.1.4. Marine organisms with potential risk of exposure to MNPs

Bivalve mollusks are widely used as bioindicators for monitoring coastal water anthropogenic pollution due to several reasons. Firstly, they are filter-feeding organisms, able to filtrate large volumes of water per day, meaning they drain in nutrients along with a high variety of pollutants (i.e., metals, nano-contaminants, microplastics, pesticides). Secondly, they are present in temperate coastal seas worldwide, they are sessile, forming beds in shallow waters, which enables the collection of location-specific information, as well as easiness in cultures and collections.[42,43] Additionally, they are of medium size, and a single individual provides sufficient tissue for analysis.

Besides shellfish, macroalgae have also been considered as important indicators of water pollutants, due to their ability to uptake contaminants in their tissues. Their size, abundance in various aquatic systems, cost-effective farming and ability to effectively reflect changes in water quality, makes them a good monitoring system.[44,45] Seaweed are also important species at commercial level, due to their ability to produce compounds like vitamins, bioactive agents, amino acids, proteins, and different classes of polysaccharides. The production of these compounds finds its use in a wide range of sectors, from pharmaceutical and beauty care products to food industry and biofuels production.[46]

On the other side, given the ability to easily interact with contaminants, the interactions living organisms-pollutants can pose a risk for all aquatic ecosystem and ultimately to humans. Due to the high nutritional values in fact, seafood provides beneficial effects when integrated in human diet, being therefore extensively farmed in the aquaculture sector. Seaweed instead, already exploited in Eastern countries, are being consumed as human food in many parts of the world, representing one of the possible solutions to feed the growing human population.[47,48]

Whitin this study, mussels, clams and two types of marine seaweeds, are used to assess the bioaccumulation and biodistribution impact of nano-contaminants in their tissues. Sample preparation techniques are discussed in Chapter 2, while an extensive investigation about distribution and localization of NPs within their tissue is addressed in Chapter 3.

1.2. Techniques for identification, quantification and localization of MNPs

There are clearly two key challenges to estimate/establish the potential impact of MNPs in marine environment and human health: 1) to understand MNPs interaction with the marine organisms not only in terms of bioaccumulation, but also biodistribution and possible NPs transformations in the tissue and, 2) the development of new tools for in-situ detection and quantification of these MNPs in seawater that allow decentralized monitoring and quick implementation of measures for risk mitigation.

To analyze NPs interactions with tissues, analytical techniques must have sufficient spatial resolution to identify and localize particles with size lower than 100 nm associated and/or uptaken by cells. Moreover, sample preparation for this analysis is of vital importance to avoid alterations of the tissue and NPs and to be able to achieve correct conclusions on the impact of NPs exposure on tissue microstructures and biodistribution and possible NPs transformations.[49]

Related to the 2nd challenge, progresses have been made for the monitoring of water parameters such as pH, temperature, dissolved oxygen and turbidity, by using multiparametric sensors for real-time and online monitoring. As concerned methods for the detection of other classes of contaminants such as pathogens, and organic pollutant, research is far behind and the main conventional techniques, such as liquid or gas chromatography (LC, GS) combined with mass spectrometry (MS) and enzyme-linked immunosorbent assay (ELISA), are often expensive, require qualified professionals and

complex equipment, do not allow direct measurements in the field and do not provide immediate results. Also, sampling, sample preservation, transport and laboratory analysis are all parameters that affect the final costs. Regarding MNPs monitoring, there are only few reports related to the detection of Ag NPs and TiO_2 NPs in seawater using single particle Inductively Coupled Plasma Mass Spectrometry (sp-ICP-MS)[50,51]we employed sector-field inductively coupled mass spectrometry to assess the presence of ENPs in coastal seawater samples collected from the Black Sea in regions suffering different anthropogenic impacts. Ultrafiltration through commercial 3 kDa membrane filters was shown to be feasible to separate the ENPs from the bulk seawater, and the subsequent ultrasound-mediated acidic dissolution makes the metals constituting the ENPs amenable to analysis. This procedure allowed the ENPs bearing Cu, Zn, V, Mo, and Sn to be for the first time quantitated in seashore surface water, their concentration ranging from 0.1 to 1.0 μg L−1 (as metal and only one so far related to their monitoring using portable systems, but compromised on detection limit and time of analysis.[52] Therefore, there is the need to develop low-cost, accessible, and easy-to-handle devices for the in-situ analysis of MNPs in seawater.

In this thesis work, attempts have been made in order to face these weaknesses by developing in situ sensors for the rapid detection and assessment of the new emerging contaminants at the nano-scale level and by investigating the potential interaction of marine organisms after exposure to MNPs.

In the following sections, three different approaches for the quantification and localization of NPs in water and tissue are presented. At first, is given an overview of sp-ICP-MS, performed at laboratory scale. Here, this technique is mainly used as support for further developments and analysis. After, an entire chapter is dedicated to the introduction of electron microscopy techniques for the assessment of bioaccumulation and biodistribution of MNPs in marine organisms and lastly, an explanation about SERS principles, on which the portable system for the monitoring of the MNPs is based, is presented.

1.2.1. *MNPs quantification using single particle-ICP-MS*

Inductively coupled plasma mass spectrometry (ICP-MS) is an analytical technique that can be used to measure elements at the trace level.[53,54] Liquid samples are introduced into a nebulizer by a peristaltic pump or self-aspiration system and, after creating an aerosol of fine droplets, are transferred to an argon plasma. The high temperature of the plasma evaporates the solvent while atomizing and ionizing the

remaining part. Ions that passed through the interface are analyzed by a spectrometer based on their mass/charge (m/z) ratio, reaching elemental quantification of parts per trillion (ppt) level. The whole system operates under vacuum conditions, to avoid that the ions, travelling towards the detector, collide with any other gas molecules.[55]

Single-particle-ICP-MS (sp-ICP-MS), instead, utilizes the standard setup of ICP-MS, taking advantage from sensitivity and elemental specificity, while performing measurements on a "particle by particle" basis. Its use in the study of colloidal analysis was reported by Degueldre and Favarger, becoming afterwards a method of choice when detection, determination and characterization of nanomaterials was required.[56] For environmental applications, as well as for pharmaceuticals and food analysis, sp-ICP-MS plays an important role since extremely sensitive methods are necessary to assess the presence of MNPs and predict their environmental cycle.[57–59]

The very low limit of detection (LoD), besides providing information about elemental chemical composition, sample concentration, size, and number size distribution, has made sp-ICP-MS a suitable technique for the characterization of nanomaterials at environmentally relevant concentrations.

By channeling single particles to the instrument, they are detected as separate pulses in a time-resolved mode. The intensity of each pulse is proportional to the element mass per particle and can be converted to particle size given prior knowledge on the particle's density, shape, and element mass fraction. Detection depends mainly on two factors: the concentrations of the NPs, that needs to be enough to allow the counting of a minimum number of events, and their size or element mass per NPs, that needs to be large enough to generate a pulse of ions detectable by the spectrometer, distinct from the baseline produced by the continuous background in a time scan.

Despite most of the time the sample is ready to be analyzed, often requiring only dilutions, when it comes to environmental samples, sample preparation is one of the key steps in determining the possibility of the analysis. The removal of the matrix while preserving the nature of the NPs under investigation, is extremely important for the success of the measurement.[60]

Extraction methods like acid, alkaline and enzymatic digestions, besides microwave assisted techniques are laid down in Chapter 2.

1.2.2. *Biodistribution and transformation studies using electron microscopy techniques*

An effective way to assess the presence of anything anywhere, is to have a look at it. And one of the tools available to do so, especially at lower scale, is microscopy.

Three are the most known and used branches within the microscopy field, 1) optical, 2) electron and 3) scanning probe microscopy, which are named after the way in which the probe interacts with the material to generate the image. In the context of optical microscopy, where the light interacts with the sample, the major limitation is the optical resolution limit, stated to be of around 0.2 μm, which makes the technique being ineffective when smaller particles are contemplated. The electron microscopy uses an electron beam to create an image being able to significantly improve the resolution, while, for the scanning probe microscopy, a nanoscale probing tip is scanned across the sample surface being able to detect topography and materials properties.[61]

Considering the above and the fact that particles at the nanoscale range (i.e., 1-100 nm) are involved in this study, electron microscopy is an excellent technique to perform the analysis and thus a more extensive explanation about the methodology will be given here.

It was Ernst Ruska and Max Knoll, a physicist and an electrical engineer respectively, from the University of Berlin, who created the first prototype of an electron microscope in 1931.[62,63] By replacing the use of light with electrons that could pass through the sample and form an image, they discovered the first transmission electron microscope (TEM). Ten years later, Ruska created a similar yet different approach using a focused electron to scan the surface of a sample to deliver information about its topography and composition. Unlike TEM, the image from this new scanning electron microscope (SEM) was created after the microscope collected and counted the scattered electrons.

Starting from the top of the column, the key components of a TEM microscope involve an electron gun filament, a small wire heated to a high temperature that emits electrons, coupled with a high voltage source to define the acceleration voltage of the electron beam, set to be from 80 to 300 kV; electron gun lenses and apertures, located throughout the microscope's column, to focus the beam onto the sample, minimize distortions and magnify the resulting image and, a vacuum system, with several pumps, valves and filters, to keep the microscope under vacuum conditions, allowing the beam to travel through the sample avoiding any other kind of interactions. The sample is placed onto a specific specimen holder, located at the center of the microscope column and it is designed to hold the sample at a precise

location in the beam of electrons, with the possibility of being rotated at will. It can also be equipped with heating or cooling systems to control the temperature of the sample (Figure 2).

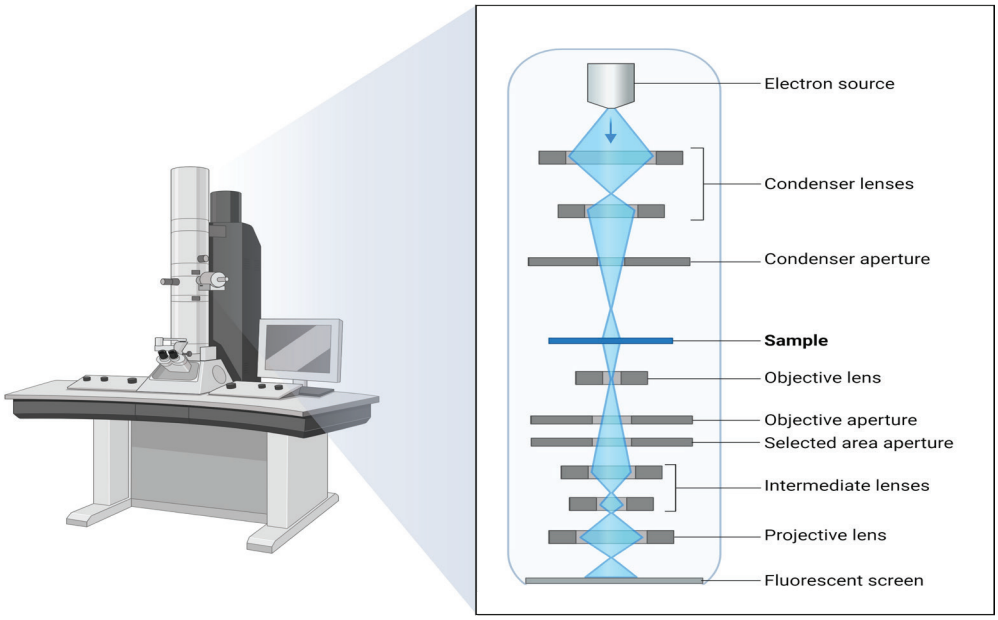

Figure 2. Scheme of TEM structure and components *(Created with BioRender.com).*

Changes in mass and thickness of the sample are responsible for the variation of the amplitude with which the electrons are transmitted through the sample or scattered at different angles, leading to the formation of bright or dark field images. In the first case, that is the traditional way of imaging, only the electrons that are transmitted through the sample are collected to form the image, excluding the scattered one. Vice versa, there is a dark field image formation. Especially when it comes to the detection and localization of NPs in biological compartments, TEM turns out to be a valuable technique, because of its extremely high resolution (< 1 nm with aberration correction) and the possibility to investigate the status of the particles (aggregation, dissolution, transformation processes).[64,65]

Similar to the TEM, in SEM mode, electrons are emitted from an electron gun placed at the top of the column, accelerated and driven through a combination of lenses and apertures to produce a focused beam of electrons that hit the surface of the sample. This time the sample is mounted on a stage in the chamber area at desired pressure and voltage conditions.

The position of the electron beam on the sample is controlled by scan coils situated above the objective lens that allow the scanning of a specific area of the sample, generating several signals, such as secondary electrons (SE) and backscattered

electrons (BSE), depending on the deepness of sample interaction. Therefore, different information can be extracted: more surface details, when SE are collected and more information regarding sample composition, when BSE are detected, since differences in contrast will depend on the atomic number of the element (the higher, the brighter). However, the beam is able to penetrate the sample to a depth of few microns, depending on the acceleration voltage and density of the sample, achieving resolutions of around 1 to 20 nm.

More recent is another imaging mode that can be also useful in the analysis of biological samples, the scanning transmission electron microscopy (STEM) mode where, an annular detector (HAADF: high angle annular dark field) is used to image only highly scattered electrons passing through the sample, decreasing the noise and increasing the signal coming from high mass materials (i.e., nanoparticles) (Table 1).

Electron microscopy techniques

	Spatial resolution	***Analysis conditions***
Transmission EM	~ 0.2 nm	200 kV
Scanning EM	1 – 20 nm	~ 30 kV
Aberration Corrected - TEM	≤ 0.063 nm	300 kV
Aberration Corrected - STEM	≤ 0.063 nm	300 kV

Table 1. Comparison between different EM techniques spatial resolution.

One of the additional analyses that can be performed in TEM, SEM or STEM mode is the X-Ray spectroscopy. X-Rays are produced when an incident electron penetrates the inner-shell electrons. If enough energy is transferred from the incident electron to the inner-shell electron, then the atom in the sample will become ionized, leaving a "hole" in the inner shell. When the electron is displaced, an electron from the outer shell (higher energy) fills the vacancy (lower energy) and the energy difference is released in the form of an X-Ray. Since each element has unique energy level in the electron shell, the X-Rays are representative of the sample composition. To detect X-Rays, an energy dispersive X-Ray (EDS) detector is placed right above the sample being able to generate both, qualitative and quantitative analysis.

Due to the high magnification level and resolution that it is possible to achieve, electron microscopy is mostly used to study structures and properties of materials at the

atomic and molecular level and it is extensively used in several fields including material science and life science applications.[66]

In order to obtain high-quality images, sample preparation is a key point to preserve the integrity of the sample.[67] Sample size and thickness are important to allow the electron beam to pass through the sample and interact with it. Results coming from the use of electron microscopy to assess the biodistribution and transformation process that involve Ag and TiO_2 NPs upon interaction with marine organisms are discussed more in detail in Chapter 3.

1.2.3. *In-situ MNPs monitoring in seawater by Surface-enhanced Raman scattering (SERS)*

The Raman scattering (RS), named in the honor of its inventor, C. V. Raman in 1928, is the inelastic scattering of an incident radiation after interaction with vibrating molecules.[68] When a monochromatic radiation hits a sample, it scatters in all directions after interacting. The majority of this scattered radiation has a frequency which is equal to the frequency of the incident radiation and constitutes the Rayleigh scattering. Only a small fraction of this scattered radiation has a frequency different from the one of the incident radiation and constitutes the so-called Raman scattering (i.e., inelastic scattering). This frequency difference (shift), corresponds to the excitation of the vibrational levels of the molecule, shifted to higher or lower frequencies from the incident light.

When the frequency of the incident radiation is higher than the frequency of the scattered one, it is called *Stokes shift*. Otherwise, when the frequency of the incident radiation is lower than the frequency of the scattered radiation, it is called *anti-Stokes* shift. The Stokes shifts are the ones measured in Raman spectroscopy (Figure 3).

Low sensitivity due to weak Raman scattering is the major limitation associated with this technique, which can be overcome by the resonance Raman scattering (RRS), in which the frequency of the incident radiation is in the order of the electronic transition of the molecule. In this way, the virtual state becomes resonant with one of the electronic levels in the molecule, resulting in an increase of the scattering efficiency of the molecule of up to 6 orders of magnitude.[69] Any molecule that absorbs in the vicinity of the incident laser wavelength is subject to RRS.

However, Raman spectroscopy was not widely used for long time for sensing application until the surface enhanced Raman Effect was discovered. SERS is a modified technique in which the sample is adsorbed onto a colloidal metallic surface enhancing the

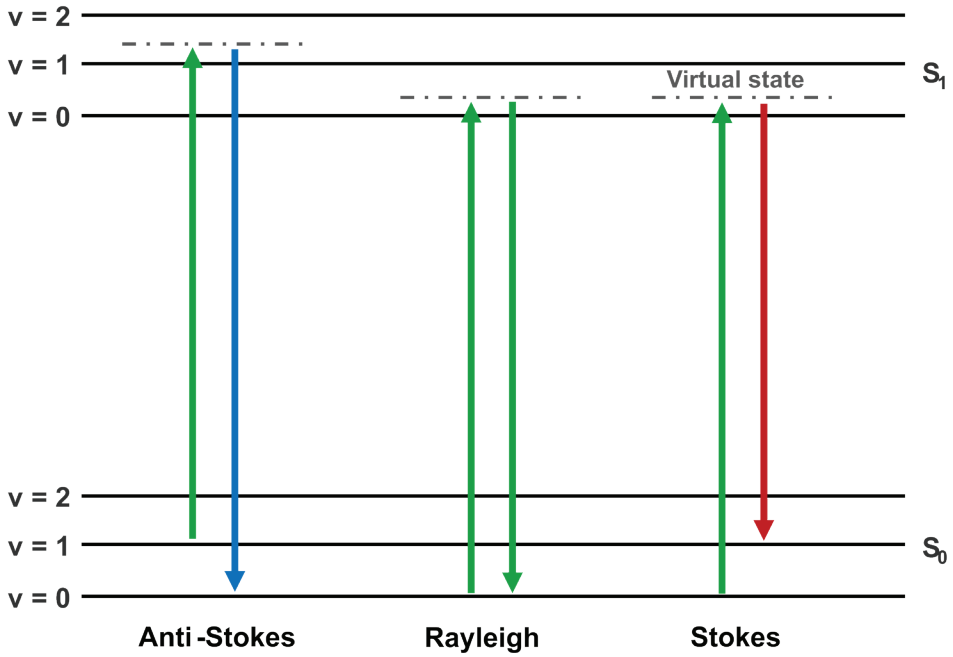

Figure 4. Schematic diagram of the energy transition involved in Raman scattering and Rayleigh scattering.

intensity of the Raman signal. This phenomenon was first observed in 1974 by Fleischmann, Hendra, and McQuillan, who reported an unexpectedly large Raman signal from pyridine adsorbed on a roughened silver electrode.[70]

The combination of the two, RRS and SERS techniques (i.e., Surface Enhanced Resonance Raman scattering (SERRS)), can amplify the sensitivity up to fifteen orders of magnitude as compared to Raman spectroscopy.[71] Being a surface technique, the effect becomes higher if the molecule gets closer to the metallic nanostructure, due to the coupling between the two. Typical metallic nanostructures used to obtain this enhancement are noble metal particles, such as gold and silver, due to their chemical stability and to their plasmon resonance frequencies being within the visible and the near-infrared (NIR) region. Other transition metals have also been assessed for their enhancement effects, such as platinum and iron, showing however lower enhancement levels than those seen for gold, silver or copper.[72]

To understand the enhancement effect of SERS, two mechanisms have been proposed: the electromagnetic (EM) mechanism and the chemical (CT) mechanism, where the EM is believed to make the most contribution to SERS effect. The origin of EM on the nanoscale derives from the collective oscillation of electrons excited by the incident light on

the metal surface. This collective oscillation is called localized surface plasmon resonance (LSPR) and it is influenced by the size, morphology and distance and orientation between the molecule and the SERS substrate. When the electromagnetic field is concentrated in a specific point of the SERS substrate, the so-called hot-spots, the LSPR frequency could be altered, resulting in a further SERS enhancement (Figure 4).[73] In these hot-spots, the electromagnetic field is highly concentrated due to: 1) the coupling between two or more NPs with closely spaced feature (few nanometers distance) or 2) the shape anisotropy, i.e., the morphology involves sharp features such as nanotriangles, nanorods and nanostars.[74] The CT mechanism provides enhanced sensitivity via chemical interactions between the analyte and the nanostructured substrate. It occurs when there is an exchange of electrons between the Fermi level of the metal and the lowest unoccupied molecular orbital (LUMO) or highest occupied molecular orbital (HOMO) of the molecule.[75] Separation between sample and substrate for the enhancement to occur is in the order of angstroms, making it a short-range effect.

Considering both mechanisms, it is crucial to select a proper SERS-active substrate to obtain the desired enhancement and allow analyte traces detection besides compatibility with the target molecules. Targeting the analyte onto the metallic surface can help on this aspect. Reproducibility is also a

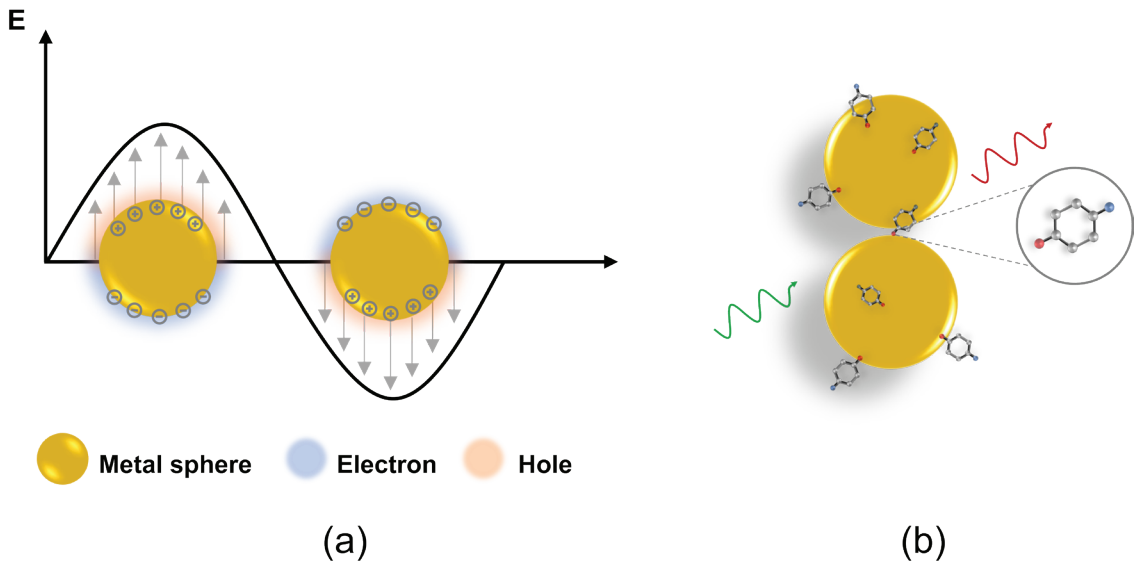

Figure 4. Schematic diagram of (a) LSPR effect in metallic sphere showing the displacement of the conductive electron cloud relative to the nuclei and (b) SERS phenomena upon NPs-molecule interaction.

critical point to consider, especially when quantitative measurements are required.[76]

Metallic nanoparticles (NPs) are recognized as the most studied substrates after the discovery of SERS effect.[77] Despite the formation of aggregates by adding salt has poor reproducibility due to the randomness of interparticle distance and arrangement, making the enhancement effect not predictable, self-assembly methods, in which the NPs form a thin film onto a surface via functional groups (i.e., amine, thiol) could overcome this problem.[78,79] This may improve the portability and versatility of the SERS analysis, over the regular physical fabrication techniques such as sputtering, physical vapor deposition or electron beam lithography, which are difficult to find in conventional laboratories.

In the last years, one of the most significant developments in SERS has been the exponential increase in synthetic capabilities for homogeneous anisotropic metal nanoparticles. It has been demonstrated that anisotropic nanoparticles often exhibit superior optical properties compared to spherical ones, due to intense electric field localization near sharp geometric features and a broadly tunable LSPR. Among these, rods, triangular prisms, cubes and stars morphologies have been described where the concentration of electromagnetic field has been found to be at the triangles corners, ends of nanorods, edges of cubes and tips of nanostars.[80,81] As a result, anisotropic nanoparticles are attractive building blocks for surface-enhanced Raman spectroscopy (SERS) substrates.

A dedicated chapter, Chapter 4, will deeply focus on the investigation and the development of a SERS-based portable sensor for the assessment of Ag NPs in environmental waters, taking into accounts all the advantages and limitations of the device.

References

1. Tolaymat, T., El Badawy, A., Genaidy, A., Abdelraheem, W. & Sequeira, R. Analysis of metallic and metal oxide nanomaterial environmental emissions. J. Clean. Prod. 143, 401–412 (2017).
2. Keller, A. A. et al. Stability and Aggregation of Metal Oxide Nanoparticles in Natural Aqueous Matrices. Environ. Sci. Technol. 44, 1962–1967 (2010).
3. European Commission. Overview of EU aquaculture (fish farming). https://oceans-and-fisheries.ec.europa.eu/ocean/blue-economy/aquaculture/overview-eu-aquaculture-fish-farming_en#related-links (2022).
4. Wang, Z. et al. Trophic transfer of TiO 2 nanoparticles from marine microalga (Nitzschia closterium) to scallop (Chlamys farreri) and related toxicity. Environ. Sci. Nano 4, 415–424 (2017).
5. Johari, S. A., Kalbassi, M. R., Soltani, M. & Yu, I. J. Study of fungicidal properties of colloidal silver nanoparticles (AgNPs) on trout egg pathogen, Saprolegnia sp. Int. J. Aquat. Biol. 3, 191–198 (2015).
6. Pati, R. et al. Topical application of zinc oxide nanoparticles reduces bacterial skin infection in mice and exhibits antibacterial activity by inducing oxidative stress response and cell membrane disintegration in macrophages. Nanomedicine Nanotechnology, Biol. Med. 10, 1195–1208 (2014).
7. Magaña-López, R., Zaragoza-Sánchez, P. I., Jiménez-Cisneros, B. E. & Chávez-Mejía, A. C. The Use of TiO2 as a Disinfectant in Water Sanitation Applications. Water 13, 1641 (2021).
8. Zhou, X., Wang, Y., Gu, Q. & Li, W. Effects of different dietary selenium sources (selenium nanoparticle and selenomethionine) on growth performance, muscle composition and glutathione peroxidase enzyme activity of crucian carp (Carassius auratus gibelio). Aquaculture 291, 78–81 (2009).
9. Rather, M. A. et al. Chitosan-Nanoconjugated Hormone Nanoparticles for Sustained Surge of Gonadotropins and Enhanced Reproductive Output in Female Fish. PLoS One 8, e57094 (2013).
10. Ramsden, C. S., Smith, T. J., Shaw, B. J. & Handy, R. D. Dietary exposure to titanium dioxide nanoparticles in rainbow trout, (Oncorhynchus mykiss): no effect on growth, but subtle biochemical disturbances in the brain. Ecotoxicology 18, 939–951 (2009).
11. FEDERICI, G., SHAW, B. & HANDY, R. Toxicity of titanium dioxide nanoparticles to rainbow trout (Oncorhynchus mykiss): Gill injury, oxidative stress, and other physiological effects. Aquat. Toxicol. 84, 415–430 (2007).
12. Vidmar, J., Milačič, R. & Ščančar, J. Sizing and simultaneous quantification of nanoscale titanium dioxide and a dissolved titanium form by single particle inductively coupled plasma mass spectrometry. Microchem. J. 132, 391–400 (2017).
13. Gea, M. et al. Shape-engineered titanium dioxide nanoparticles (TiO2-NPs): cytotoxicity and genotoxicity in bronchial epithelial cells. Food Chem. Toxicol. 127, 89–100 (2019).
14. Court of Justice of the European Union. The General Court annuls the Commission

Delegated Regulation of 2019 in so far as it concerns the harmonised classification and labelling of titanium dioxide as a carcinogenic substance by inhalation in certain powder forms. 3–5 (2022).
15. Commission, E. Commission Delegated Regulation (EU) 2020/217. Official Journal Of The European Union (2020).
16. Dedman, C. J., King, A. M., Christie-Oleza, J. A. & Davies, G.-L. Environmentally relevant concentrations of titanium dioxide nanoparticles pose negligible risk to marine microbes. Environ. Sci. Nano 8, 1236–1255 (2021).
17. Matranga, V. & Corsi, I. Toxic effects of engineered nanoparticles in the marine environment: Model organisms and molecular approaches. Mar. Environ. Res. 76, 32–40 (2012).
18. Tovar-Sánchez, A. et al. Sunscreen Products as Emerging Pollutants to Coastal Waters. PLoS One 8, e65451 (2013).
19. Baker, T. J., Tyler, C. R. & Galloway, T. S. Impacts of metal and metal oxide nanoparticles on marine organisms. Environ. Pollut. 186, 257–271 (2014).
20. Wang, Z., Yin, L., Zhao, J. & Xing, B. Trophic transfer and accumulation of TiO2 nanoparticles from clamworm (Perinereis aibuhitensis) to juvenile turbot (Scophthalmus maximus) along a marine benthic food chain. Water Res. 95, 250–259 (2016).
21. Hurum, D. C., Agrios, A. G., Gray, K. A., Rajh, T. & Thurnauer, M. C. Explaining the Enhanced Photocatalytic Activity of Degussa P25 Mixed-Phase TiO 2 Using EPR. J. Phys. Chem. B 107, 4545–4549 (2003).
22. Smijs, T. & Pavel. Titanium dioxide and zinc oxide nanoparticles in sunscreens: focus on their safety and effectiveness. Nanotechnol. Sci. Appl. 95 (2011) doi:10.2147/NSA.S19419.
23. Du, J. et al. Antibacterial activity of a novel Forsythia suspensa fruit mediated green silver nanoparticles against food-borne pathogens and mechanisms investigation. Mater. Sci. Eng. C 102, 247–253 (2019).
24. Kokura, S. et al. Silver nanoparticles as a safe preservative for use in cosmetics. Nanomedicine Nanotechnology, Biol. Med. 6, 570–574 (2010).
25. Yu, R., Liz-Marzán, L. M. & García de Abajo, F. J. Universal analytical modeling of plasmonic nanoparticles. Chem. Soc. Rev. 46, 6710–6724 (2017).
26. Li, W.-R. et al. Antibacterial activity and mechanism of silver nanoparticles on Escherichia coli. Appl. Microbiol. Biotechnol. 85, 1115–1122 (2010).
27. Sondi, I. & Salopek-Sondi, B. Silver nanoparticles as antimicrobial agent: a case study on E. coli as a model for Gram-negative bacteria. J. Colloid Interface Sci. 275, 177–182 (2004).
28. Elamawi, R. M., Al-Harbi, R. E. & Hendi, A. A. Biosynthesis and characterization of silver nanoparticles using Trichoderma longibrachiatum and their effect on phytopathogenic fungi. Egypt. J. Biol. Pest Control 28, 28 (2018).
29. Logeswari, P., Silambarasan, S. & Abraham, J. Synthesis of silver nanoparticles using plants extract and analysis of their antimicrobial property. J. Saudi Chem. Soc. 19, 311–317 (2015).
30. Guo, Y. et al. AgNPs Change Microbial Community Structures of Wastewater. Front. Microbiol. 9, (2019).
31. Gottschalk, F., Sonderer, T., Scholz, R. W. & Nowack, B. Modeled Environmental Concentrations of Engineered Nanomaterials (TiO 2 , ZnO, Ag, CNT, Fullerenes) for Different Regions. Environ. Sci. Technol. 43, 9216–9222 (2009).
32. Li, Y. & Cummins, E. A semi-quantitative risk ranking of potential human exposure to engineered nanoparticles (ENPs) in Europe. Sci. Total Environ.

778, 146232 (2021).
33. Levard, C. et al. Sulfidation Processes of PVP-Coated Silver Nanoparticles in Aqueous Solution: Impact on Dissolution Rate. Environ. Sci. Technol. 45, 5260–5266 (2011).
34. Levard, C. et al. Probing Ag nanoparticle surface oxidation in contact with (in)organics: an X-ray scattering and fluorescence yield approach. J. Synchrotron Radiat. 18, 871–878 (2011).
35. Liu, J. & Hurt, R. H. Ion Release Kinetics and Particle Persistence in Aqueous Nano-Silver Colloids. Environ. Sci. Technol. 44, 2169–2175 (2010).
36. Gharibshahi, L., Saion, E., Gharibshahi, E., Shaari, A. H. & Matori, K. A. Influence of Poly(vinylpyrrolidone) concentration on properties of silver nanoparticles manufactured by modified thermal treatment method. PLoS One 12, e0186094 (2017).
37. Biba, R. et al. Coating-Dependent Effects of Silver Nanoparticles on Tobacco Seed Germination and Early Growth. Int. J. Mol. Sci. 21, 3441 (2020).
38. Krishnakumar, T. et al. Structural, optical and electrical characterization of antimony-substituted tin oxide nanoparticles. J. Phys. Chem. Solids 70, 993–999(2009).
39. Baytak, A. K., Teker, T., Duzmen, S. & Aslanoglu, M. A novel voltammetric sensor based on carbon nanotubes and nanoparticles of antimony tin oxide for the determination of ractopamine. Mater. Sci. Eng. C 59, 368–374 (2016).
40. Luo, H. et al. High Surface Area Antimony-Doped Tin Oxide Electrodes Templated by Graft Copolymerization. Applications in Electrochemical and Photoelectrochemical Catalysis. ACS Appl. Mater. Interfaces 7, 25121–25128 (2015).
41. Bessa, M. J. et al. Unveiling the Toxicity of Fine and Nano-Sized Airborne Particles Generated from Industrial Thermal Spraying Processes in Human Alveolar Epithelial Cells. Int. J. Mol. Sci. 23, 4278 (2022).
42. Li, J. et al. Using mussel as a global bioindicator of coastal microplastic pollution. Environ. Pollut. 244, 522–533 (2019).
43. Beyer, J. et al. Blue mussels (Mytilus edulis spp.) as sentinel organisms in coastal pollution monitoring: A review. Mar. Environ. Res. 130, 338–365 (2017).
44. Zokm, G. M. El, Ismail, M. M. & Okbah, M. A. E. Seaweed as bioindicators of organic micropollutants polycyclic aromatic hydrocarbons (PAHs) and organochlorine pesticides (OCPs). Environ. Sci. Pollut. Res. 29, 34738–34748 (2022).
45. Ismail, G. A. & Ismail, M. M. Variation in oxidative stress indices of two green seaweeds growing under different heavy metal stresses. Environ. Monit. Assess. 189, 68 (2017).
46. El-Naggar, N. E.-A., Hussein, M. H., Shaaban-Dessuuki, S. A. & Dalal, S. R. Production, extraction and characterization of Chlorella vulgaris soluble polysaccharides and their applications in AgNPs biosynthesis and biostimulation of plant growth. Sci. Rep. 10, 3011 (2020).
47. Bouga, M. & Combet, E. Emergence of Seaweed and Seaweed-Containing Foods in the UK: Focus on Labeling, Iodine Content, Toxicity and Nutrition. Foods 4, 240–253 (2015).
48. Mahadevan, K. Seaweeds: a sustainable food source. in Seaweed Sustainability 347–364 (Elsevier, 2015). doi:10.1016/B978-0-12-418697-2.00013-1.
49. CHEN, S. et al. Avoiding artefacts during electron microscopy of silver nanomaterials exposed to biological environments. J. Microsc. 261, 157–166 (2016).
50. Kuznetsova, O. V., Keppler, B. K. & Timerbaev, A. R. Analysis of Engineered Nanoparticles in Seawater Using ICP-MS-Based Technology: From Negative to Positive Samples. Molecules 28, 994 (2023).
51. López-Mayán, J. J. et al. Evaluation of a cloud point extraction method for the pre-

concentration and quantification of silver nanoparticles in water samples by ETA-AS. Int. J. Environ. Anal. Chem. 98, 1434–1447 (2018).
52. Cheng, W., Stuart, E. J. E., Tschulik, K., Cullen, J. T. & Compton, R. G. A disposable sticky electrode for the detection of commercial silver NPs in seawater. Nanotechnology 24, 505501 (2013).
53. Ataro, A., McCrindle, R. I., Botha, B. M., McCrindle, C. M. E. & Ndibewu, P. P. Quantification of trace elements in raw cow's milk by inductively coupled plasma mass spectrometry (ICP-MS). Food Chem. 111, 243–248 (2008).
54. Garbe-Schonberg, C.-D. Simultaneus Determination of thirty-seven trace element in twenty-eight international rock standards by ICP-MS. Geostand. Geoanalytical Res. 17, 81–97 (1993).
55. Tanner, S. D. & Baranov, V. I. A dynamic reaction cell for inductively coupled plasma mass spectrometry (ICP-DRC-MS). II. Reduction of interferences produced within the cell. J. Am. Soc. Mass Spectrom. 10, 1083–1094 (1999).
56. Degueldre, C. & Favarger, P.-Y. Colloid analysis by single particle inductively coupled plasma-mass spectroscopy: a feasibility study. Colloids Surfaces A Physicochem. Eng. Asp. 217, 137–142 (2003).
57. Moor, C., Lymberopoulou, T. & Dietrich, V. J. Determination of Heavy Metals in Soils, Sediments and Geological Materials by ICP-AES and ICP-MS. Microchim. Acta 136, 123–128 (2001).
58. de la Calle, I., Menta, M., Klein, M. & Séby, F. Screening of TiO 2 and Au nanoparticles in cosmetics and determination of elemental impurities by multiple techniques (DLS, SP-ICP-MS, ICP-MS and ICP-OES). Talanta 171, 291–306 (2017).
59. Careri, M., Elviri, L., Mangia, A. & Mucchino, C. ICP-MS as a novel detection system for quantitative element-tagged immunoassay of hidden peanut allergens in foods. Anal. Bioanal. Chem. 387, 1851–1854 (2007).
60. Falciani, R., Novaro, E., Marchesini, M. & Gucciardi, M. Multi-element analysis of soil and sediment by ICP-MS after a microwave assisted digestion method. J. Anal. At. Spectrom. 15, 561–565 (2000).
61. de Lange, F. et al. Cell biology beyond the diffraction limit: near-field scanning optical microscopy. J. Cell Sci. 114, 4153–4160 (2001).
62. Knoll, M. & Ruska, E. Das Elektronenmikroskop. Zeitschrift for Phys. 78, 318–339 (1932).
63. Ruska, E. The development of the electron microscope and of electron microscopy. Rev. Mod. Phys. 59, 627–638 (1987).
64. Schrand, A. M., Schlager, J. J., Dai, L. & Hussain, S. M. Preparation of cells for assessing ultrastructural localization of nanoparticles with transmission electron microscopy. Nat. Protoc. 5, 744–757 (2010).
65. Al-Rawi, M., Diabaté, S. & Weiss, C. Uptake and intracellular localization of submicron and nano-sized SiO2 particles in HeLa cells. Arch. Toxicol. 85, 813–826 (2011).
66. King, W. E. et al. Ultrafast electron microscopy in materials science, biology, and chemistry. J. Appl. Phys. 97, 111101 (2005).
67. Tizro, P., Choi, C. & Khanlou, N. Sample Preparation for Transmission Electron Microscopy. in 417–424 (2019). doi:10.1007/978-1-4939-8935-5_33.
68. Raman, C. V. & Krishnan, K. S. A new type of secondary radiation [11]. Nature 121, 501–502 (1928).
69. Efremov, E. V., Ariese, F. & Gooijer, C. Achievements in resonance Raman spectroscopy. Anal. Chim. Acta 606, 119–134 (2008).
70. Fleischmann, M., Hendra, P. J. & McQuillan, A. J. Raman spectra of pyridine adsorbed at a silver electrode. Chem. Phys. Lett. 26, 163–166 (1974).

71. Kneipp, K. et al. Single Molecule Detection Using Surface-Enhanced Raman Scattering (SERS). Phys. Rev. Lett. 78, 1667–1670 (1997).
72. Pérez-Jiménez, A. I., Lyu, D., Lu, Z., Liu, G. & Ren, B. Surface-enhanced Raman spectroscopy: benefits, trade-offs and future developments. Chem. Sci. 11, 4563–4577 (2020).
73. Gabudean, A. M., Biro, D. & Astilean, S. Localized surface plasmon resonance (LSPR) and surface-enhanced Raman scattering (SERS) studies of 4-aminothiophenol adsorption on gold nanorods. J. Mol. Struct. 993, 420–424 (2011).
74. Alvarez-Puebla, R., Liz-Marzán, L. M. & García de Abajo, F. J. Light Concentration at the Nanometer Scale. J. Phys. Chem. Lett. 1, 2428–2434 (2010).
75. Morton, S. M. & Jensen, L. Understanding the Molecule−Surface Chemical Coupling in SERS. J. Am. Chem. Soc. 131, 4090–4098 (2009).
76. Tantra, R., Brown, R. J. C. & Milton, M. J. T. Strategy to improve the reproducibility of colloidal SERS. J. Raman Spectrosc. 38, 1469–1479 (2007).
77. Yang, Y., Xiong, L., Shi, J. & Nogami, M. Aligned silver nanorod arrays for surface-enhanced Raman scattering. Nanotechnology 17, 2670–2674 (2006).
78. Zhong, L.-B. et al. Self-Assembly of Au Nanoparticles on PMMA Template as Flexible, Transparent, and Highly Active SERS Substrates. Anal. Chem. 86, 6262–6267 (2014).
79. Chen, R., Shi, J., Liu, C., Li, J. & Cao, S. In situ self-assembly of gold nanorods with thermal-responsive microgel for multi-synergistic remote drug delivery. Adv. Compos. Hybrid Mater. 5, 2223–2234 (2022).
80. Banholzer, M. J., Millstone, J. E., Qin, L. & Mirkin, C. A. Rationally designed nanostructures for surface-enhanced Raman spectroscopy. Chem. Soc. Rev. 37, 885 (2008).
81. Rodríguez-Lorenzo, L., Álvarez-Puebla, R. A., de Abajo, F. J. G. & Liz-Marzán, L. M. Surface Enhanced Raman Scattering Using Star-Shaped Gold Colloidal Nanoparticles. J. Phys. Chem. C 114, 7336–7340 (2010).

Chapter 2

Sample preparation methods for extraction, pre-concentration and detection of metallic nanoparticles from biota and water samples

Metallic nanoparticles (MNPs) are introduced into the environment through several intentional or unintentional mechanisms. As mentioned in chapter 1, these MNPs can end up in water bodies increasing the probability of interaction with the biota and consequently the exposure to humans. Several detection techniques have been investigated and, despite their high sensitivity and specificity, the misinterpretation of the results increases with the complexity of the matrix studied. In addition, these MNPs can be taken up from different biota and waters, provoking the need of diverse sample treatments to efficiently extract and isolate the particles prior to instrumental analysis. Therefore, there is a growing need for analytical methods to safely extract, purify and detect MNPs present in complex matrices with the minimum impact on their physicochemical properties.

This chapter is focused on the development of sample preparation methodologies to extract and pre-concentrate MNPs from biota and water, crucial for the reliable and reproducible quantification in complex media. At first, the full characterization of the MNPs (i.e., ATO, TiO_2 and Ag NPs) used among this thesis work is presented. Their primary size and morphology were characterized by electron microscopy and X-Ray powder diffraction. The colloidal stability in both, ultrapure water and artificial seawater, was assessed by dynamic light scattering, zeta potential and UV-Vis spectroscopy. The efficiency of sample preparation methodology for their extraction from biota and water was assessed by single particle inductively coupled plasma mass spectrometry (sp-ICP-MS) and ICP atomic emission spectroscopy (ICP-OES) using ultrasound-assisted alkaline digestion and cloud point extraction (CPE), respectively.

Results show that ultrasound-assisted alkaline digestion and CPE of bivalves (i.e., mussels) and water (i.e., seawater), respectively, are promising techniques for the extraction, purification, and pre-concentration of these MNPs.

Chapter 2

2.1. Introduction

Engineered nanomaterials (ENMs) production is rapidly increasing and becoming an essential component of many industrial and consumer products. Their detection and characterization within complex media (i.e., consumer products) is essential to understand their benefits and potential risks and to implement measures, if needed. Despite their benefits, in fact, there is a growing concern about their possible release and spread into the environment, where they can persist and accumulate in various ecosystems.[1,2] Once released, they can travel through air, water, and soil, leading to their widespread distribution and potential impacts on various organisms. Depending on their surface properties, surface charge, ligands, coatings, shape and size, nanoparticles (NPs) can have different ways of interacting with the surroundings.[3] Their physicochemical parameters are the major responsible for influencing their fate and behavior, preventing or promoting transformation processes and organisms interactions, and being in some cases responsible for toxicity events.[4]

Thus, the potential adverse effects of ENMs are the subject of ongoing research and have led to calls for implementing regulations and monitoring their production and release into the environment. As a consequence, this has led to highlight the importance of having techniques to allow NPs detection in different environmental compartments where, the diverse physicochemical properties and transformations that ENMs undergo once released and the subsequent potential interaction with biota make the development of analytical methods for their detection very challenging.[5–7]

The majority of the investigations are carried out in medically oriented studies where, higher particle concentrations, usually modified or functionalized, are involved.

Fluorescence-labelled NPs are commonly adopted and followed to investigate their bioaccumulation and biodistribution within in-vitro or in-vivo toxicity assays.[8,9] However, modified NPs barely reproduce the behavior of the unmodified ones, thus not representing a good prediction model.[10]

In addition, when interacting with living organisms, the particles end up being embedded in more complex matrices, a phenomenon that also occurs after their incorporation into consumer products. This makes even more difficult to use standard techniques, like electron microscopy (EM), mass spectrometry (MS) or light scattering (LS) ones, without previous sample treatment. Also, at environmental level, very low concentrations are usually investigated, which leads researchers to deal with the limitations of the techniques. Therefore, there is an urgent need to develop methodologies integrating samples preparation steps for extraction, purification, and pre-concentration of MNPs from complex matrices and their subsequent identification and quantification, in order to advance in understanding their fate and possible toxicity effects.

One of the techniques largely used to investigate elemental particle composition is inductively coupled plasma mass spectrometry (ICP-MS) or single particle-inductively coupled plasma-mass spectrometry (sp-ICP-MS) for NPs analysis.[11,12] However, when it comes to complex media, even these established techniques become challenging, completely relying on NPs extraction efficiency and precise sample preparation.

Among the sample preparation techniques, a first distinction in sample pre-treatment allows discrimination between in-situ and ex-situ analysis, in relation to the method of investigation. The in-situ analysis, does not involve any extraction process, allowing the analysis of the NPs within their precise location. EM techniques are usually the ones employed in these studies and their use is addressed in the next chapter (Chapter 3). As the name itself suggests, the ex-situ analysis, involves the extraction of the particles from the matrix, using reliable methods that do not cause unexpected modifications to the particles, in terms of size, shape and aggregation level.

Within the sample preparation methods using for ex-situ analysis, the acid digestion is the most common method to purify and isolate nanoparticles for various applications, such as material science, biomedical research, and environmental analysis.[13,14] It involves using a concentrated acid or a mixture of acids to extract ionic elements or NPs from complex inorganic and organic matrices, such as biological tissues. In relation to the nature of NPs, concentrated oxidizing agents, such as nitric acid (HNO_3) or hydrochloric acid (HCl), are extensively used to digest organic matrices and keep

NPs integrity. NPs can then be isolated using centrifugation or other physical separation techniques to remove matrix residues for their analysis. Using these acids in combination with hydrogen peroxide (H_2O_2) and microwave-assisted techniques, the method can also promote the complete dissolution of NPs to perform total elemental quantification.

Alternatives to acid digestion methods are those based on the use of alkaline reagents. The alkaline-based extraction method involves the use of basic solutions, such as sodium hydroxide (NaOH) or potassium hydroxide (KOH), to dissolve and extract NPs from complex matrices.[15]The basic solution reacts with the matrix, breaking down its structure and releasing the target particles into the solution. The NPs can then be isolated using physical separation techniques, such as centrifugation or filtration. The use of alkaline extraction is, in some cases, preferred over acid-based methods as it provides a gentler and less aggressive extraction process, resulting in fewer alterations of the structure and properties of the extracted NPs. The most common alkali solubilizer, having high efficiency for MNPs, is tetramethylammonium hydroxide (TMAH), while NaOH or KOH are believed to cause particles aggregation.[10,16] Depending on the physicochemical properties, there are NPs resistant to the majority of acids and bases, such as antimony tin oxide (ATO), TiO_2 and silicon dioxide (SiO_2) NPs, while others, such as Ag, copper oxide (CuO) or zinc oxide (ZnO) NPs, that easily dissolve under almost any acidic or basic conditions. For these kinds of NPs, sample preparation methodology with softer conditions should be selected and the enzymatic digestions could be a successful alternative.

The enzyme-assisted extraction method in fact, is gaining attention as an efficient, greener, sustainable alternative to conventional extraction techniques.[17,18] It involves the use of enzymes to selectively degrade the complex matrix without damaging the particles. The enzymes are chosen to target specific components of the matrix, such as proteins, carbohydrates, or lipids, allowing for a selective NPs extraction. Proteases or pectinases are usually used to digest animal tissues, while cellulase is mostly used for cell wall disruption. Sodium dodecyl sulphate (SDS) is often added to the solution as a stabilizer.[19] In order to obtain high extraction efficiency, several parameters need to be optimized, such as temperature, pH, extraction time and substrate/enzyme ratio. One of the limitations of this method is the high cost of the enzymes that are not optimal for processing large samples volume or scaling up the process to an industrial scale. Also, tissue residues not completely degraded by the enzymes can cause lower transport efficiency when the quantification is performed. For this reason, the water-soluble TMAH may be a useful alternative to overcome this limitation for base resistant NPs extraction.

Despite digestion methods allow the extraction and isolation of NPs from biota, their concentrations can be lower than the limit of detection of the most used analytical techniques, which could still lead to bioaccumulation provoking potential toxicological responses.

Moreover, since it has been reported that the predicted environmental concentrations of some MNPs, such as Ag NPs, are in the ng/L range in surface water, a pre-concentration step is in these cases recommended. Cloud point extraction (CPE) proves to be a suitable approach to address this challenge. CPE is a liquid-liquid extraction technique used to separate and concentrate target compounds prior to further analysis, being useful for environmental samples as their expected NPs concentrations are very low. It can be used as a pre-concentration technique itself, concentrating NPs in a relatively small volume or as a following step in combination with extraction techniques.[20,21] CPE commonly involves the use of non-ionic surfactants at concentrations above the critical micellar concentration (CMC) and the cloud point temperature (CPT).[22] At these conditions, which are surfactant specific, the solution becomes cloudy and partitions into two different phases, a small volume containing the surfactant-rich phase in which the analyte is included and a more aqueous one. The surfactant-rich phase is created over micelles formation and aggregation, with subsequential precipitation. Triton X-45, Triton X-100, and Triton X-114 are some of the most used non-ionic surfactant reagents,[23] where, Triton X-114 has a relatively low cloud point, allowing phase separation already at 23 °C.

In this chapter, the development and optimization of sample preparation methods for MNPs with different physicochemical properties upon bioaccumulation in biota and water is addressed. To this end, representative MNPs were chosen based to their physicochemical properties: ATO and TiO_2 as stable crystalline NPs, while Ag as reactive crystalline NPs that tend to dissolve under various conditions. These NPs, dispersed in artificial seawater, were fully characterized by electron microscopies, XRD, dynamic light scattering, zeta potential and UV-vis spectroscopy. After understanding their behaviour in seawater, specific ones were selected to test the efficiency of the sample preparation methods developed in this chapter.

The ultrasound-assisted alkaline digestion was selected for the extraction of ATO NPs from mussels (*Mytilus galloprovincialis*) and its performance was evaluated using sp-ICP-MS. After optimization, the assessment of the potential bioaccumulation of ATO NPs in marine mussels during 28 days of exposure was evaluated. Meanwhile, CPE using TX-114 was optimized for the pre-concentration of Ag and TiO_2 NPs dispersed in seawater containing organic matter (i.e., seawater collected from aquarium where bioaccumulation assays with mussels were performed). CPE performance was

then assessed by ICP-OES. NPs with different sizes and colloidal stability were tested to understand the impact of their physicochemical properties on the CPE efficiency.

2.2. Results and Discussion

2.2.1. Characterization of MNPs in artificial seawater

The MNPs studied in this work were fully characterized in ultrapure water, as a reference medium, and synthetic seawater. ATO NPs were dispersed without any stabilizer, while both Ag NPs and TiO_2 NPs were stabilized using polyvinylpyrrolidone (PVP) and sodium citrate, respectively (more details in Annex I, section 1). Two of the Ag NPs, PVP-15nm Ag NPs and PVP-50–80nm Ag NPs, studied here, contained PVP in their commercial formulation, demonstrating that PVP is a well-known stabilizer agent and widely used as a stabilizer for Ag NPs.[24] However, the third Ag NPs were stabilized by ethylene glycol and a purification process to replace it and coat the particles with PVP was performed. Both procedures were characterized by DLS and UV-Vis spectroscopy, showing that the particles remain colloidally stable after purification and PVP functionalization (Figure 1). In the case of TiO_2 NPs, three different NPs were selected and stabilized with sodium citrate: citrate-5nm TiO_2 NPs, citrate-25nm TiO_2 NPs and citrate-45nm TiO_2 NPs. Sodium citrate was selected as stabilizer to enhance the colloidal stability of these NPs in water since it is well-known

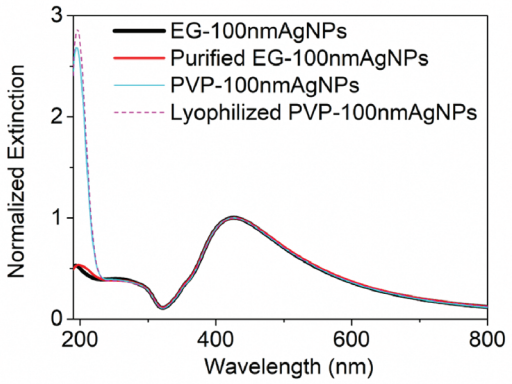

NPs	[NPs] / mg/L	D_H[a] (PDI)[b] / nm
		Ultrapure water
EG[C]-100nmAgNPs	13.3	120 ± 1 (0.19 ± 0.06)
Purified EG-100nmAgNPs	60	110 ± 2 (0.28 ± 0.04)
PVP-100nmAgNPs	60	120 ± 1 (0.29 ± 0.04)
Lyophilazed PVP-100nmAgNPs	60	131 ± 1 (0.25 ± 0.04)

[a] *Mean hydrodynamic diameter was obtained by DLS at room temperature and at a scattering angle of 90° for 60 s. DLS measurements were carried out on 5 runs: Mean ± Standard desviation (SD).*
[b] *Polydispersity index*
[C] *EC=Ethylene glycol*

Figure 1. Physicochemical properties characterization of 100 nm Ag NPs as a function of each purification and functionalization step.

that citrate is an excellent capping agent and stabilizer for TiO_2 in aqueous suspensions.[25]

Figure 2 shows transmission EM (TEM) images of all NPs dispersed in ultrapure water. The analysis reveals that all NPs present a pseudo-spherical shape. However, only PVP-15nm Ag NPs and PVP-100nm Ag NPs were well-dispersed on the grid, while PVP-50–80nm Ag NPs, ATO NPs and the three TiO_2 NPs tended to form aggregates. The NPs primary size was estimated to be: 24 ± 7 nm for PVP-15nm Ag NPs, 42 ± 21 nm for PVP-50–80nm Ag NPs, and 96 ± 25 nm for PVP-100nm Ag NPs, 29 ± 10 nm for citrate-25nm TiO_2 NPs and 44 ± 22nm for citrate-45nm TiO_2 NPs. It should be noted that, despite high resolution TEM (HRTEM) was used, it was not possible to obtain the primary size estimation for citrate-5nm TiO_2 NPs and ATO NPs, because of their polydispersity and overlapping NPs in the aggregates. Therefore, the nano crystallite size for both NPs was calculated by X-Ray diffraction (XRD) pattern using the Scherrer equation, obtaining a size of 8.6 nm for citrate-5nm TiO_2 NPs and 16.8 nm for ATO NPs (Figure 3).[26]

Knowing the influence that high salt concentration can have on NPs by affecting their colloidal stability and availability to interact with specific organisms, different physicochemical properties were investigated in synthetic seawater, besides ultrapure water.

Taking advantage of the plasmonic properties of Ag NPs, their extinction spectra in both, ultrapure water and synthetic seawater, were measured by UV-Vis spectroscopy as shown in Figure 4. The extinction spectra of PVP-15nm Ag NPs and PVP-100nm Ag NPs displays a single LSPR band centered at 412 nm and 425 nm in both media, which demonstrates that these nanoparticles are colloidally stable in media with high ionic strength like artificial seawater. This is due to the presence of PVP since this polymer stabilizes the NPs by electrosteric repulsion.[27] However, the extinction spectrum of PVP-50–80nm Ag NPs shows a broad LSPR band developed in the visible-near-infrared region and a decrease of the concentration when in artificial seawater. These features can be attributed to the aggregation of Ag NPs, i.e., the plasmonic coupling between closely packed NPs, especially in the presence of high ionic strength. Due to the polymer shell it can act as a dielectric spacer and be an effective insulator, which may hinder additional coupling of LSPR oscillations between associated particles provoking the decrease of the sensitivity of the UV-Vis spectroscopy on the aggregation monitoring.[28] DLS overcomes this obstacle and therefore the hydrodynamic size of Ag NPs was also characterized, together with ATO and TiO_2 NPs. Table 1 summarizes the results obtained by DLS and zeta potential.

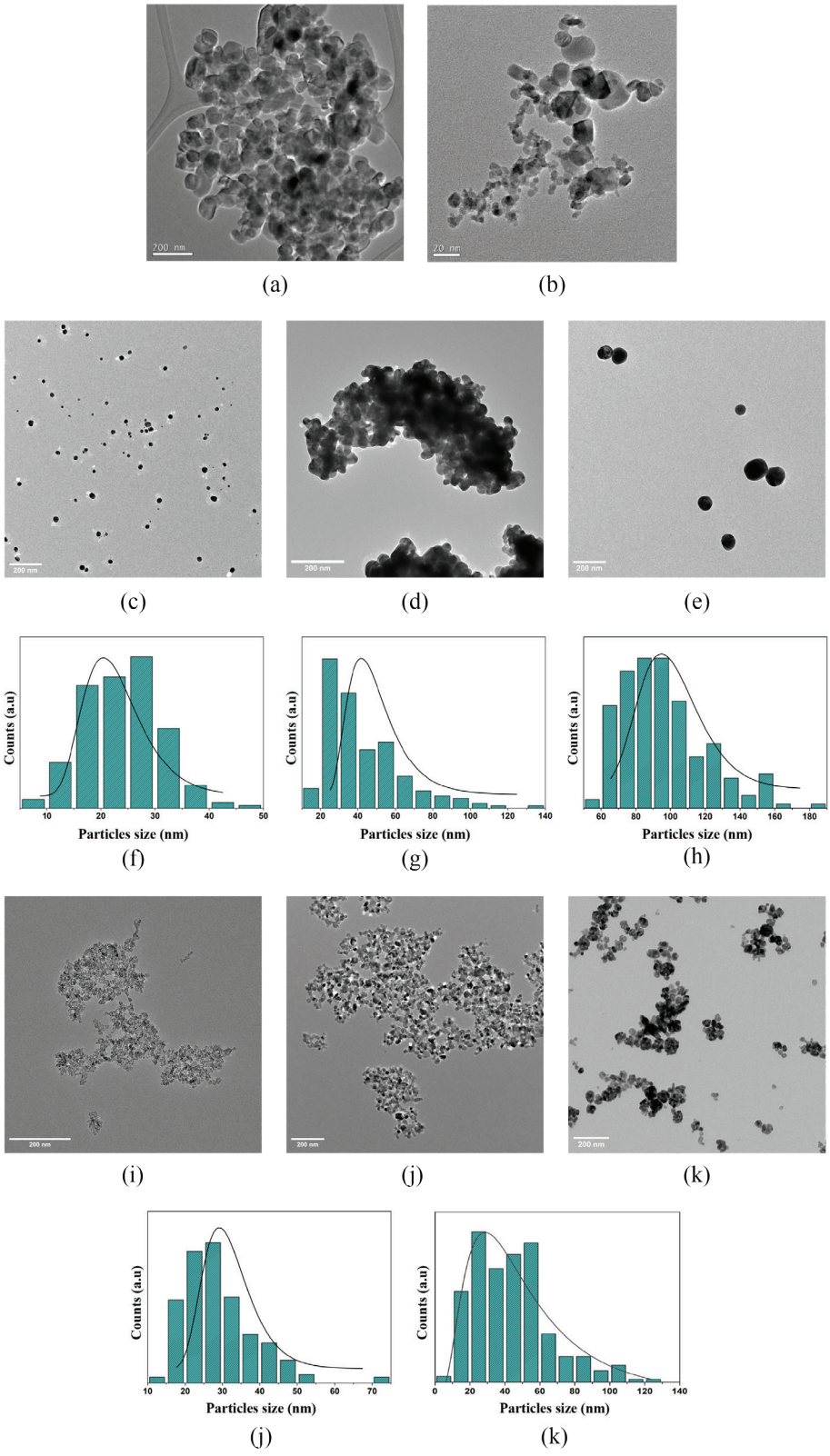

Figure 2. TEM analysis showing morphology and dispersion of (a, b) ATO NPs, (c – e) PVP-15nm Ag NPs, PVP-50–80nm Ag NPs and PVP-100nm Ag NPs respectively and (i – k) citrate-5nm TiO2 NPs, citrate-25nm TiO2 NPs and citrate-45nm TiO2 NPs respectively. Scale bar of 200 nm and (b) 20 nm. Particle size distribution of (f – h) Ag NPs and (l, m) citrate-25nm TiO2 NPs and citrate-45nm TiO2 NPs respectively, estimated by measuring an average of 200 particles per sample. Gaussian fitting is represented by histograms and continuous line respectively. ATO NPs TEM analysis was performed in CEMES/CNRS (29, rue Jeanne Marvig, 31055 Toulouse, France).

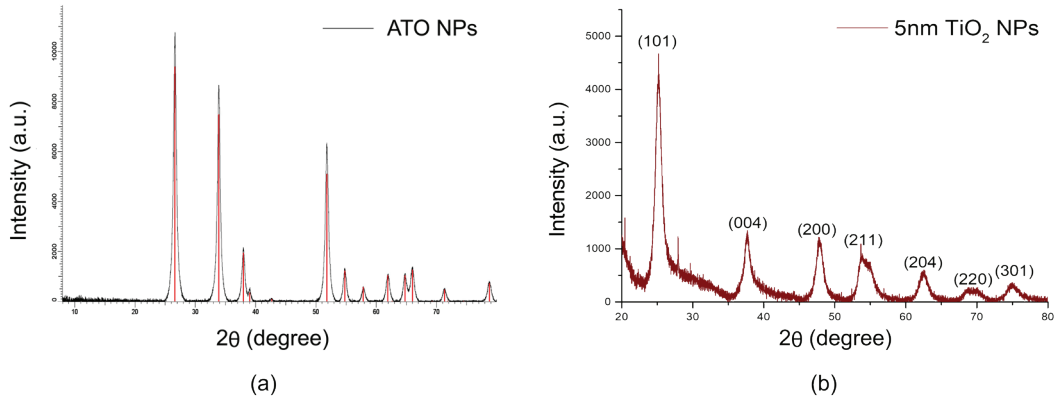

Figure 3. X-ray diffraction (XRD) pattern of (a) ATO NPs and (b) anatase 5 nm TiO2 NPs. The nano crystalline size was calculated using Scherrer equation $L=K\lambda/\beta\cos\theta$ (L = nano crystallite size; λ (nm) = XRD radiation of wavelength; β = full width at half maximum of peaks; θ = peak centered at 2θ in the pattern. The crystalline nanosize obtained was 16.8 and 8.6 nm, respectively. XRD analysis of ATO NPs was performed in CEMES/CNRS (29, rue Jeanne Marvig, 31055 Toulouse, France).

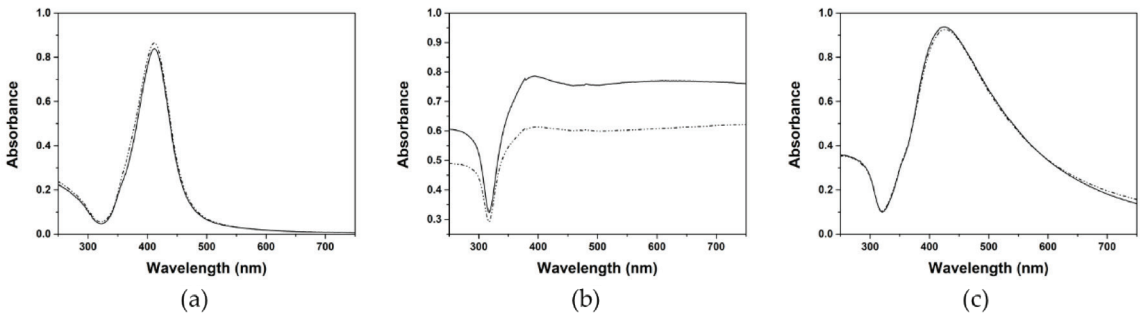

Figure 4. UV-Vis extinction spectra of (a) PVP-15nm Ag NPs, (b) PVP-50–80nm Ag NPs and (c) PVP-100nm Ag NPs. Particles stability was tested in ultrapure water and artificial seawater, represented by continuous and dashed lines respectively.

The hydrodynamic size of Ag NPs estimated by DLS in ultrapure water confirmed the UV-Vis results (Table 1). PVP-15nm Ag NPs and PVP-100nm Ag NPs showed a size of 49 ± 3 nm and 139 ± 2 nm, respectively, which are higher diameters than the ones obtained by TEM. This is due to the presence of PVP layer around Ag NPs. PVP-50–80nm Ag NPs presented a hydrodynamic size of 619 ± 75 nm confirming the aggregation of these Ag NPs. In all cases, a negative surface charge was measured by zeta potential when Ag NPs were dispersed in ultrapure water, confirming the repulsion between similarly charged particles in the dispersion (Table 1). These values can be attributed to the negatively charged PVP

	Ultrapure water			*Synthetic seawater*		
	Hydrodynamic diameter[1] (nm)	*PDI[2]*	*Z potential[3] (mV)*	*Hydrodynamic diameter[1] (nm)*	*PDI[2]*	*Z potential[3] (mV)*
ATO NPs	107 ± 2	0.32 ± 0.04	– 32 ± 4	9665 ± 820	0.67 ± 0.28	– 1 ± 4
PVP-15nm Ag NPs	49 ± 3	0.6 ± 0.07	– 24 ± 5	47 ± 2	0.4 ± 0.03	– 9 ± 16
PVP-50-80nm Ag NPs	618 ± 83	0.2 ± 0.02	– 83 ± 6	1348 ± 407	0.3 ± 0.04	– 5 ± 10
PVP-100nm Ag NPs	139 ± 2	1.5 ± 0.11	– 21 ± 12	97 ± 1	0.8 ± 0.12	– 6 ± 10
citrate-5nm TiO_2 NPs	53 ± 2	0.47 ± 0.06	– 31 ± 1	2478 ± 166	0.48 ± 0.17	– 1 ± 3
citrate-25nm TiO_2 NPs	166 ± 3	0.19 ± 0.03	– 79 ± 2	7589 ± 2291	2.11 ± 0.99	– 1 ± 2
citrate-45nm TiO_2 NPs	174 ± 56	0.54 ± 0.15	– 72 ± 16	5708 ± 1012	3.04 ± 0.70	1 ± 4

[1] Mean hydrodynamic diameter and [2] polydispersity index obtained by DLS at a scattering angle of 173° and 25 °C. DLS measurements were carried by quintupled: mean ± standard deviation (SD).
[3] Zeta potentials were measured in 5 runs (mean ± SD).

Table 1. NPs physicochemical characterization.

polymer (zeta potential – 30 mV) offering a stabilization of Ag NPs due to the combined electrosteric repulsion.[27] A higher negative value of – 83 ± 6 mV was recorded for PVP-50–80nm Ag NPs demonstrating, once again, that the initial aggregates were stable.

The presence of PVP is crucial especially when the particles are dispersed in artificial seawater. Hydrodynamic diameters of 47 ± 2 nm and 97 ± 1 nm were recorded for PVP-15nm Ag NPs and PVP-100nm Ag NPs, showing that the presence of salts does not destabilize these NPs. However, the hydrodynamic size of PVP-50–80nm Ag NPs in seawater was bigger, 1348 ± 407 nm, than in ultrapure water, which can be attributed to the fact that the concentration of PVP is lower than in the other two NPs (0.2% vs 75%). This lower amount of PVP was not enough to prevent aggregation to occur and the particles re-arranged themselves into newly formed aggregates. Interestingly, zeta-potential measurements reveal a decrease of surface charge in seawater. In fact, all Ag NPs in seawater showed zeta potential values of – 9 ± 16, – 6 ± 10 and – 5 ± 10 mV for PVP-15nm Ag NPs, PVP-100nm Ag NPs and PVP-50–80nm Ag NPs, respectively. This decrease likely is due to the compression of the electric double layer (EDL) promoted by the presence of highly ionic strength in seawater. This compression of EDL induces aggregation when the only repulse force is electrostatic; however, in this case, the steric remain due to the

presence of PVP on the surface, keeping Ag NPs stable. In the case of PVP-50–80nm Ag NPs an increase of the hydrodynamic size in seawater was observed, meaning that the amount of PVP was not enough to keep stable the aggregates by steric repulsion forces.

DLS data from all TiO_2 NPs and ATO NPs dispersed in ultrapure water showed higher hydrodynamic diameter that the ones reported by TEM analysis: 107 ± 2 nm for ATO NPs, 53 ± 2 nm for citrate-5nm TiO_2 NPs, 166 ± 3 nm for citrate-25nm TiO_2 NPs and 174 ± 56 nm for citrate-45nm TiO_2 NPs. These values confirmed that ATO and TiO_2 NPs tend to easily aggregate, despite using a stabilizer, as confirmed by TEM (Figure 2). Once in seawater, all NPs immediately form even bigger aggregates, as shown in DLS analysis (Table 1). This destabilization is due to the decrease of zeta potential from negative values (range from -79 to -32 mV) to almost null surface charge, caused by the compression of the electric double layer (EDL) promoted by the presence of high ionic strength in seawater. The absence of stabilizers (i.e., polymer instead of citrate) to shield the electrostatic repulsion between the particles, promotes the occurrence of aggregation processes. Also, the synthetic seawater used in the study, does not contain any natural (NOM) or particulate organic matter, which could help in increasing particles stability.

2.2.2. MNPs extraction from marine mussels using ultrasound-assisted alkaline digestion: the case of Antimony Tin Oxide NPs

As mentioned in chapter 1, marine mussels production represents more than one third of the EU aquaculture. Therefore, it is of vital importance to understand the potential bioaccumulation of MNPs in this specie. It is well-known that marine mussels are filter-feeding mollusks that retain particles between 5 to 35 μm in diameter, being the maximum retention efficiency reported for particles with a size of 30 – 35 μm. However, mussels may efficiently retained (i.e., 100%) smaller particles down up 7 μm.[29] Taking into account this range, ATO NPs were selected to study their potential bioaccumulation in mussels, since their average hydrodynamic diameter in artificial seawater was close to 10 μm (Table 1) making feasible their efficient retention into mussels digestive system.

To study the bioaccumulation, control trials were performed over 28 days of exposure at 0, 0.1 and 1 mg/L of ATO NPs by triplicate (more details in Annex I, section 3.1). Mussels were collected after each time point of exposure (i.e., 0, 7, 14, 21 and 28 days). Before treating the real samples, some optimizations of ATO NPs extraction from mussels were carried out by spiking ATO NPs to individual mussels.

As explained in the section above, the sample preparation for ex-situ analysis has an impact in the recovery of the whole analytical method. It is well-known that acid digestion can destroy the soft tissues; however only few acidic mixtures keep the total integrity of the NPs (e.g., HNO_3).[30] The lack of acidic mixtures to extract MNPs without altering size and morphology limits the use of this acid digestion. Therefore, the remaining extraction methods mentioned before were tested: 1) enzymatic digestion using papain or a mixture of lipase:pancreatin and 2) ultrasound-assisted TMAH alkaline digestion. Table 2 shows the conditions used for the extraction of ATO NPs from mussels tissue.

		Digestion methods for 1 g of sample
Enzymatic		
	Papain	- activation buffer (EDTA, L-cysteine, dimercaptopropanol) - pH > 2.8 - filtration (5 µm filter size)
	Lipase:Pancreatine (0.8%:0.8% (w/v))	- buffer solution (NaH2PO4, NaOH) - pH = 7.40 - filtration (5 µm filter size)
Alkaline		
	TMAH (10%)	- aqueous solution - bath sonicator incubation - centrifugation steps

Table 2. NPs extraction methods.

Cleaner extracts were obtained after TMAH alkaline digestion, which may reduce the loss of NPs in the filtration, as the extracts in the SEM images show (Figure 5), prior to single particle ICP-MS, which was the analytical technique selected to quantify the bioaccumulation. The particulate material obtained after enzymatic digestion was bigger than the one obtained by alkaline digestion (> 50 µm for enzymatic digestion VS < 10 µm for alkaline digestion). Thus, ultrasound-assisted TMAH digestion was selected as extraction method of ATO NPs from mussel. The TMAH alkaline digestion method was validated by adding ATO NPs to mussels in the range 0 – 2 mg/L. After alkaline digestion, the extracts were analyzed by ICP-MS. The recovery was estimated related to the total and NPs concentration of Sb and Sn measured by ICP-MS and sp-ICP-MS in comparison with the theorical content of each element into the composition of ATO (Sb_2O_5:SnO_2 15:85% wt). Thus, a recovery up to 90% was achieved when 1.5 and 2 mg/L were analyzed, demonstrating that the alkaline digestion is a potential pre-treatment approach to be used when complex matrices are involved (Figure 6).

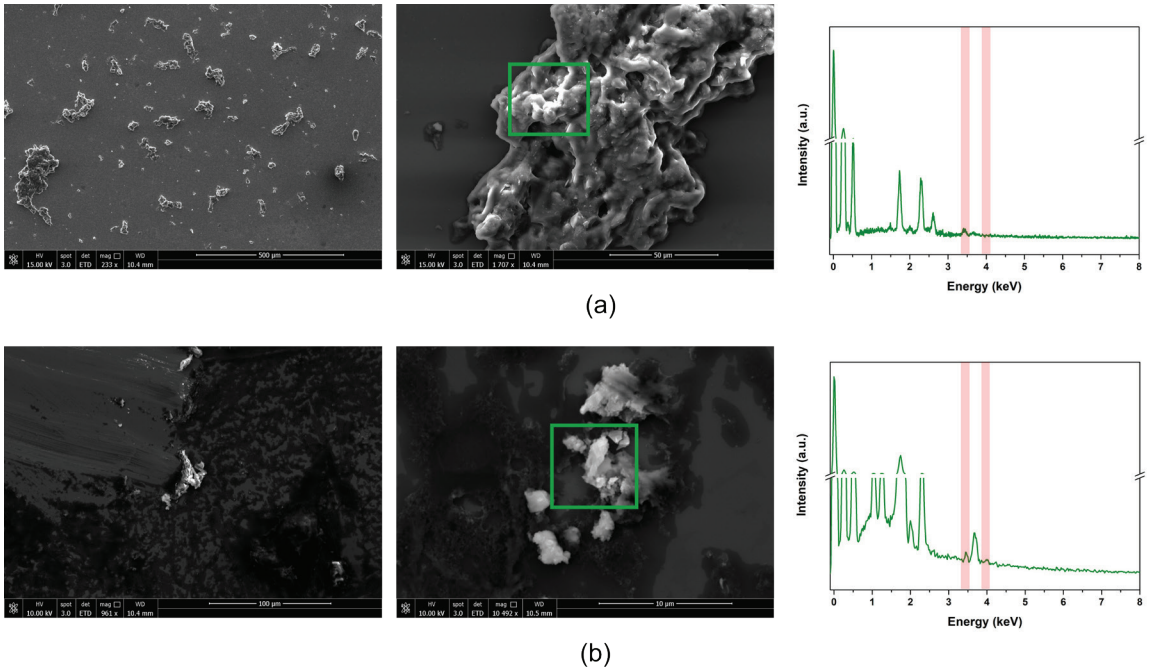

Figure 5. ATO NPs after (a) enzymatic extraction using papain and (b) alkaline digestion using TMAH.

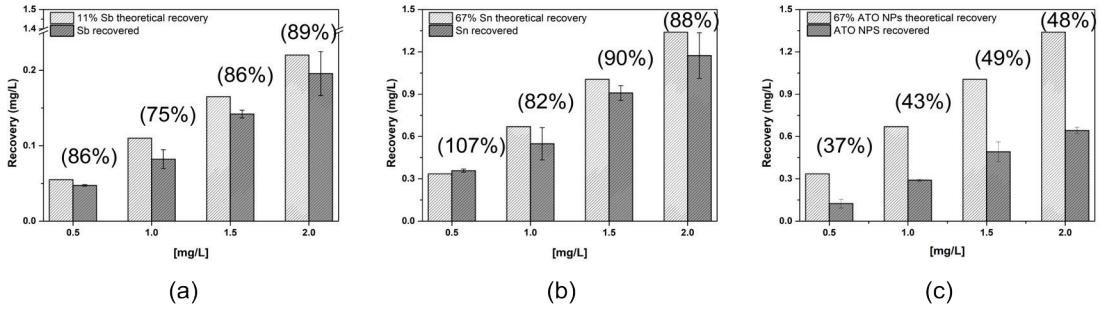

Figure 6. Dissolved concentrations of Sb (left) and Sn (right) recovered after mussels alkaline digestion of spiked samples at different concentrations. Error bars correspond to the SD of three experimental replicates.

After the optimization of the analytical methodology for extraction and quantification of ATO NPs from mussels, the samples collected from the bioaccumulation assays were analyzed. Six different mussels from three independent replicates for each of the condition (0, 0.1 and 1 mg/L of ATO NPs) and time of exposure (i.e., 0, 7, 14, 21 and 28 days) were analyzed for Sb and Sn elemental and NPs quantification by ICP-MS and sp-ICP-MS, after being subjected to TMAH alkaline digestion. However, for the quantification of NPs by sp-ICP-MS, only Sn was selected since it represents the 67% of the total mass of ATO, while Sb represents only the 11%.

ATO NPs concentration showed time and dose-dependent accumulation trend, reaching the highest level of $2.31 \times 10^6 \pm 7.39 \times 10^5$ NPs /g of dry weight in the last

time point, after 28 days of exposure (Figure 7). Higher variability in the highest concentration quantified was observed (i.e., higher standard deviation (SD) value), which could be attributed to the systematic error for the several dilutions performed prior sp-ICP-MS analysis. The sp-ICP-MS in nano configuration allows measuring both ionic and particulate concentration of the selected element (Sn in this case). This value can help in understanding the possible NPs transformation as a function of dissolution and aggregation processes. Figure 7a shows that a low concentration of dissolved Sn was measured in the nano configuration in any of the time points of exposure, indicating that the analytical methodology developed does not affect the integrity of ATO NPs in terms of dissolution. It is as well interesting to point out that there is no trend in dose or time-dependency on the ionic concentration, indicating that there is no significant dissolution of ATO NPs into mussels tissue. Moreover, the average size of the NPs obtained was similar in all time points analyzed as shown in Figure 7b. The sp-ICP-MS size was comparable to the one obtained by DLS when ATO NPs were dispersed in ultrapure water (Table 1). This could be attributed to the stabilization effect during the extraction procedure due to the presence of proteins, fatty acid and lipids from the mussels, together with the effect of sonication performed during the TMAH extraction process.[31] The presence of some NPs observed in the control condition could suggest that NPs that contain Sn in their composition were already accumulated into mussels at the starting time of the experiment.

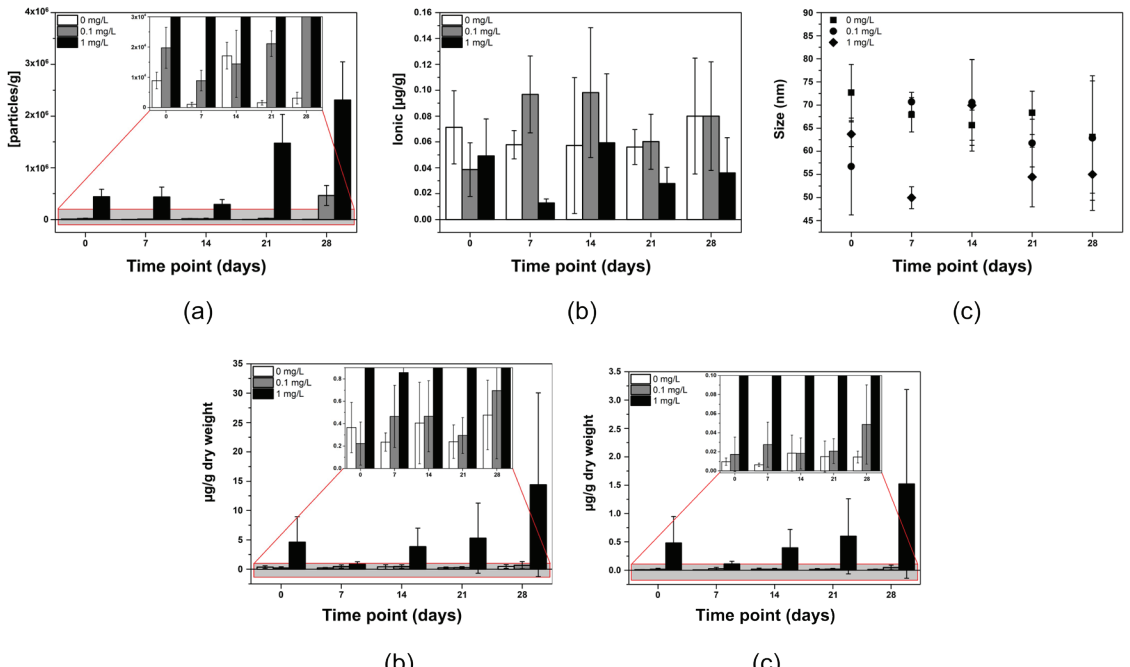

Figure 7. Recovery of (a) ATO NPs (67%, Sn fraction), (b) ionic concentration and (c) NPs diameter after mussels alkaline digestion at different time points using sp-ICP-MS. (d) Total Sn and (e) total Sb concentration measured by ICP-MS. Error bars correspond to the SD of three experimental replicates.

As concerned the total Sb and Sn recovery, the measured element amount increased related to the time of exposure, especially at higher concentrations, which is in agreement with the results obtained by sp-ICP-MS (Figure 7, c – d).

Despite the fact that there is an existing time-dependent accumulation of ATO NPs in mussels and that available studies confirm the digestive gland being the main organ for ENMs accumulation in bivalve molluscs,[32] NPs could not be found in digestive gland and mantle tissue analyzed by TEM, since the number of ATO NPs was not enough to allow any detection. In any case, tissues from mussels exposed to ATO NPs were analyzed and the results did not show any ultrastructural difference when compared to the control (Figure 8).

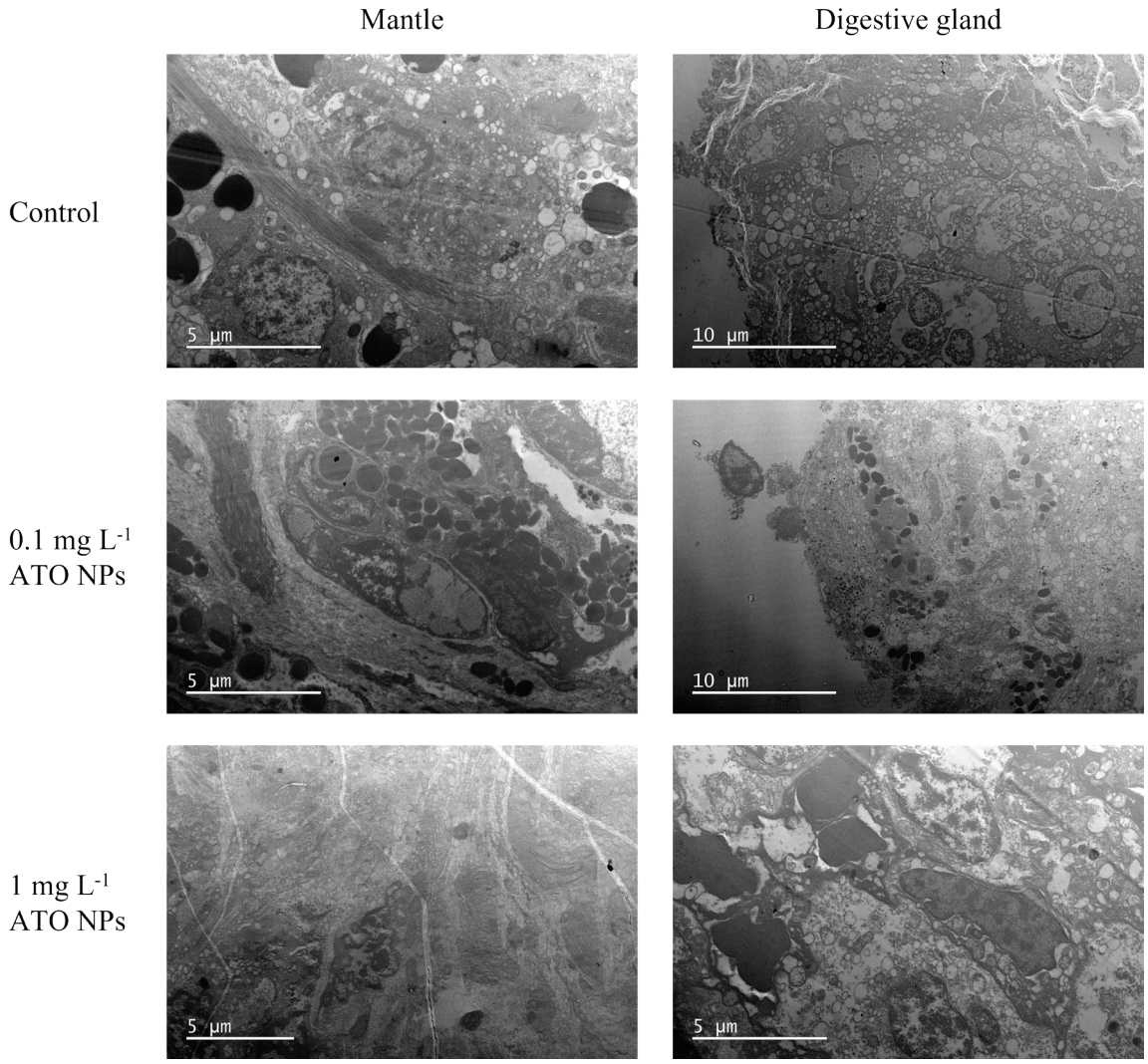

Figure 8. Transmission electron microscopy analysis of mussels tissues (mantle, left panel; digestive gland, right panel) upon 28 days of dietary exposure to 0, 0.1 and 1 mg/L of ATO NPs.

2.2.3. Separation and pre-concentration of MNPs from water samples using Cloud Point Extraction technique

The characterization of MNPs from environmental samples is necessary to better understand their fate, behavior and potential toxicity. Despite techniques availability, one of the problems often encountered is the limit of detection (LOD), being too high for environmentally relevant concentrations.

Here, CPE was selected as a sample preparation to concentrate MNPs from water samples prior analysis with conventional analytical tools, such as ICP-OES. In order to study the effect of the nature of the NPs, size and aggregation degree, Ag and TiO_2 NPs were selected. Their full characterization was deeply addressed in section 2.2.1 of this chapter. However, particokinetics were additionally studied in both, ultrapure water and artificial seawater, by UV-Vis spectroscopy and DLS.

Figure 9 shows the particokinetics analysis for the three Ag NPs: PVP-15nm Ag NPs, PVP-100nm Ag NPs and PVP-50–80nm Ag NPs. The LSPR spectra evolution of PVP-15nm Ag NPs and PVP-100nm Ag NPs dispersed in both, ultrapure water and seawater, demonstrated that these NPs remained in suspension over 28 days (Figure 9, a – f). This is due to the presence of PVP since this polymer stabilizes the NPs by electrosteric repulsion.[27]

Interestingly, these Ag NPs when dispersed in ultrapure water present different NPs population with different sedimentation rate as shown in the time evolution of the hydrodynamic size (Figure 9, h). The presence of PVP is crucial especially when the particles are dispersed in artificial seawater. Hydrodynamic diameters of 47 ± 2 nm and 97 ± 1 nm are recorded for PVP-15nm Ag NPs and PVP-100nm Ag NPs, showing that the presence of salts does not destabilize the NPs even after 28 days of exposure to the medium (Figure 9). The value of 1348 ± 407 nm reported for PVP-50–80nm Ag NPs proves instead that the lower amount of PVP is not enough to prevent aggregation to occur and the particles re-arranged themselves into newly formed aggregates. Moreover, these Ag NPs sedimented completely after 1 day of being dispersed in seawater as shown in the time evolution of the UV-Vis extinction spectrum (Figure 9, g) and the decrease in the DLS intensity (kcounts) over time (Figure 9, j). The hydrodynamic size of PVP-50–80nm Ag NPs displayed an increase in the first 2 h when dispersed in seawater, reaching then an equilibrium while maintaining a similar aggregate size before complete sedimentation (Figure 9, i). The PVP-50–80nm Ag NPs were redispersed after complete sedimentation and their hydrodynamic

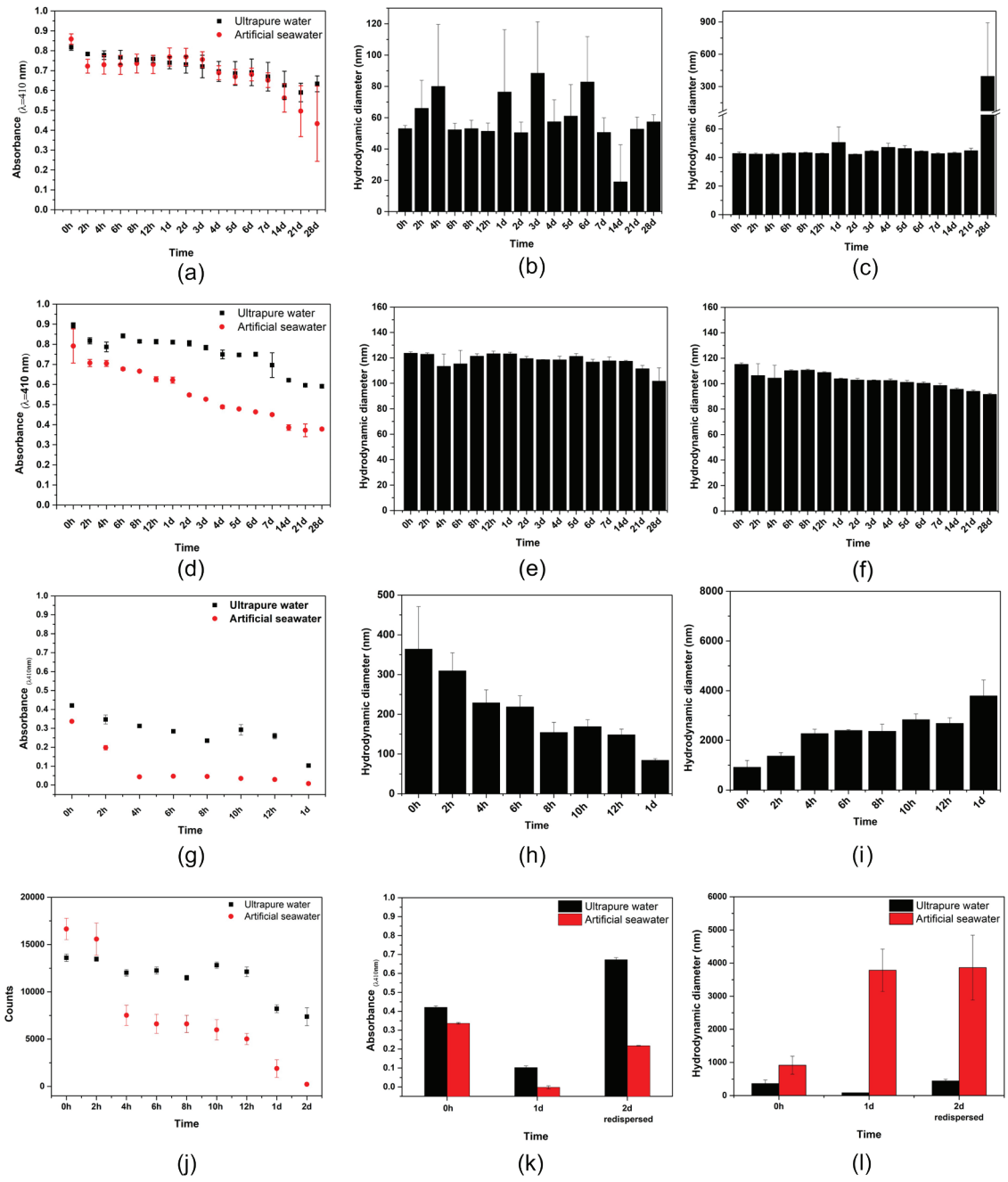

Figure 9. (a, d, g) Spectral evolution of optical absorbance and hydrodynamic size evolution (obtained by DLS, scattering angle of 173° and 20 °C) of PVP-Ag15nm NPs (first line), PVP-Ag-100nm NPs (second line), PVP-Ag50–80nm NPs (third line). The NPs are dispersed in both (b, e, h) ultrapure water and (c, f, i) artificial seawater. The particles were monitored over 30 days for single particles and 1 day for the aggregates at room temperature. In the case of PVP-Ag15nm NPs, the particles stay colloidally stable over time. In the case of PVP-100nmAg NPs, a decay of LSPR band is observed over time, which is due to likely sedimentation of the NPs. In the last case, PVP-Ag50–80nm NPs show not only a decay of LSPR band due to the fast sedimentation but also a variation in the hydrodynamic size where the sedimentation of big aggregates occurs since the first hours. (j, k) Particles counts of PVP-Ag50–80nm NPs demonstrating that after 1 day, complete sedimentation occurs. This is also confirmed by the decay of LSPR band at 1 day and its consequently increase after redispersion. (l) Hydrodynamic size evolution of PVP-Ag50–80nm NPs when in ultrapure water and artificial seawater revealing that, despite the fast sedimentation, the particles keep the same size after redispersion.

size was measured by DLS. A similar size was obtained before and after redispersion (Figure 9, k - l). Clearly, PVP-50–80nm Ag NPs were discarded for the optimization of CPE since they sediment almost completely after 2 h.

In the case of TiO_2 NPs, the particokinetics results are shown in Figure 10. The presence of citrate was enough to prevent the sedimentation of these NPs in ultrapure water even after 7 days of incubation, but not in presence of high ionic strength. When NPs were dispersed in seawater, the values of 2478 ± 166 nm, 7589 ± 2291 nm and 5708 ± 1012 nm reported for citrate-5nm TiO_2 NPs, citrate-25nm TiO_2 NPs and citrate-45nm TiO_2 NPs respectively, demonstrated that the presence of salts destabilizes the NPs, leading to the formation of bigger aggregates that easily sediment by time. This was confirmed by UV-Vis and DLS results obtained following the sedimentation and NPs size evolution over 7 days (Figure 10, a – i). In fact, the NPs started to settle already 2 hours after being in suspension, until they completely sedimented after 1 day, as shown in the UV-Vis spectral evolution (Figure 10, a – d – g) and by the decrease in the DLS intensity (kcounts) over time (Figure 10, j – k – l). Therefore, in this case, citrate-5nm and citrate-45nm TiO_2 NPs were selected for CPE optimization since they have the same ratio citrate:TiO_2 (1.5:1 wt:wt) and they have very different primary size (Figure 2 and Figure 3).

Details about CPE procedure are described in Annex I, section 2.2. Briefly, a final volume of 40 mL of MNPs dispersed in artificial seawater or mussel seawater was reached after addition of 4 mM Triton X-114 (TX-114) at room temperature and pH adjustment at 3 – 3.5. 1 h incubation time in boiling water followed, leading to the observation of a clear phase separation, without the need to perform any further centrifugation step to accelerate the process. TX-114, a polyethylene glycol tert-octylphenyl ether, was selected due to its physicochemical properties that improve the phase separation in short time, such as low could point temperature (23 – 36 ºC) and high density of the surfactant-rich phase, among others.[33] Temperature close to the boiling point of water (around 80 ºC), which was higher than the CPT of TX-114, was used since in these conditions the higher dehydration of the surfactant contributes to micelles aggregation and consequent precipitation.[34] As the idea is to promote the encapsulation of the MNPs inside the Triton micelles, the hydrophobic interaction between MNPs and TX-114 need to be enhanced. To do so, the surface charge of MNPs should be close to zero, which was already promoted when dispersed in seawater (see Table 1). The pH 3 – 3.5 was selected to promote also the protonation for any component in the mixture (e.g., citrate, PVP, particulate organic matter) favoring the hydrogen bond formation.[33] Also, it has been reported that the presence of salt and acidic pH, enhances

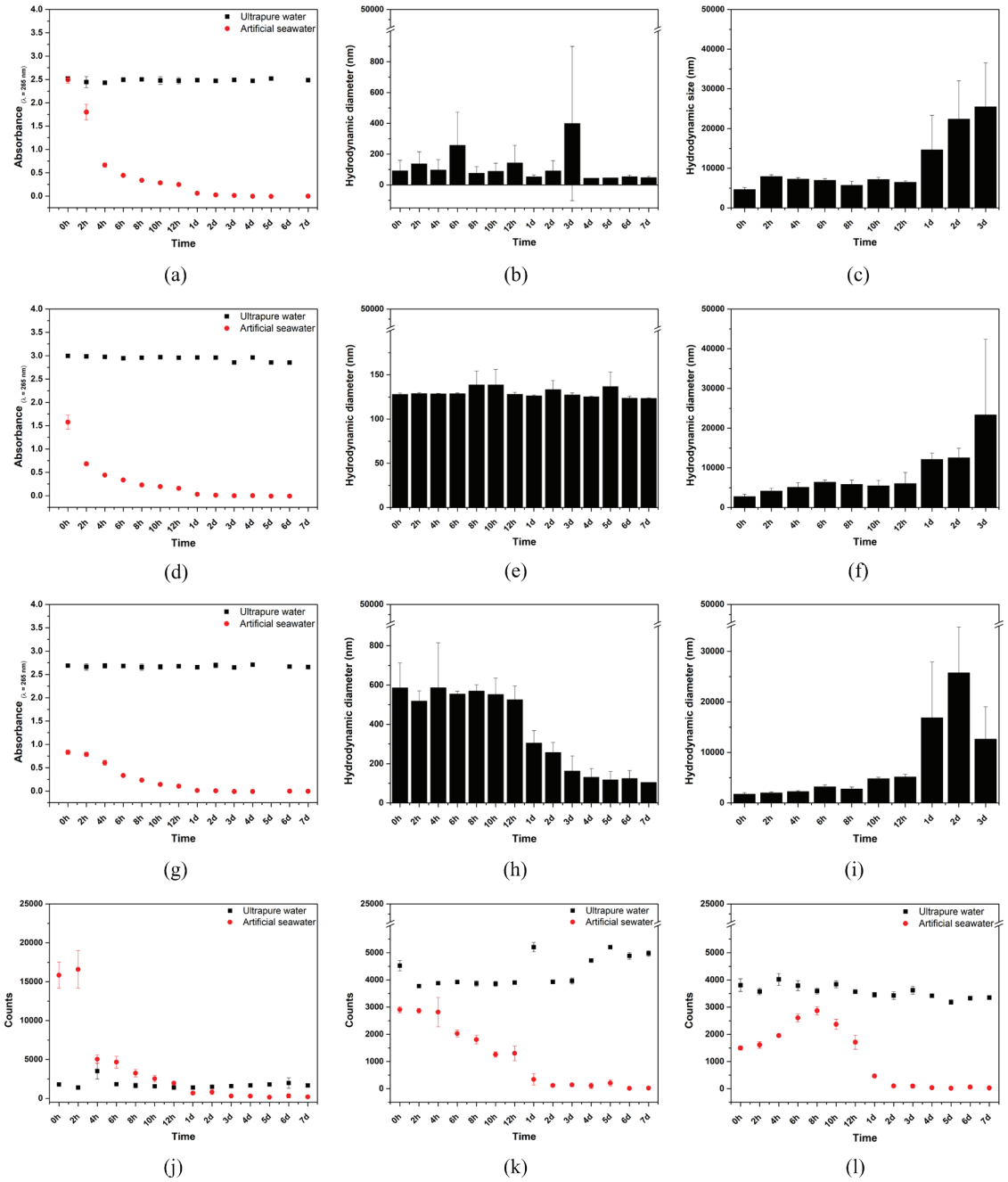

Figure 10. (a - i) Spectral evolution of optical absorbance and hydrodynamic size evolution (obtained by DLS, scattering angle of 173° and 20 °C) of citrate-5nm TiO_2 NPs (first line), citrate-25nm TiO_2 NPs (second line) and citrate-45nm TiO_2 NPs (third line). The NPs are dispersed in both (b, e, h) ultrapure water and (c, f, i) artificial seawater at initial concentration of 50 mg/L. The particles were monitored over 7 days for single particles and 3 days for the aggregates at room temperature. When in ultrapure water, the particles stay colloidally stable over time. In the case of artificial seawater, a decay of absorbance band is observed over time, as well as a variation in the hydrodynamic size where the sedimentation of big aggregates occurs since the first hours.

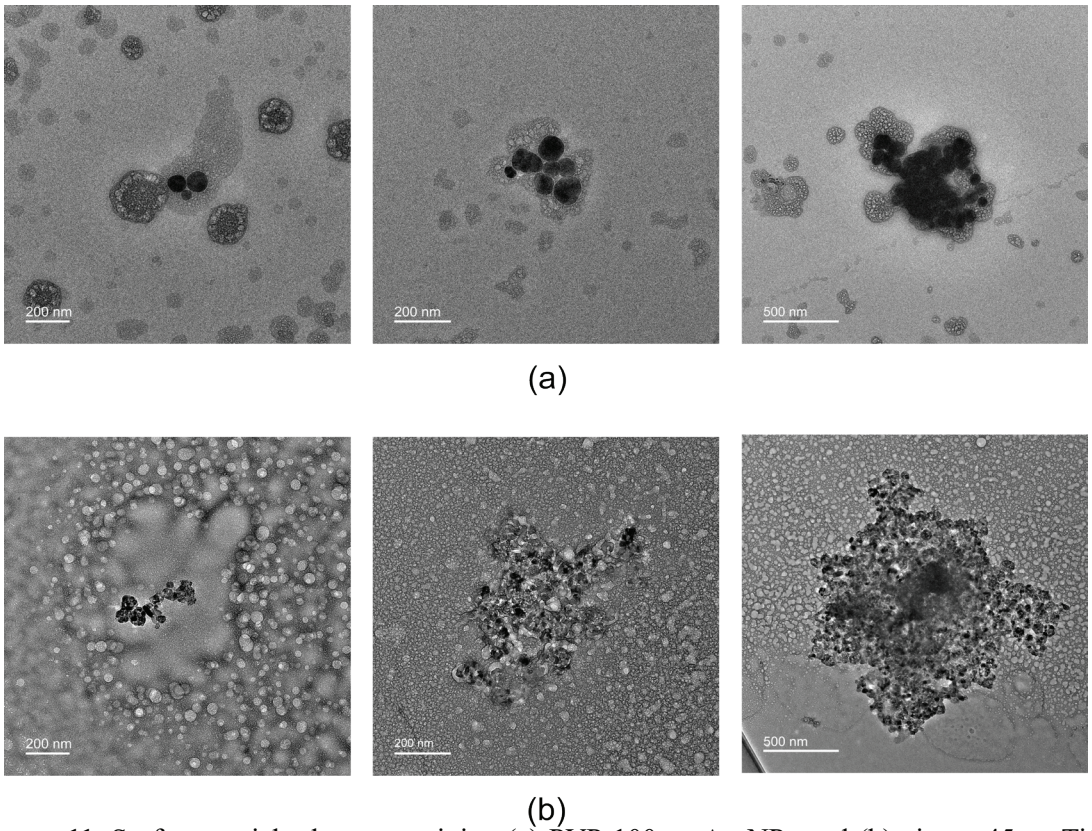

Figure 11. Surfactant rich phase containing (a) PVP-100nm Ag NPs and (b) citrate-45nm TiO_2 NPs after CPE.

the NPs extraction efficiency by CPE, due to the reduction of Coulomb repulsion between the charged NPs in TX-114 micelles and, as a consequence, the increase of the phase separation occurs.[35]

CPE efficiency was assessed by using four selected MNPs as mentioned before in this section: PVP-15nm Ag NPs, PVP-100nm Ag NPs, citrate-5nm TiO_2 NPs and citrate-45nm TiO_2 NPs and two different media: synthetic seawater and seawater collected from aquarium in which mussels were cultured, named here as "mussel seawater". TEM analysis was performed after surfactant-rich phase extraction. Results showing PVP-100nm Ag NPs and citrate-45nm TiO_2 NPs surrounded by micelles are shown in Figure 11, confirming the MNPs interaction with TX-114.

Elemental analysis of Ag NPs and TiO_2 NPs in the TX-114-rich phase were quantified by ICP-OES. Results are shown in Figure 12. The CPE recoveries were NP size- and medium- dependent being the tendency for NPs size: citrate-45nm TiO2 NPs >> citrate- 5 nm TiO2 NPs > PVP-100nm Ag NPs >>> PVP-15nm Ag NPs and for medium: mussel seawater > artificial seawater. These differences can be attributed to the fact that both TiO_2

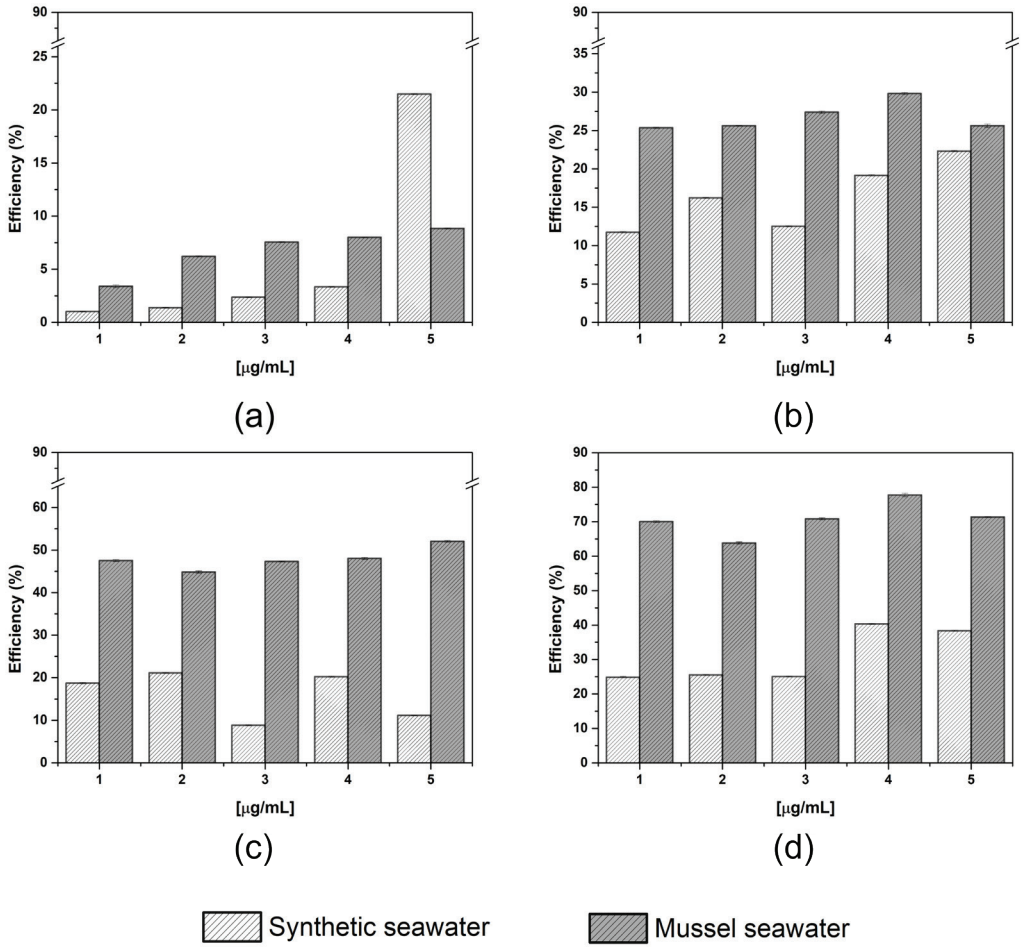

Figure 12. CPE recovery efficiency by ICP-OES analysis of (a) PVP-15nm Ag NPs, (b) PVP-100nm Ag NPs, (c) citrate-5nm NPs and (d) citrate-45nm NPs

NPs formed very big aggregates (> 5000 nm in hydrodynamic size, Table 1) when they were dispersed in seawater, while both Ag NPs remained stable. However, the difference in the coating, PVP for Ag NPs vs citrate for TiO_2 NPs, could contribute to the variation of CPE recovery. PVP also exhibits a clouding behavior upon heating of the solution.[36] Its presence as coating in Ag NPs could modify the could point of TX-114 in the conditions optimized here. The enhancement of the CPE efficiency in mussel seawater could be due to the presence of natural organic matter (NOM). It is well-known that the solubility of some components of NOM in water decreases at higher ionic strengths.[37] This, together with the protonation of NOM at acidic pH may improve the interaction of MNPs-NOM complexes with the micellar aggregates, enhancing the extraction process.[20]

2.3 Conclusions

A set of MNPs were selected taking into account their availability in the market, as well as their physicochemical properties, such as primary size and the surface functionality (i.e., the coating). The coating and its concentrations have a strong impact on the colloidal stability of the MNPs in artificial seawater: PVP-15nm and PVP-100nm Ag NPs remained colloidally stable during 28 days in seawater, while citrate-coated TiO_2 NPs and uncoated ATO NPs formed aggregates immediately after dispersion in the media. Understanding their behavior in seawater allowed a better selection of the MNPs as a model for the development and optimization of sample preparation methods for their extraction, purification and pre-concentration from biota (e.g., mussels) and water.

Ultrasound-assisted TMAH digestion was used for the extraction of ATO NPs from mussels and subsequently analysis of their potential bioaccumulation by sp-ICP-MS. The TMAH digestion showed higher recoveries (> 90 %) of ATO NPs via analysis of total Sb and Sn. This could be attributed to the fact that the extracts obtained using this sample preparation were cleaner, which avoided losses of NPs due to their adsorption on particulate organic matter. Additionally, the bioaccumulation of these NPs in marine mussel Mytilus sp. were studied using the methodology optimized here. The results indicated that, despite being scarce ($2.31 \times 10^6 \pm 9.05 \times 10^5$ particles/g), the bioaccumulation of ATO NPs into mussels was observed. TEM analysis of the potential biodistribution was carried out. However, no ATO NPs could be localized and visualized in the tissues analyzed (i.e., mantle and digestive gland) due to the relatively low concentration, as well as no significant alterations were observed in cells ultrastructure.

CPE, using a non-ionic Triton X-114 surfactant, was able to successfully separate and concentrate both, Ag and TiO_2 NPs, in seawater during 1 hour and without the need of centrifugation. An influence of the size and aggregation level as well as the medium composition was observed in the CPE efficiency evaluated using ICP-OES. For stable PVP-coated Ag NPs, higher efficiency was observed for PVP-100nm Ag NPs compared to PVP-15nm Ag NPs, but recoveries were lower (< 30%) than citrate-coated TiO_2 aggregates (≤ 80%). In addition, the presence of particulate organic matter in seawater improved the CPE efficiency in all cases analyzed, being 2-fold higher for both citrate-5nm and citrate-45nm TiO_2 NPs. Therefore, it was demonstrated that CPE was more efficient in presence of particulate organic matter and for MNPs with bigger hydrodynamic size.

References

1. Ferry, J. L. *et al.* Transfer of gold nanoparticles from the water column to the estuarine food web. *Nat. Nanotechnol.* **4**, 441–444 (2009).
2. Keller, A. A., McFerran, S., Lazareva, A. & Suh, S. Global life cycle releases of engineered nanomaterials. *J. Nanoparticle Res.* **15**, 1692 (2013).
3. Chithrani, B. D., Ghazani, A. A. & Chan, W. C. W. Determining the Size and Shape Dependence of Gold Nanoparticle Uptake into Mammalian Cells. *Nano Lett.* **6**, 662–668 (2006).
4. Gambardella, C. *et al.* Effect of silver nanoparticles on marine organisms belonging to different trophic levels. *Mar. Environ. Res.* **111**, 41–49 (2015).
5. Cedervall, T. *et al.* Understanding the nanoparticle–protein corona using methods to quantify exchange rates and affinities of proteins for nanoparticles. *Proc. Natl. Acad. Sci.* **104**, 2050–2055 (2007).
6. Baveye, P. & Laba, M. Aggregation and Toxicology of Titanium Dioxide Nanoparticles. *Environ. Health Perspect.* **116**, (2008).
7. Li, X., Lenhart, J. J. & Walker, H. W. Dissolution-Accompanied Aggregation Kinetics of Silver Nanoparticles. *Langmuir* **26**, 16690–16698 (2010).
8. Ghormade, V. *et al.* Fluorescent cadmium telluride quantum dots embedded chitosan nanoparticles: a stable, biocompatible preparation for bioimaging. *J. Biomater. Sci. Polym. Ed.* **26**, 42–56 (2015).
9. Caballero-Díaz, E. *et al.* The Toxicity of Silver Nanoparticles Depends on Their Uptake by Cells and Thus on Their Surface Chemistry. *Part. Part. Syst. Charact.* **30**, 1079–1085 (2013).
10. Abdolahpur Monikh, F. *et al.* Method for Extraction and Quantification of Metal-Based Nanoparticles in Biological Media: Number-Based Biodistribution and Bioconcentration. *Environ. Sci. Technol.* **53**, 946–953 (2019).
11. Mansor, M. *et al.* Application of Single-Particle ICP-MS to Determine the Mass Distribution and Number Concentrations of Environmental Nanoparticles and Colloids. *Environ. Sci. Technol. Lett.* **8**, 589–595 (2021).
12. Navratilova, J. *et al.* Detection of Engineered Copper Nanoparticles in Soil Using Single Particle ICP-MS. *Int. J. Environ. Res. Public Health* **12**, 15756–15768 (2015).
13. Li, L., Leopold, K. & Schuster, M. Effective and selective extraction of noble metal nanoparticles from environmental water through a noncovalent reversible reaction on an ionic exchange resin. *Chem. Commun.* **48**, 9165 (2012).
14. He, M., Chen, B., Wang, H. & Hu, B. Microfluidic chip-inductively coupled plasma mass spectrometry for trace elements and their species analysis in cells. *Appl. Spectrosc. Rev.* **54**, 250–263 (2019).

15. Vitale, R. J., Mussoline, G. R., Petura, J. C. & James, B. R. Hexavalent Chromium Extraction from Soils: Evaluation of an Alkaline Digestion Method. *J. Environ. Qual.* **23**, 1249–1256 (1994).

16. Loeschner, K., Brabrand, M. S. J., Sloth, J. J. & Larsen, E. H. Use of alkaline or enzymatic sample pretreatment prior to characterization of gold nanoparticles in animal tissue by single-particle ICPMS. *Anal. Bioanal. Chem.* **406**, 3845–3851 (2014).

17. Li, B., Chua, S. L., Yu, D., Chan, S. H. & Li, A. Detection, Identification and Size Distribution of Silver Nanoparticles (AgNPs) in Milk and Migration Study for Breast Milk Storage Bags. *Molecules* **27**, 2539 (2022).

18. Keller, A. A., Huang, Y. & Nelson, J. Detection of nanoparticles in edible plant tissues exposed to nano-copper using single-particle ICP-MS. *J. Nanoparticle Res.* **20**, 101 (2018).

19. Vladitsi, M., Nikolaou, C., Kalogiouri, N. P. & Samanidou, V. F. Analytical Methods for Nanomaterial Determination in Biological Matrices. *Methods Protoc.* **5**, 61 (2022).

20. El Hadri, H. & Hackley, V. A. Investigation of cloud point extraction for the analysis of metallic nanoparticles in a soil matrix. *Environ. Sci. Nano* **4**, 105–116 (2017).

21. WANG, L. *et al.* Determination of estrogens in water by HPLC–UV using cloud point extraction. *Talanta* **70**, 47–51 (2006).

22. Tani, H., Kamidate, T. & Watanabe, H. Micelle-mediated extraction. *J. Chromatogr. A* **780**, 229–241 (1997).

23. Arya, S. S., Kaimal, A. M., Chib, M., Sonawane, S. K. & Show, P. L. Novel, energy efficient and green cloud point extraction: technology and applications in food processing. *J. Food Sci. Technol.* **56**, 524–534 (2019).

24. Slistan-Grijalva, A. *et al.* Synthesis of silver nanoparticles in a polyvinylpyrrolidone (PVP) paste, and their optical properties in a film and in ethylene glycol. *Mater. Res. Bull.* **43**, 90–96 (2008).

25. Mudunkotuwa, I. A. & Grassian, V. H. Citric Acid Adsorption on TiO 2 Nanoparticles in Aqueous Suspensions at Acidic and Circumneutral pH: Surface Coverage, Surface Speciation, and Its Impact on Nanoparticle− Nanoparticle Interactions. *J. Am. Chem. Soc.* **132**, 14986–14994 (2010).

26. Canchanya-Huaman, Y. *et al.* Strain and Grain Size Determination of CeO2 and TiO2 Nanoparticles: Comparing Integral Breadth Methods versus Rietveld, μ-Raman, and TEM. *Nanomaterials* **11**, 2311 (2021).

27. Moore, T. L. *et al.* Nanoparticle colloidal stability in cell culture media and impact on cellular interactions. *Chem. Soc. Rev.* **44**, 6287–6305 (2015).

28. Vanderkooy, A., Chen, Y., Gonzaga, F. & Brook, M. A. Silica Shell/Gold Core Nanoparticles: Correlating Shell Thickness with the Plasmonic Red Shift upon Aggregation. *ACS Appl. Mater. Interfaces* **3**, 3942–3947 (2011).

29. Strohmeier, T. *et al.* Response of Mytilus edulis to enhanced phytoplankton availability by controlled upwelling in an oligotrophic fjord. *Mar. Ecol. Prog. Ser.* **518**, 139–152 (2015).

30. Costa-Fernández, J. M., Menéndez-Miranda, M., Bouzas-Ramos, D., Encinar, J. R. & Sanz-Medel, A. Mass spectrometry for the characterization and quantification of engineered inorganic nanoparticles. *TrAC Trends Anal. Chem.* **84**, 139–148 (2016).

31. Hasan Nia, M. *et al.* Stabilizing and dispersing methods of TiO 2 nanoparticles in biological studies. *J. Paramed. Sci. Spring* **6**, 2008–4978 (2015).

32. Rocha, T. L., Gomes, T., Sousa, V. S., Mestre, N. C. & Bebianno, M. J. Ecotoxicological impact of engineered nanomaterials in bivalve molluscs: An overview. *Mar. Environ. Res.* **111**, 74–88 (2015).

33. Ji, Y. *et al.* Facile Cloud Point Extraction for the Separation and Determination of Phenolic Acids from Dandelion. *ACS Omega* **6**, 13508–13515 (2021).

34. Szymczyk, K. & Taraba, A. Aggregation behavior of Triton X-114 and Tween 80 at various temperatures and concentrations studied by density and viscosity measurements. *J. Therm. Anal. Calorim.* **126**, 315–326 (2016).

35. Liu, J. *et al.* Cloud Point Extraction as an Advantageous Preconcentration Approach for Analysis of Trace Silver Nanoparticles in Environmental Waters. *Anal. Chem.* **81**, 6496–6502 (2009).

36. Dan, A., Ghosh, S. & Moulik, S. P. The Solution Behavior of Poly(vinylpyrrolidone): Its Clouding in Salt Solution, Solvation by Water and Isopropanol, and Interaction with Sodium Dodecyl Sulfate. *J. Phys. Chem. B* **112**, 3617–3624 (2008).

37. Adusei-Gyamfi, J., Ouddane, B., Rietveld, L., Cornard, J.-P. & Criquet, J. Natural organic matter-cations complexation and its impact on water treatment: A critical review. *Water Res.* **160**, 130–147 (2019).

Chapter 3

Bioaccumulation and biodistribution of polyvinylpyrrolidone-coated silver nanoparticles and citrate-coated titanium dioxide nanoparticles in marine organisms destined to human consumption

Biodistribution and bioaccumulation of metal nanoparticles (MNPs) in marine species refers to the process by which these particles can be taken up and distributed within aquatic organisms, such as fish, mollusks, and algae. Among others, Ag NPs and TiO_2 NPs are commonly used in a variety of consumer products, including food packaging, textiles, cosmetics, and paints and are also released into the environment through industrial and agricultural activities. As a result, they can enter aquatic ecosystems and accumulate in the biota, posing a potential final risk to human health. Besides clams, which are already widely consumed by humans, seaweeds have been identified as promising food resource due to their rich nutrient content and sustainability. However, studies assessing the potential bioaccumulation and subsequent transformation of MNPs after being uptaken by marine organisms, are very few, also due to challenges during the analysis. In this work, the biodistribution and transformation of polyvinylpyrrolidone-coated silver nanoparticles (PVP-Ag NPs) and citrate-coated titanium dioxide nanoparticles (TiO_2 NPs) into Asiatic clams (*Ruditapes philippinarum*) and two different seaweeds, *Palmaria palmata* and *Ulva fenestrata*, using a complementary set of analytical techniques, focused on electron microscopy coupled with energy-dispersive X-Ray analysis, were investigated. The bioaccumulation was analyzed by sp-ICP-MS at University of Santiago de Compostela showing that the concentration of MNPs per grams of biota was different in relation to clams exposure: □ 10^6 NPs/g for citrate-45nm TiO_2 NPs and □10^{10} NPs/g for PVP-100nm

Ag NPs. While similar concentrations of NPs were quantified in both seaweeds regardless the MNPs type. However, the biodistribution and transformation observed was highly dependent on the seaweed and MNPs type. These results indicate that special attention needs to be given to the distribution and transformation of MNPs in seaweed and clams for human consumption and not only to the bioaccumulation, since the first two parameters could heavily impact their behavior in humans, when ingested, and the risk mitigation strategies.

Chapter 3

3.1. Introduction

As the production of nanomaterials is in continuous expansion, there is a corresponding increase in their potential release into the environment, leading to a growing concern about fate and effects, including the consideration of potential interactions with living matters.[1] As a consequence of their extensive applications and broad commercialization,[2–4] silver nanoparticles (Ag NPs) and titanium dioxide nanoparticles (TiO_2 NPs) may have high potential impact on marine ecosystem, posing a health risk not only to aquatic organisms and plants but also humans.[5]

Li & Cummins have developed a semi-quantitative risk ranking for human health assessment of engineered nanomaterials highlighting that TiO_2 NPs are ranked as the highest potential health risk through consumer product exposure, while Ag NPs present the highest health concern by exposure via natural water sources.[6]

While seafood (i.e., clams) is currently accepted as an essential food for humans, providing basic nutritional needs and being considered a major source of protein for many coastal and island population,[7] seaweed, fully exploited in Eastern countries, are not yet part of the traditional diet in the Western countries, but represents one of the possible solutions to feed the growing human population.[8] In addition, seaweeds owe their importance at the commercial level in a wide range of sectors, from pharmaceutical to food industry, to their ability to produce several compounds like vitamins, bioactive agents, amino acids, proteins, and different classes of polysaccharides.[9]

Not surprisingly, due to the widespread of oceans pollution, the possibility that living organisms can interact with components dissolved or/and suspended in water bodies, such as nanocontaminants, is significantly high, especially considering the absorption

capacity of seaweed and the filtration ability of clams.[10] Therefore, they can be considered a good biomonitoring system, due to their ability to accumulate and rapidly respond to the presence of contaminants but, at the same time, being at the lowest level of the aquatic food chain, these interactions can also pose a risk for all the aquatic ecosystem and ultimately to humans.[11,12]

As a consequence, the increasing amount of shellfish and edible seaweed consumed to achieve adequate nutrients intake needs to be balanced considering the equally increase of contaminants ingestion, which can become sufficiently high to be of toxicological concern.

Several studies investigated the toxicity of dissolved metals in marine seaweeds but very few literatures addressed the potential risk of these metals in their nano-sized form.[13,14] Among them, Turner et al., investigated the toxicity of Ag NPs in marine macroalgae Ulva lactuca by monitoring the photosystem II.[15] Miao et al., addressed the Ag NPs toxicity into marine diatoms by studying cell growth and photosynthetic activity,[16] while studies about the use of sp-ICP-MS to assess the presence of metal NPS (MNPs), such as TiO_2 and Au NPs in clams, have been already published.[17,18] Unfortunately, most of the works do not address the potential uptake and localization of NPs to better understanding their correlation and impact of the toxicity responses observed. Only Siddiqui et al., performed NPs localization within seaweed tissues, showing that the assessment of the presence of NPs by using SEM-EDX was only achieved for CuO NPs but not for Ag NPs, when the same strategy was used,[19] while for in-vitro clams studies, scanning transmission electron microscopy in scanning electron microscopy (STEM-in-SEM) was employed to assess Au NPs localization within tissues.[20]

The identification and localization of MNPs within the tissue is extremely challenging and particles related, depending on their size and to the possible transformations they can undergo once interacting with the organisms. For example, Ag NPs oxidation processes (i.e., dissolution) can easily lead to the release of ionic silver, particles size reduction and complexation processes with chloride or sulfide that completely modify NP physico-chemical properties inducing acute toxicity and kinetics mechanisms that could interfere with NPs bioavailability.[21]

Electron microscopy (EM) and more specific transmission EM (TEM) can therefore be an excellent tool to address this challenge since it offers resolution of few nanometers in conventional TEM and even atomic resolution by using aberration-corrected high resolution TEM (HRTEM).[22] Moreover, TEM allows the visualization and localization of electron-dense NPs into tissues without any specific labelling or priori information about their composition. TEM can also provide an estimation about the number of particles

inside a specific tissue compartment (e.g., cell wall, cell membrane, among others). High-angle annular dark-field scanning transmission EM (HAADF STEM) coupled with energy dispersive x-ray spectroscopy (EDX) can extract more information not only in terms of ultrastructures of the tissue, without performing any extra post-staining on the grid and by acquiring high contrast images, but also in terms of NP compositions, which may open the opportunity to study NP transformations inside the tissue. The integration of EDX analysis also allows the discrimination between electron-dense NPs that could be found in real samples, by elemental chemical composition. Despite all these advantages, very few works have explored the potential biodistribution and transformation of Ag NPs and TiO_2 NPs in seaweed, as well as clams, by coupling EM with EDX analysis.

Within this thesis work, the biodistribution and transformation of commercially available polyvinylpyrrolidone-coated silver nanoparticles (PVP-Ag NPs) and citrate-coated titanium dioxide nanoparticles (TiO_2 NPs) into the Asiatic clam, *Ruditapes philippinarum*, and two distinct species of marine seaweed, *Ulva fenestrata* (Sea lettuce) and *Palmaria palmata* (Dulse), was investigated by using conventional TEM, high-resolution TEM (HRTEM) and HR scanning TEM (HRSTEM) coupled with EDX.

3.2. Results and Discussion

3.2.1. Clams exposure to silver and titanium dioxide NPs

PVP-100nm Ag NPs and citrate-45nm TiO_2 NPs were the selected MNPs used for the bioaccumulation studies in Asiatic clams (*Ruditapes philippinarum*). Their full characterization, in terms of size and colloidal stability can be found in Chapter 2, section 2.2.1.

Briefly, TEM images showed that both NPs have a spherical shape with an average primary diameter of 96 ± 25 nm for PVP-100nm Ag NPs and 44 ± 22nm for citrate-45nm TiO_2 NPs (Figure 2, Chapter 2). Citrate-45nm TiO_2 NPs formed small aggregates, while PVP-100nm Ag NPs were well-dispersed on the grid surface. This observation was supported by DLS analysis where the hydrodynamic size recorded was 174 ± 56 nm for citrate-45nm TiO_2 NPs and 139 ± 2 nm for PVP-100nm Ag NPs in ultrapure water. This difference in colloidal stability was more pronounced in artificial seawater, where PVP-100nm Ag NPs remained colloidally stable (hydrodynamic size of 97 ± 1 nm) during at least 28 days, while citrate-45nm TiO_2 NPs aggregated immediately after seawater dispersion (5708 ±

1012 nm). This different behavior could have an impact on their bioaccumulation in clams.

Figure 1 schematically describes the experimental design of MNPs exposure to clams carried out at the facilities of Centro Tecnológico del Cluster de la Acuicultura (CETGA, Spain). Details about bioaccumulation assays instead, are explained in Annex I, section 3.3. Briefly, clams were exposed to 0, 0.1 and 1 mg/L of MNPs, PVP-100nm Ag NPs or citrate-45nm TiO_2 NPs, through food exposure while the sampling was performed every 7 days. In this work, only the outcomes related to control conditions and highest MNPs concentration are shown.

Bioaccumulation results were analyzed by single-particle inductively coupled plasma mass spectroscopy (sp-ICP-MS), while biodistribution and NP transformation by EM techniques (i.e., TEM, STEM-EDX) after 0, 7, 14, 21 and 28 days of exposure.

sp-ICP-MS analysis was performed at University of Santiago de Compostela and used here as support for the EM analysis. For this reason,

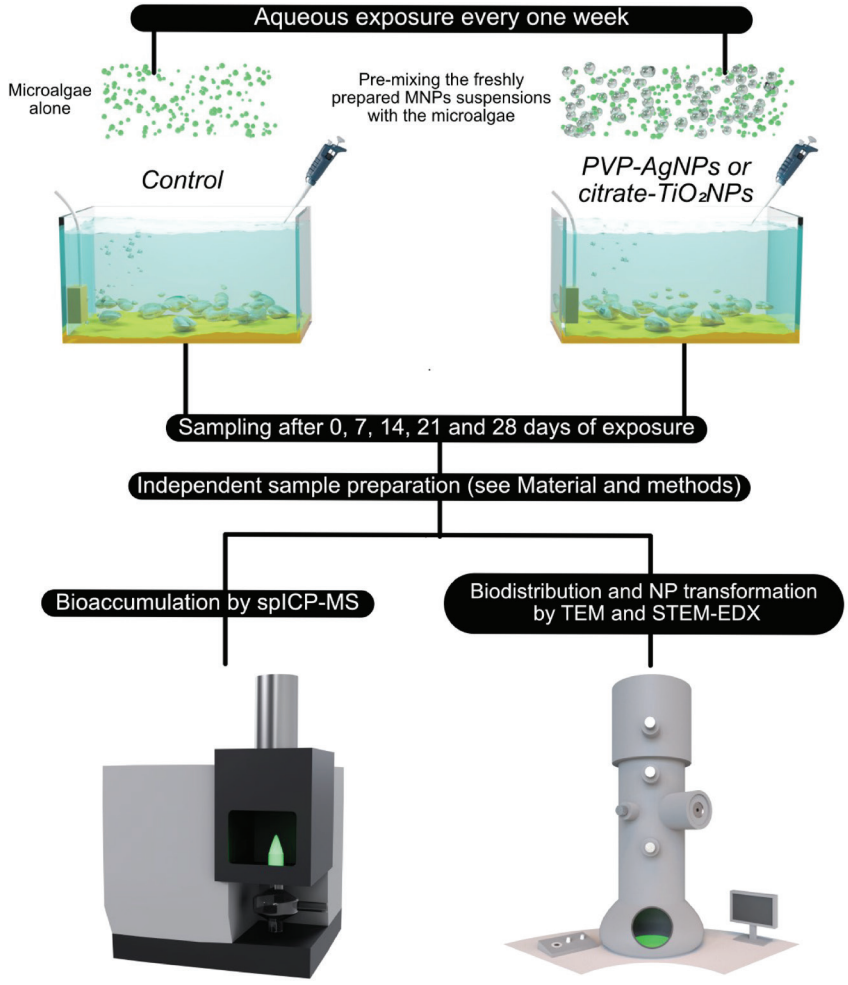

Figure 1. Schematic illustration of clams experimental set-up, exposed to 0 and 1 mg/L of MNPs.

details about data acquisition and experimental setup are not presented here.

sp-ICP-MS analysis showed that the bioaccumulation of citrate-45nm TiO_2 NPs was 3 – 4 orders of magnitude lower than the bioaccumulation of PVP-100nm Ag NPs (28 days exposure, 1 mg/L initial concentration: 8.00×10^6 NPs/g for TiO_2 NPs versus 2.50×10^{10} NPs/g for Ag NPs). As shown in Chapter 2 with ATO NPs exposure to mussels, scarce bioaccumulations did not allow the localization of any NP in the tissue by TEM. For this reason, no further investigation was performed for citrate-45nm TiO_2 NPs-exposure in clams.

As concerned clams exposure to PVP-100nm Ag NPs, in order to exploit any possible morphological change in the tissue, TEM analysis was performed after 1) exposure to 1 mg/L PVP-Ag NPs and 2) 0 mg/L as control condition where no NPs were added. 0.1 mg/L was not subjected to TEM analysis due to the low probability to encounter NPs at this concentration.

As explained in the materials and methods section, when clams were sampled, gill, digestive gland and mantle were isolated and subjected to individual analysis. Figure 2 shows low magnification TEM images of the three different organs (i.e., gill, digestive gland and mantle) after 28 days of exposure at 0 and 1 mg/L acquired to obtain a general overview of the tissue, understand its morphology and identify possible ultrastructural changes due to the presence of the particles.

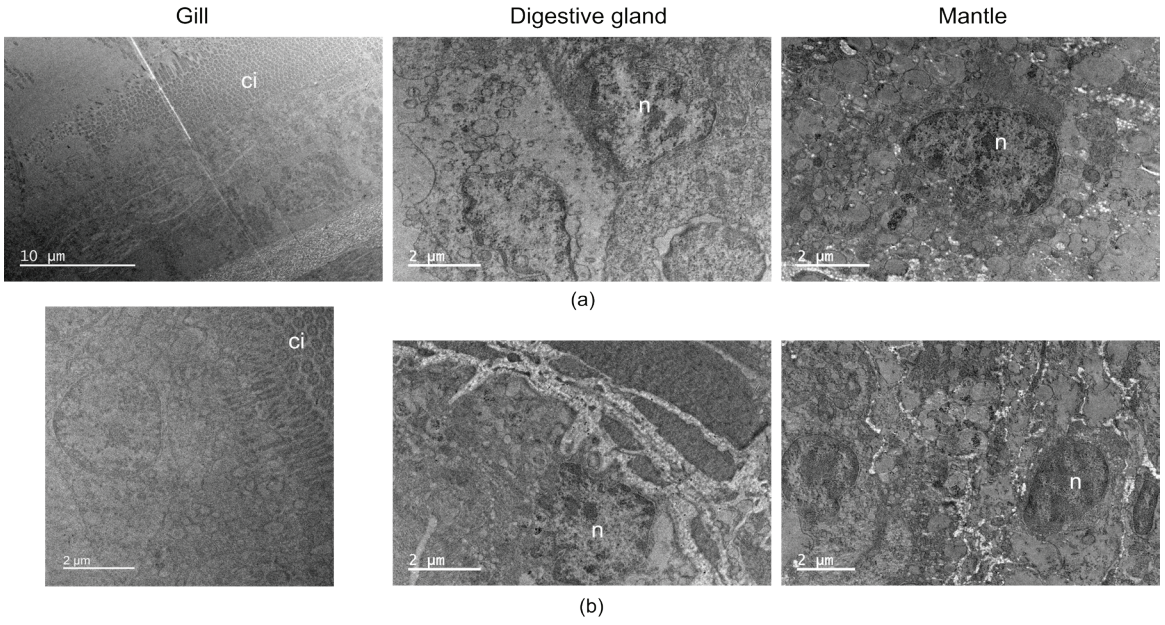

Figure 2. TEM images of clams exposed to PVP-100nm Ag NPs at (a) 0 mg/L as control condition and (b) 1 mg/L after 28 days of exposure. Gill, digestive gland and mantle are shown for each condition. Organelles are identified as: n-nucleus, ci-cilia, mi-mitochondria, rer-rough endoplasmic reticulum.

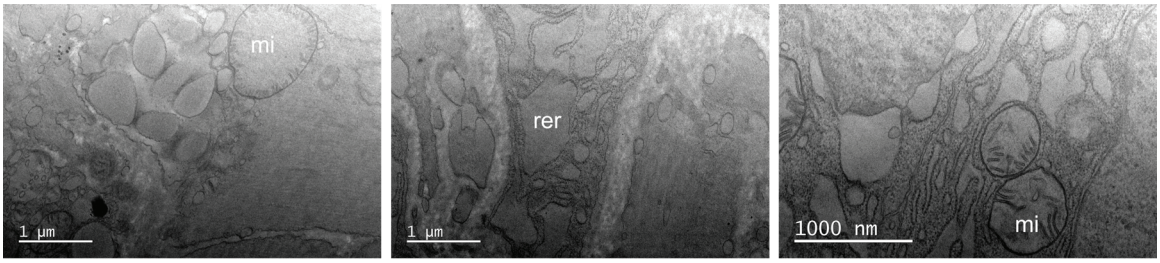

Figure 3. TEM images of clams exposed to PVP-100nm Ag NPs at 1 mg/L. (a) Gill and (b, c) digestive gland are shown. Swollen mitochondria and rough endoplasmic reticulum were observed. Organelles are identified as: mi-mitochondria, rer-rough endoplasmic reticulum.

While analyzing different time points, some differences in the structural organization of the cells could be noticed (Figure 3). An enlargement of the mitochondria as well as of the rough endoplasmic reticulum could be observed when gill and digestive gland were analyzed after NPs exposure. However, it is very difficult to attribute these changes in the ultrastructures to the mere presence of the particles. TEM sample preparation is a very tedious process and the possibility that it could interfere with the integrity of the tissue cannot be excluded. Therefore, complementary techniques (i.e., proteomics) to assess the correct functioning of cell activity after NPs exposure should be performed.

The presence of Ag NPs in gills and digestive gland was confirmed by TEM-EDX and STEM-EDX respectively. No NPs were localized in mantle. Figure 4 shows TEM images and EDX spectrum for gills exposed to 1 mg/L PVP-100nm Ag NPs after 28 days of exposure. The EDX analysis demonstrated that the electron-dense NP localized in the gills was silver. Clearly, the Ag NPs identified presented smaller size than the initial size of Ag NPs and smaller particles were visualized around of the bigger NPs, which could be indicative of the dissolution of Ag NPs.

High number of NPs were localized in digestive gland after 21 and 28 days of exposure by STEM-EDX and TEM respectively (Figure 4 and 5). This time, an EDX map was acquired for over 20 min. When in presence of small objects embedded in biological tissue, longer acquisition times are required to obtain enough signal that stands out from the background. Even so, the possibility that the tissue is resistant enough to endure the whole duration of the analysis, without leading to opening or damages, cannot be guaranteed, causing sometimes the interruption of the analysis itself (Figure 5, b). Sizes smaller than 30 nm were observed, confirming the dissolution of the Ag NPs (Figure 6).

The difference of accumulation between gills and digestive gland was previously reported. The authors showed that the coating had an impact on the

accumulation of different organs, showing that PVP-coated Ag NPs presented higher accumulation in digestive gland than in gills of *Elliptio complanata* mussels.[23] The bioaccumulation of Ag NPs in the *Ruditapes philippinarum* clam has also been studied previously by Aouini *et al.*,[24] reporting higher accumulation in digestive gland than in gills; however, the biodistribution of Ag NPs was not addressed.

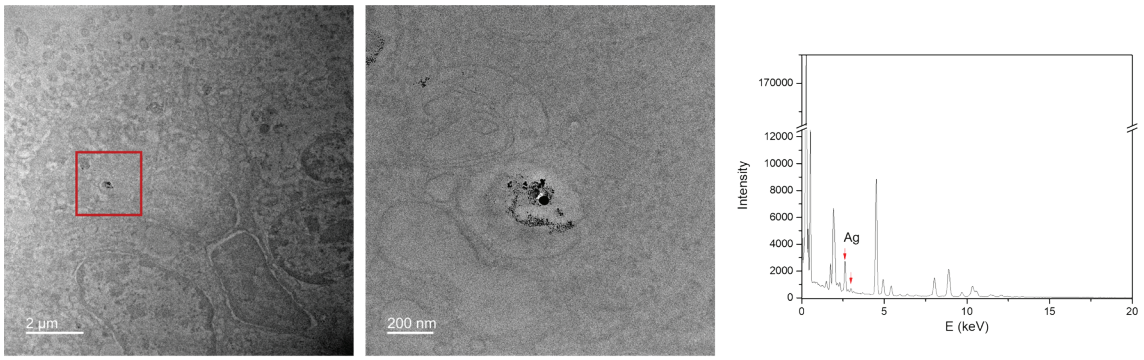

Figure 4. TEM images of (a) gill after 21 days of exposure to PVP-100nm Ag NPs at 1 mg/L and (b) related EDX spectra obtained by TEM-EDX analysis.

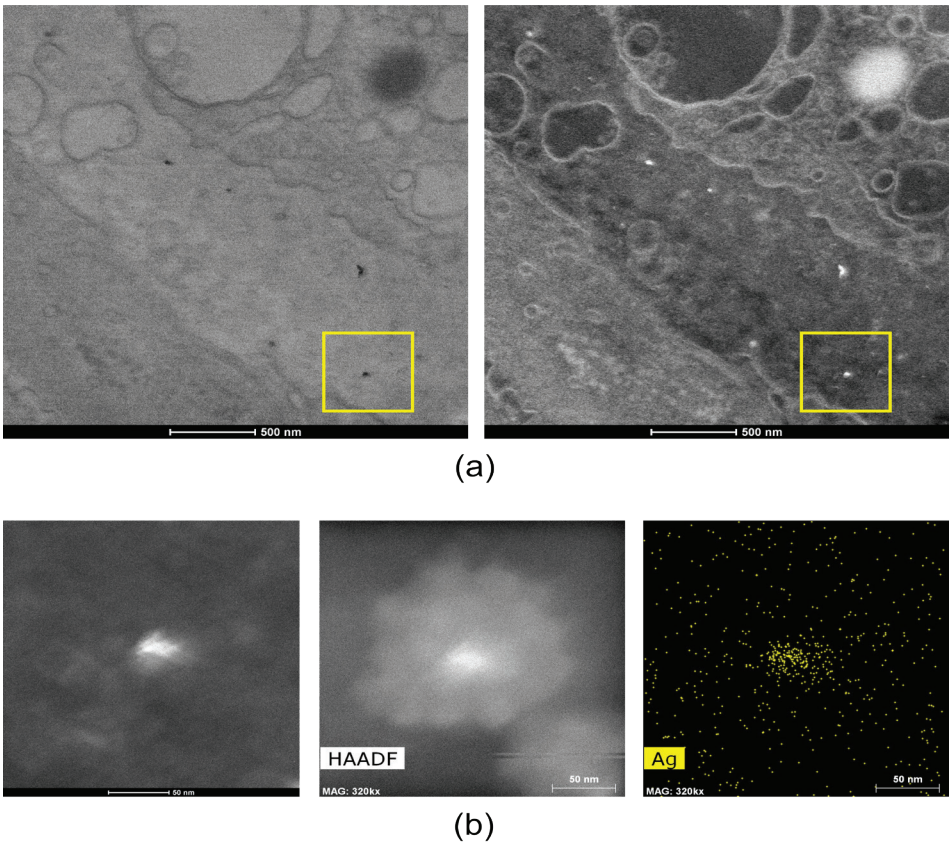

Figure 5. Bright and dark field STEM images of (a) digestive gland after 21 days of exposure to PVP-100nm Ag NPs at 1 mg/L and (b) related EDX mapping obtained by STEM-EDX analysis. HAADF image showing damages of the tissue after 20' mapping acquisition.

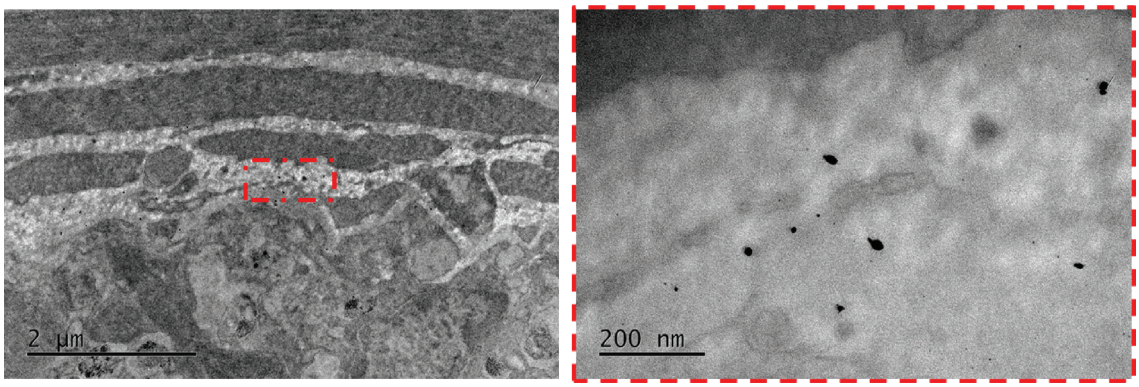

Figure 6. TEM images of digestive gland after 28 days of exposure to PVP-100nm Ag NPs at 1 mg/L.

3.2.2. Seaweed bioaccumulation of silver and titanium dioxide NPs

PVP-15nm Ag NPs and two citrate-coated TiO_2 NPs (citrate-5nm and citrate-25nm TiO_2 NPs) were the selected MNPs for the bioaccumulation study in two species of seaweed, *Ulva fenestrata* (Sea lettuce) and *Palmaria palmata* (Dulse). Their full characterization, in terms of size and colloidal stability can be found in Chapter 2, section 2.2.1. Briefly, TEM images showed that the three MNPs have a spherical shape with an average primary diameter of 24.12 ± 8.01 nm for PVP-15nm Ag NPs and 29 ± 10 nm for citrate-25nm TiO_2 NPs (Figure 2, Chapter 2). The primary crystalline size of citrate-5nm TiO_2 NPs was estimated by XRD as 8.5 nm. Both TiO_2 NPs formed small aggregates, while the PVP-15nm Ag NPs were well-dispersed on the grid surface. This observation was in agreement with DLS analysis, where the hydrodynamic size recorded was 53 ± 2 nm for citrate-5nm and 166 ± 3 nm for citrate-25 nm TiO_2 NPs in ultrapure water, while PVP-15nm Ag NPs presented a size of 49 ± 3 nm (Table 1, Chapter 2).

This difference in colloidal stability was more pronounced in artificial seawater, whereas PVP-15nm Ag NPs remained stable (hydrodynamic size of 47 ± 2 nm) during at least 28 days, while both TiO_2 NPs aggregated immediately after dispersion in seawater (hydrodynamic sizes: 2478 ± 166 nm for 5 nm and 7589 ± 2291 nm for 25 nm). This different behavior could have an impact on their bioaccumulation in seaweeds.

Figure 7 schematically describes the experimental design of MNPs exposure to seaweeds carried out at the facilities of Indigo Rock Marine Research Station (Cork, Ireland). Details about bioaccumulation assays instead, are explained in Annex I, section 3.2. Briefly, both *P. palmata* and *U. fenestrata* were exposed to 0, 3 mg/L of PVP or 1.5 mg/L of sodium citrate to study the possible effect of the NP coating, and to 0.1 and 1 mg/L of MNPs (i.e., PVP-15nm Ag NPs, citrate-5nm TiO_2 NPs and citrate-25nm TiO_2 NPs), through water

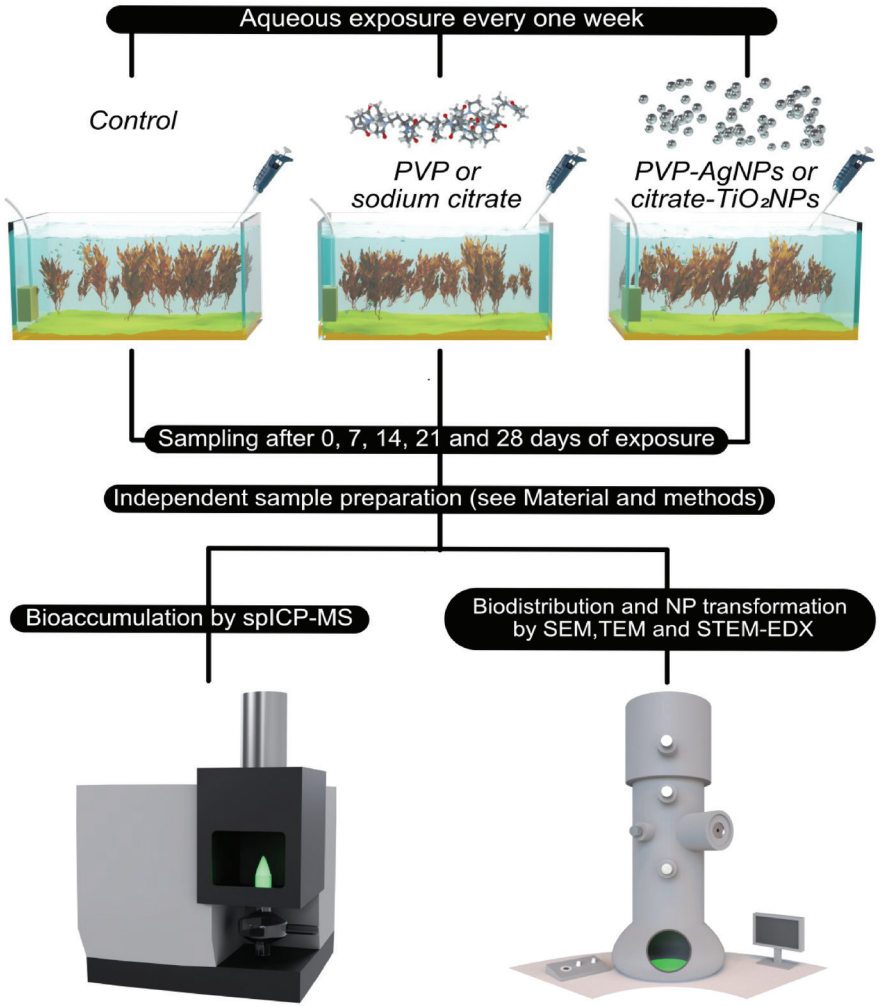

Figure 7. Schematic illustration of seaweed experimental set-up, exposed to 0, coating control and 1 mg/L of MNPs.

exposure every 7 days for a total experimental duration of 28 days. In this work, only the outcomes related to control conditions, coating control and highest concentration of MNPs are shown. Bioaccumulation results were analyzed by sp-ICP-MS, while biodistribution and NP transformation by EM techniques (i.e., SEM, TEM and STEM-EDX), after 0, 7, 14, 21 and 28 days of exposure. sp-ICP-MS analysis was performed at University of Santiago de Compostela and used here only as support for the EM analysis. For this reason, details about data acquisition and experimental setup are not presented here.

sp-ICP-MS analysis showed that the bioaccumulation of the three MNPs in both seaweeds was similar in terms of MNPs amount per gram of algae, in the range of 1.15×10^9 NPs/g - 7.79×10^9 NPs/g. This range, either internalized or externally associated, was constant since early stages (i.e., 7 days) to 28 days of exposure.

To better understand the biodistribution, i.e., NP associations with tissue, internalization or/and surface adsorption, and the possible transformations of MNPs when interacting with the seaweed (i.e., aggregation, dissolution or chemical transformation), several tissue sections of both seaweeds were analyzed at different time of exposure using SEM-EDX, TEM and STEM-EDX.

At first, SEM-EDX analysis was performed, since it is well-known that seaweeds have high adsorption capacity[23] and, as a consequence, it is expected for MNPs to have a strong interaction with the algae surface. No PVP-15nm Ag NPs were localized on the surface of any of the two seaweeds, being this likely attributed to the fact that they remained colloidally stable in artificial seawater during the time of the bioaccumulation assay (more detail in Chapter 2). Therefore, the small primary size of these NPs could make difficult their localization on the surface by SEM.

In contrast, citrate-25nm TiO_2 NPs and citrate-5nm TiO_2 NPs were identified on the surface of both, *P. palmata* and *U. fenestrata*. Figure 8, 9 and 10 show SEM images acquired and the related EDX spectra at 14, 21 and 28 days of exposure, respectively. Aggregates with a size bigger than 1 μm were found in both algae and identified as titanium dioxide by EDX in the sample exposed to citrate-25nm TiO_2 NPs and citrate-5nm TiO_2 NPs. No citrate-5nm TiO_2 NPs were localized on the *P. palmata* after 28 days of exposure; however, they were detected after 14 and 21 days. After studying the surface adsorption of the selected MNPs in both seaweeds, the potential internalization was investigated by TEM and STEM-EDX.

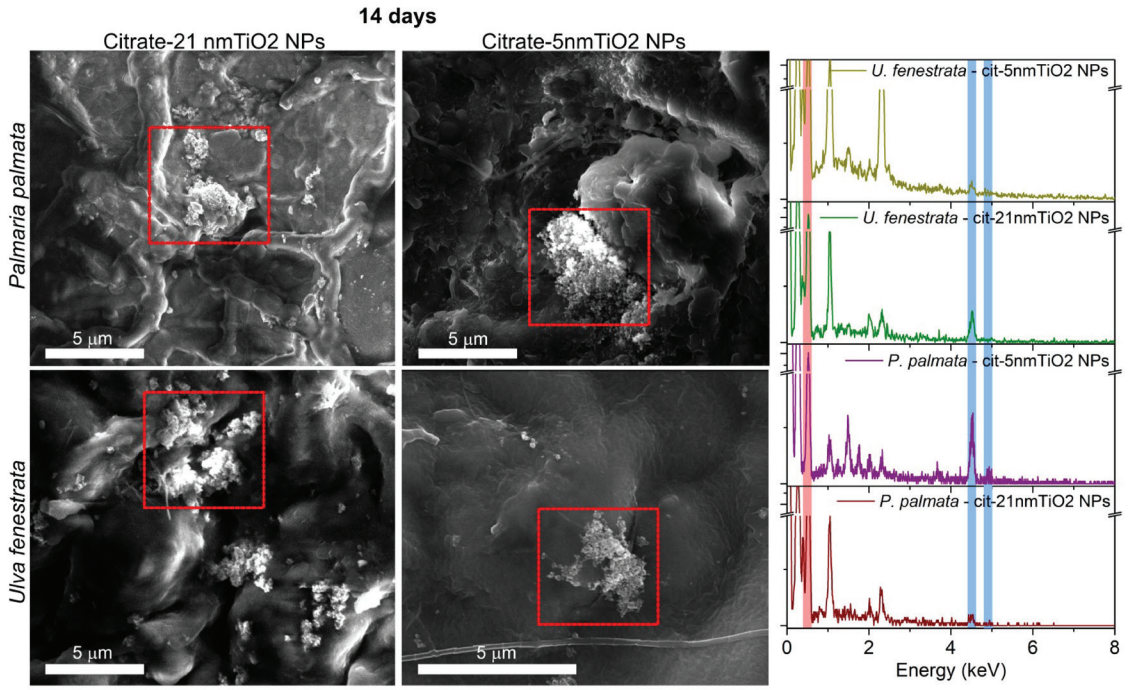

Figure 8. SEM analysis of *P. palmata* and *U. fenestrata* after 14 days of exposure to citrate-25nm TiO_2 NPs and citrate-5nm TiO_2 NPs. EDX spectra confirming Ag presence are shown.

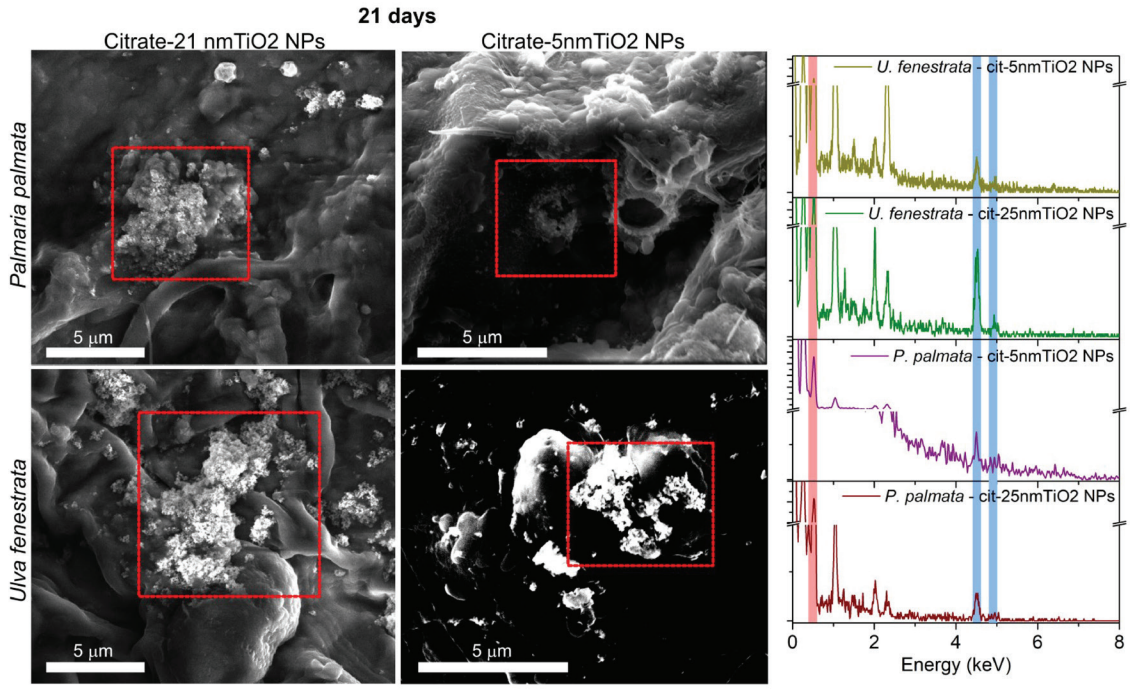

Figure 9. SEM analysis of *P. palmata* and *U. fenestrata* after 21 days of exposure to citrate-25nm TiO_2 NPs and citrate-5nm TiO_2 NPs. EDX spectra confirming Ag presence are shown.

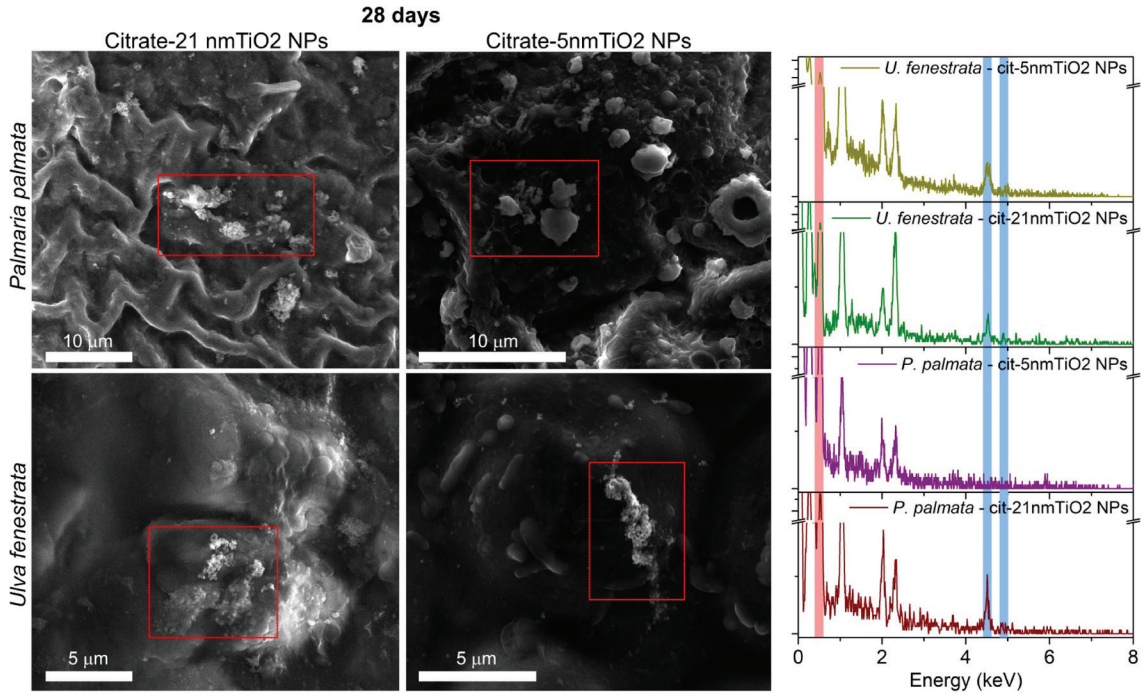

Figure 10. SEM analysis of *P. palmata* and *U. fenestrata* after 28 days of exposure to citrate-25nm TiO_2 NPs and citrate-5nm TiO_2 NPs. EDX spectra confirming Ag presence are shown.

In order to investigate any possible morphological change in seaweed tissues, low magnification TEM images were acquired and analyzed for 1) PVP-AgNPs-exposed seaweeds, 2) seaweeds exposed to 3 mg/L PVP to study the possible effect of the NP coating and 3) non-exposed seaweeds that acted as control, after 0 and 28 days of exposure. Figures 11 and 12 show the TEM images for *P. palmata* and *U. fenestrata*, respectively. Clearly, both seaweeds have a very different ultrastructures and tissue organization. *P. palmata* presents an organized structure, consisting of larger cells in the central axis surrounded by regular repetitions of smaller cortical cells. While *U. fenestrata* organization consists in two lines of elongated cells across the whole length of the tissue. No evident differences in the structural organization of the cells were observed between treatment groups and exposure time analyzed. Same remarks were made for seaweeds exposed to both citrate-coated TiO_2 NPs (data not shown).

After confirming that both seaweeds did not undergo evident adverse effects when exposed to MNPs, internalization analysis by EM were performed. Starting with TiO_2 NPs, TEM analysis showed that no TiO_2 NPs were observed/localized into *P. palmata* tissue after 28 days of exposure and, therefore, the internalization could not be confirmed by EM (Figure 13). In contrast, the internalization of both TiO_2 NPs in *U. fenestrata* could be visualized by TEM/STEM and the identity of NPs confirmed as titanium dioxide by EDX analysis (Figures 14, 16 and 17). Specifically, Figure 14 shows STEM images of *U.*

fenestrata after 28 days of exposure to citrate-5nm TiO_2 NPs. In this case, these NPs could not be detected using conventional TEM probably due to the lower electron-dense of their primary size (around 8 nm). Citrate-5nm TiO_2 NPs were localized outside the cell wall, unable to penetrate even at higher time of exposures. This could be most likely attributed to the high aggregation level of these TiO_2 NPs, as demonstrated by DLS analysis in seawater (Chapter 2) and SEM analysis, which do not favor the passive particles penetration. What is interesting to notice is how the presence of the two detectors, bright and dark field, in STEM mode, allow to obtain different sample information. It is in fact from the different contrast in dark field image that it is possible to distinguish the denser core of the aggregates from the less dense ones.

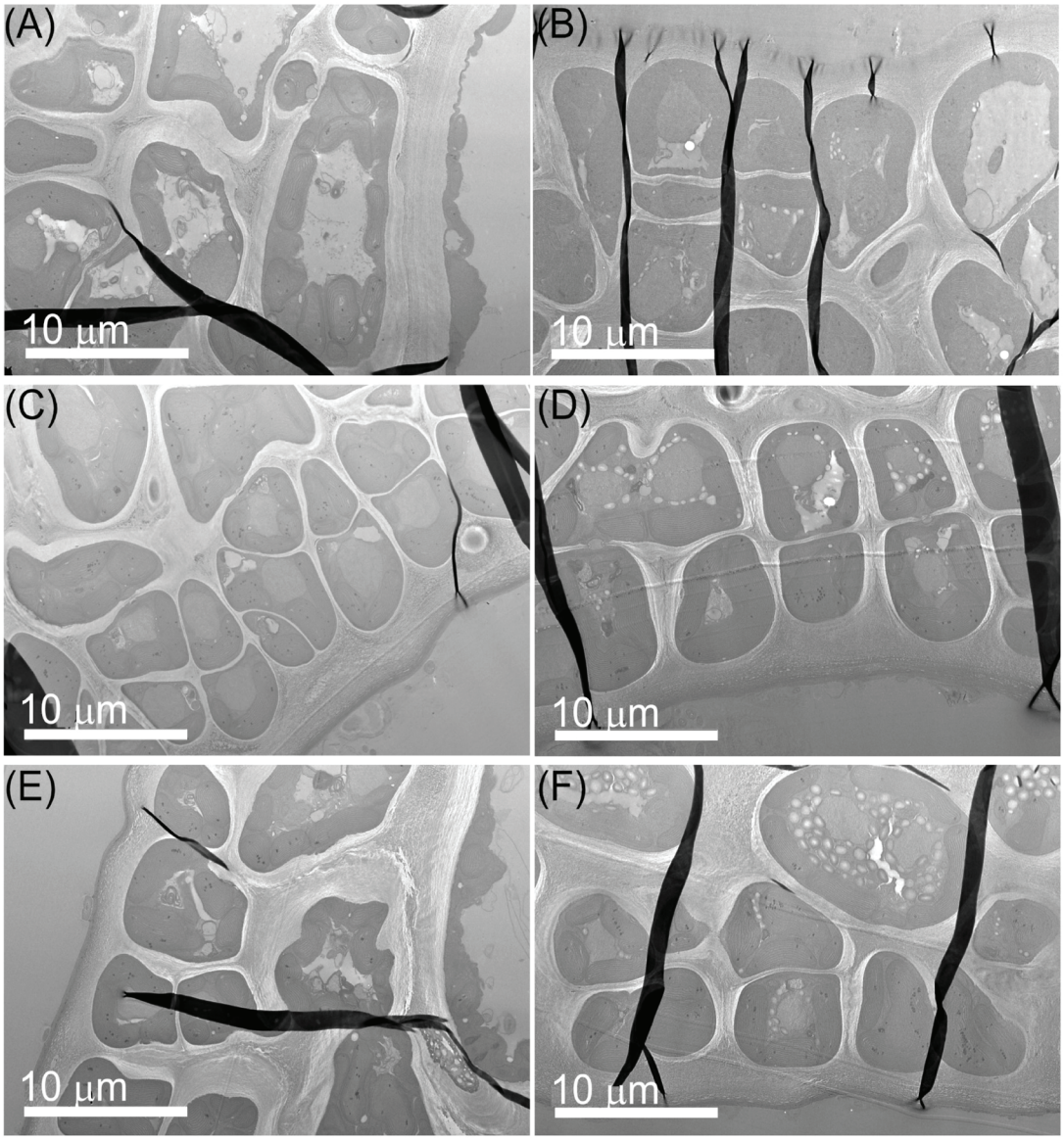

Figure 11. Representative TEM images of *P. palmata* at 0 (A, C and E) and 28 days (B, D and F) of exposure to (A and B) control, (C and D) 3 mg/L PVP and (E, F) 1 mg/L PVP-15nm Ag NPs.

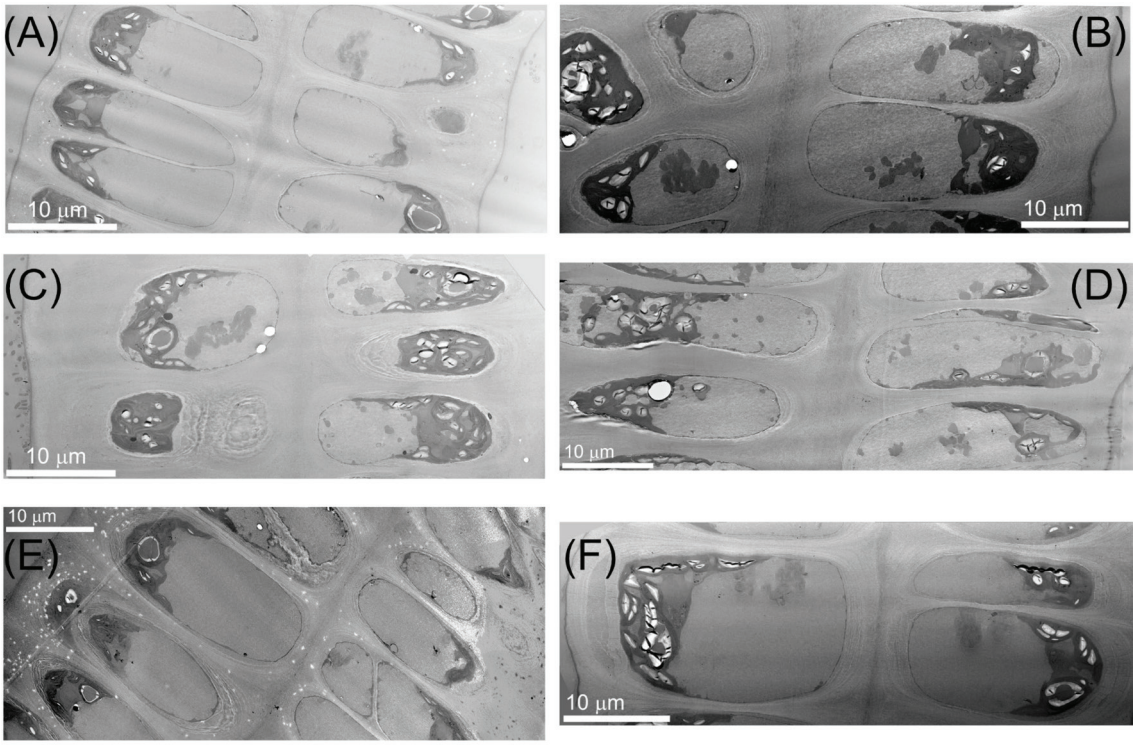

Figure 12. Representative TEM images of *U. fenestrata* at 0 (A, C and E) and 28 days (B, D and F) of exposure to (A and B) control, (C and D) 3 mg/L PVP and (E and F) 1 mg/L PVP-15nm Ag NPs.

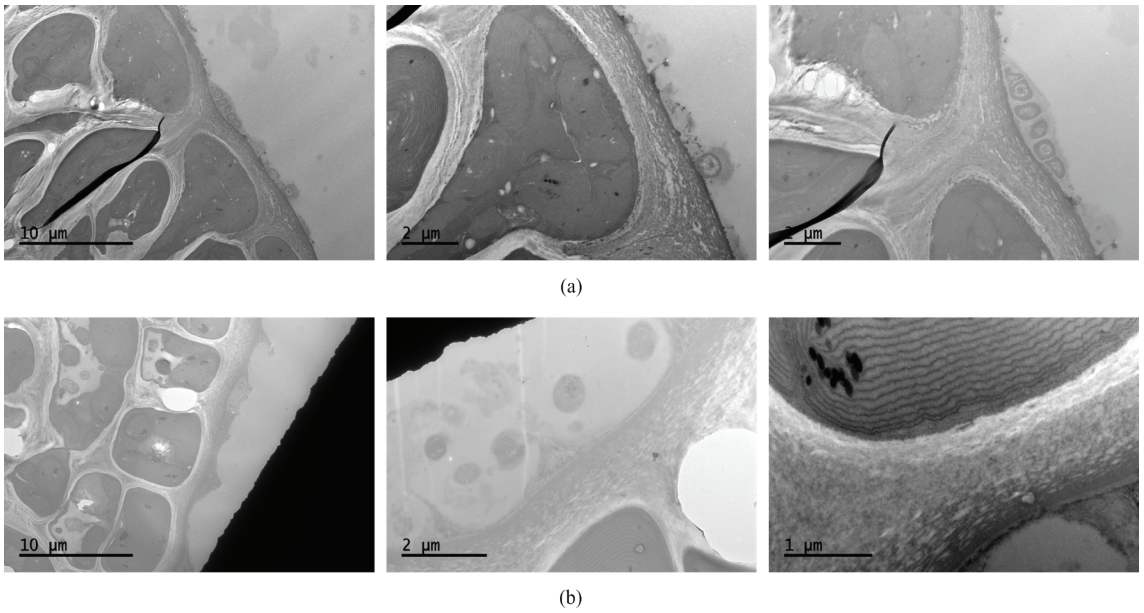

Figure 13. EM analysis showing *P. palmata* after exposure to 28 days of (a) citrate-5nm TiO_2 NPs and (b) citrate-25nm TiO_2 NPs. No particles were localized in any case.

The EDX mapping was acquired for 10 min to have enough counts for a more precise identification of TiO_2 NPs (Figure 14 c). Same tendency, i.e., no internalization, was observed when the analysis was carried out for other exposure times (i.e., 7, 14 and 21 days). Therefore, STEM-EDX images related to those time points are not shown here.

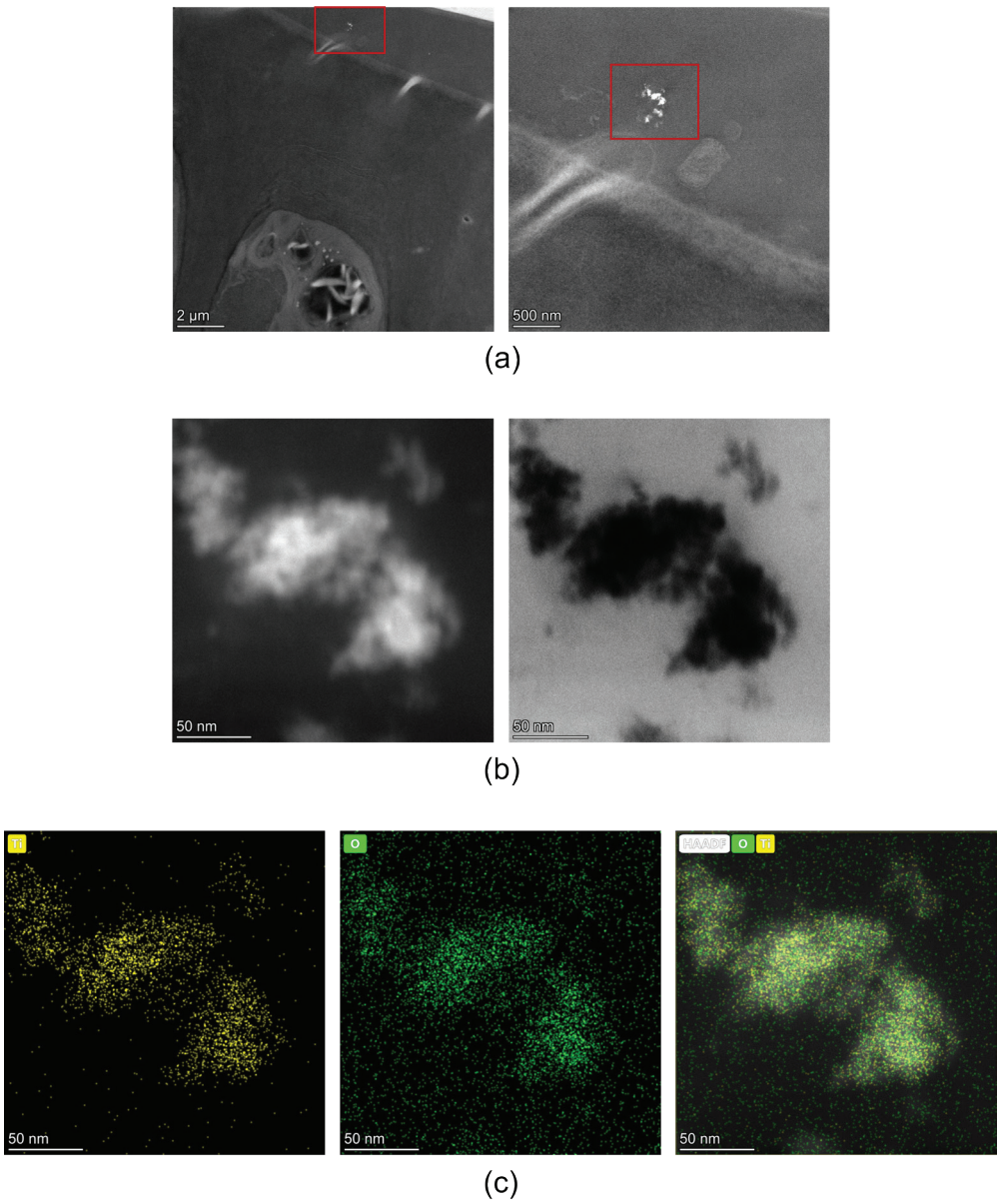

Figure 14. STEM-EDX analysis of *U. fenestrata* after 28 days of exposure to citrate-5nm TiO_2 NPs. (a) low mag images; (b) bright and dark field images and (c) EDX mapping using an acquisition time of 10'confirming the presence of TiO_2 are shown.

Interestingly, several electron-dense particles with different shape and size were found and identified as Al_2O_3 and TiO_2 in the same sample, i.e., U. fenestrata exposed to citrate-5nm TiO_2 NPs (Figure 15). However, TiO_2 NPs localized inside of the cell presented a completely different shape and size in comparison with the citrate-5nm TiO_2 NPs used in the study. These other NPs identified, most probably came from the water used in the assay, and they were able to be internalized maybe due to the smaller size. It has been reported that NPs with a size smaller or equal to 50 nm can pass through the cell walls in most of the plants, which help to explain the lack of internalization of theTiO_2 aggregates.[25]

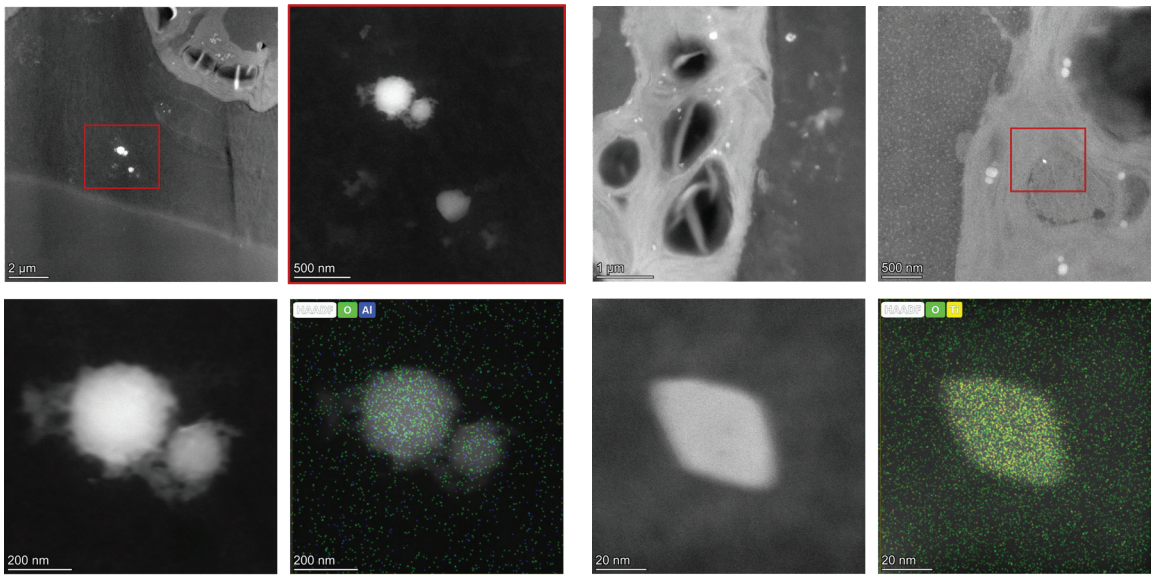

Figure 15. STEM-EDX images of different elements found in *U. fenestrata* tissue during the analysis. The mapping shows the presence of Al_2O_3 and TiO_2 NPs.

The biodistribution of citrate-25nm TiO_2 NPs in *U. fenestrata* presented the same tendency. However, size and shape of the aggregates made very easy their visualization by TEM. Figure 16 shows low magnification TEM images, where, also in this case, the particles were localized and identified as TiO_2 NPs outside the cell wall, unable to penetrate after 28 days of exposure. Also here, bright and dark field STEM images were compared (Figure 16, b), showing how, this time, was the bright field to reveal more information about particles aggregation, where particles overlapping in the aggregates could be easily identified if compared to the dark field. For this reason, only bright field images were considered in the EDX analysis (Figure 17).

Interestingly, the size of the aggregates localized by TEM with both TiO_2 NPs was smaller than the aggregates localized on the surface by SEM. The aggregates of citrate-25nm TiO_2 NPs presented high polydispersity (i.e., high variability in size distribution), while less aggregates of 5nm TiO_2NPs were localized, and the size was smaller than in the case of 25 nm NPs.

This support the hypothesis that aggregates bigger than 1 µm were firstly adsorbed on the seaweed surface via interaction with the glycoproteins and polysaccharides present in the cell wall, as previously reported.[26] In this previous report, the adsorption capacity of TiO_2NPs by algae was in the range of 59 to 5701 µg/dried g at 72 h. The initial concentration and the colloidal stability of the NPs had an effect in the adsorption kinetic. In this case, the NPs dispersed in seawater formed bigger aggregates than in ultrapure water as demonstrated

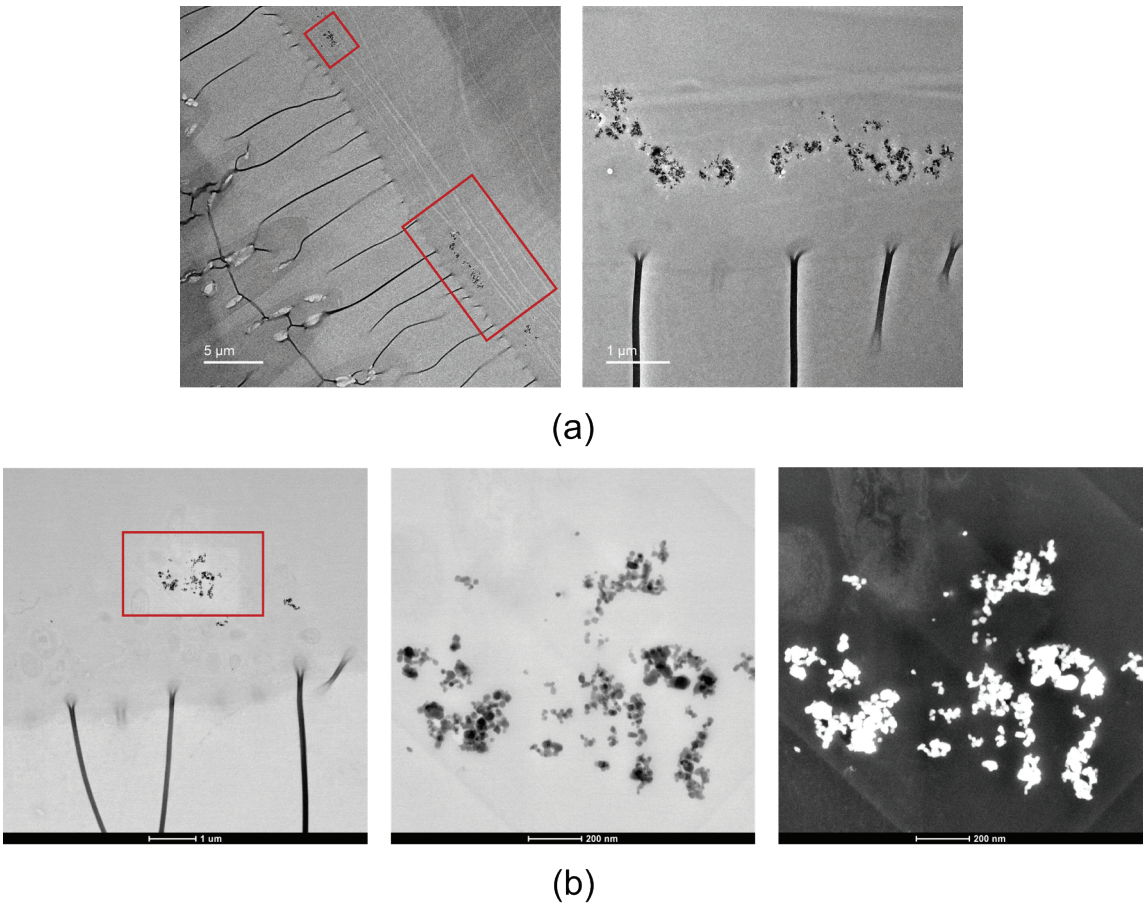

Figure 16. (a) TEM and (b) STEM images showing *U. fenestrata* after exposure to 28 days of citrate-25nm TiO_2 NPs.

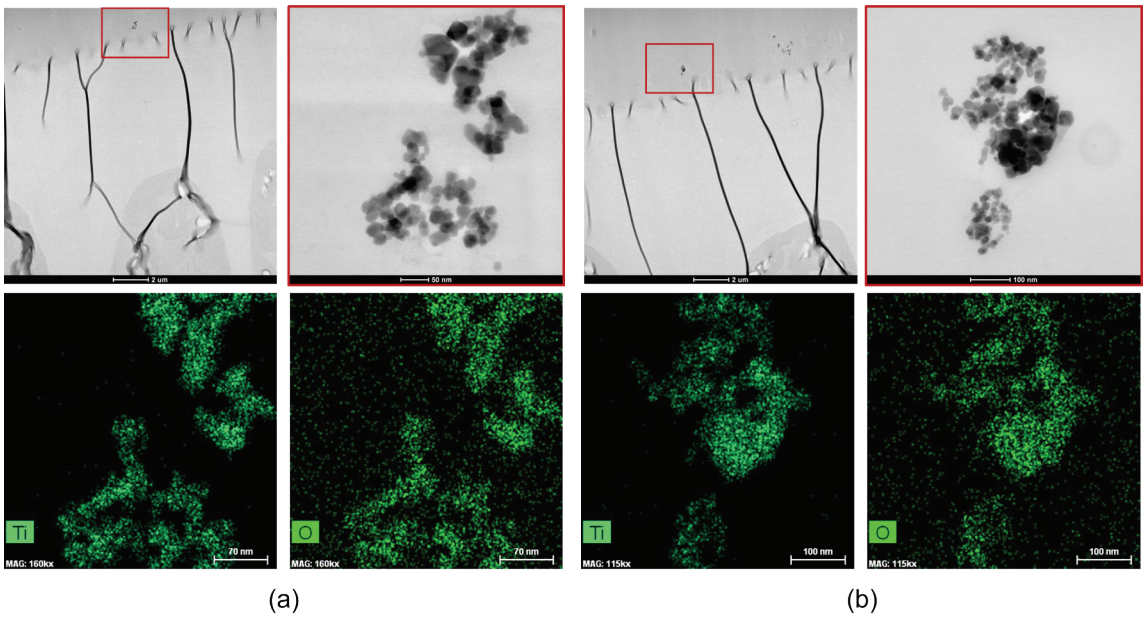

Figure 17. STEM-EDX analysis showing *U. fenestrata* after exposure to 28 days of citrate-25nm TiO_2 NPs and related EDX spectra confirming the presence of the particles.

by DLS analysis. Therefore, it is expected that the aggregates would adsorb on the surface instead of being internalized, due to their size. Then, these aggregates would "break" during the association process forming smaller aggregates embedded in the cell wall. In addition, the fact that only in *U. fenestrata*, many other inorganic particles were localized and identified, supports the idea that *U. fenestrata* cell wall composition is less selective towards particles interaction and internalization when compared to *P. palmata*.

After analyzing the biodistribution of TiO_2 NPs, it is expected to observe higher internalization in the case of PVP-15nm Ag NPs, since they were colloidally stable in seawater and their primary size was smaller than 50 nm. To better understand the biodistribution and the possible particle transformations that can involve PVP-Ag NPs (i.e., sulfidation), several sections of different time point of exposure of both seaweeds were analyzed using conventional TEM and STEM-EDX. Figures from 18 to 22 shows TEM images related to *U. fenestrata* exposure after 7, 14, 21 and 28 days of exposure to PVP-15nm Ag NPs. The distribution was found similar in all exposure time studied. NPs were able to penetrate the cuticle, mucilage and intercellular space and cell wall at early stages (i.e., 7 days, Figure 18, and Figure 19) and advance in the tissue moving between cells via inner cell wall. Ag NPs showed the same tendency in the other three time points as observed in Figure 18 and 20 for 14 days, in Figure 18 and 21, for 21 days and in Figure 18 and 22 for 28 days of exposure. A concentration gradient in Ag NPs distribution from the highest number of NPs next to the cell walls of the cortical cells (e.g., Figure 19, 20, 21 and 22) to the lowest number of NPs in the deepest localization of the tissue (Figure 18, left side) was observed. NPs size measured inside *U. fenestrata* (Figure 23) showed that the Ag NPs became smaller, 19 – 12 nm in diameter, than the initial primary size, 24 nm in diameter. This feature indicates that Ag NPs underwent dissolution, at least after tissue internalization.

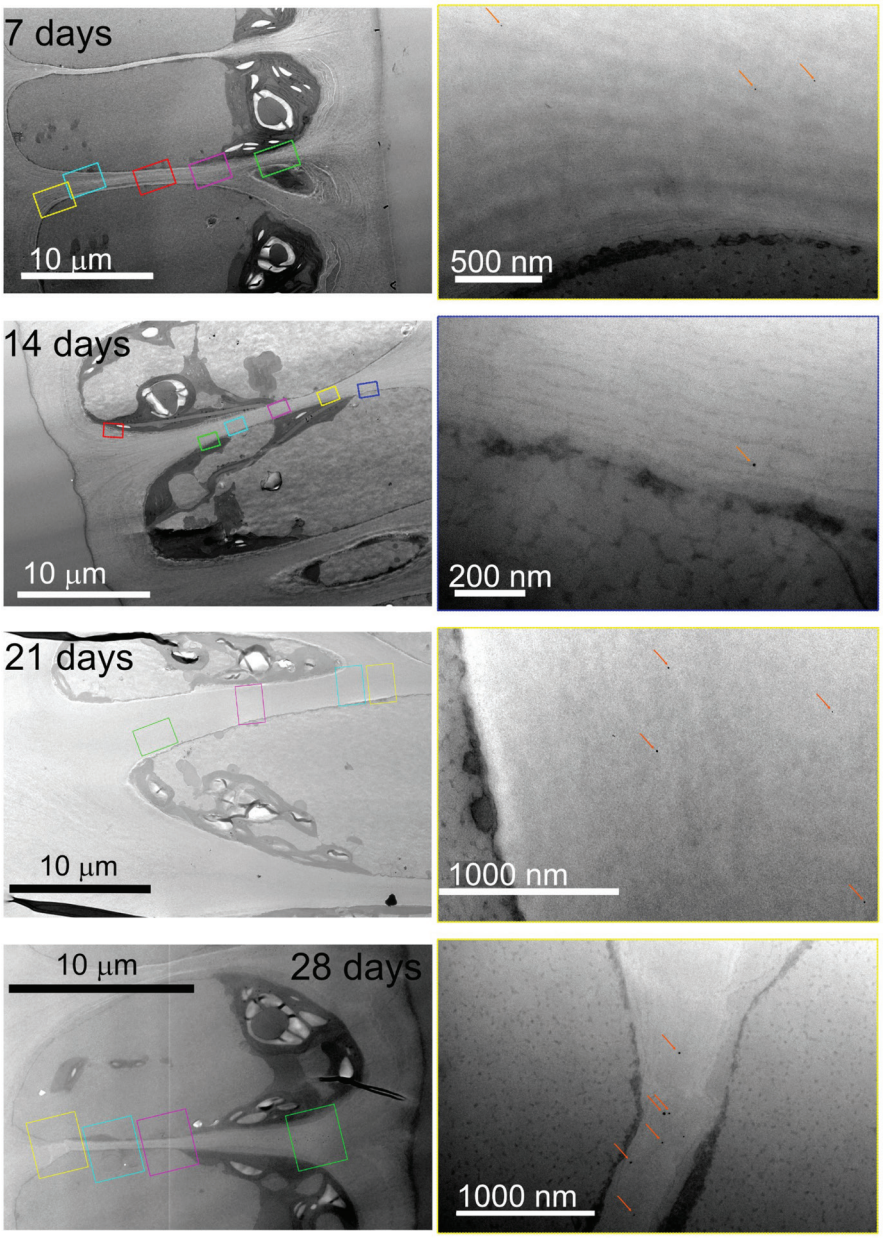

Figure 18. Biodistribution of PVP-15nm Ag NPs in *U. fenestrata* after 7, 14, 21 and 28 days of exposure. The different color squares in the lower magnification TEM images (left) indicate the tissue positions analyzed at higher magnification. TEM images on the right show Ag NPs localized in the deeper location of the tissue. The remaining color squares analyzed at higher magnification after 7, 14, 21 and 28 days of exposure can be found in Figure 19, Figure 20, Figure 21 Figure 22, respectively. The orange arrows indicate Ag NPs.

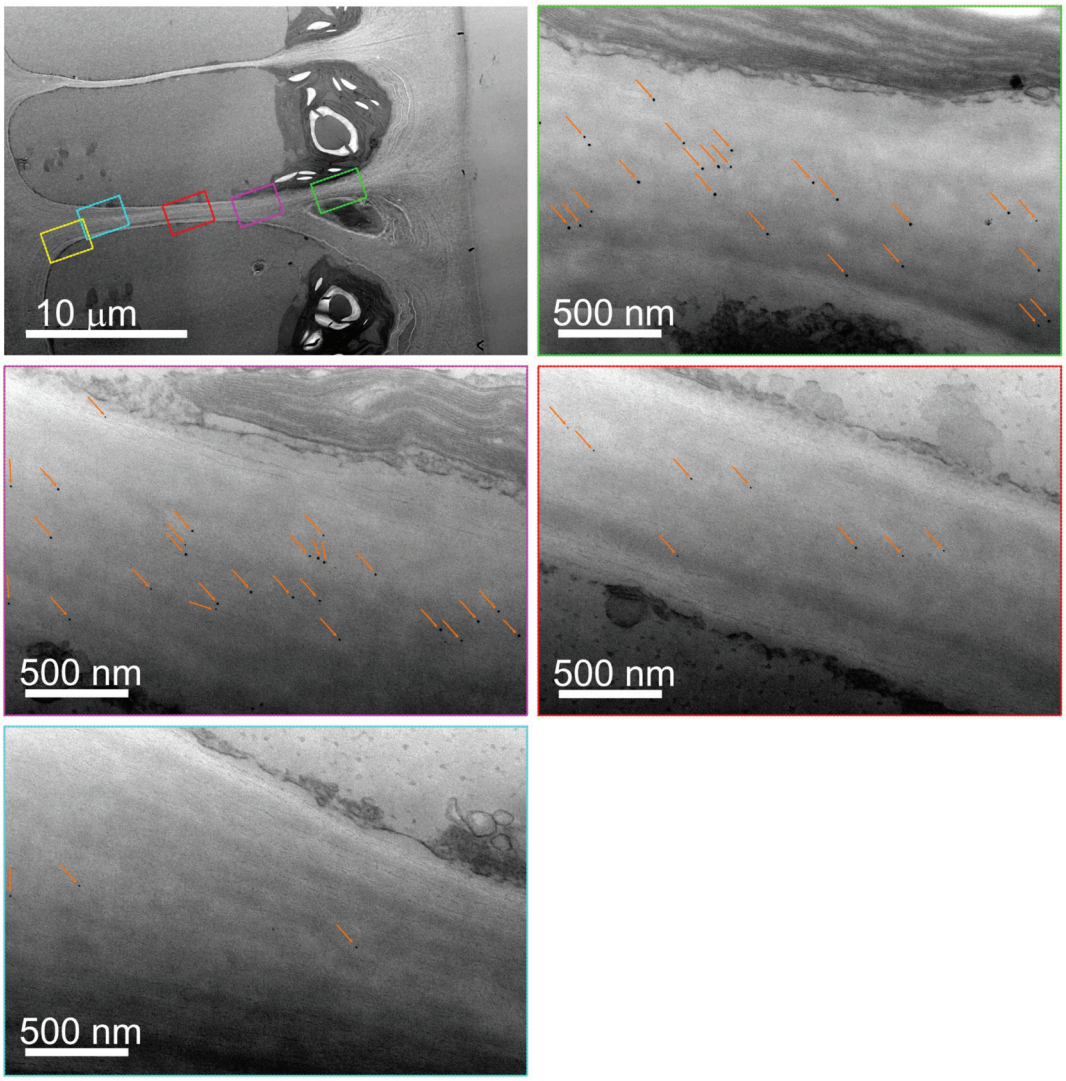

Figure 19. Biodistribution of PVP-15nm Ag NPs in *U. fenestrata* after 7 days of exposure. The different color squares in the lower magnification TEM image indicate the portions of tissue analyzed at higher magnification. Orange arrows indicated the position of Ag NPs.

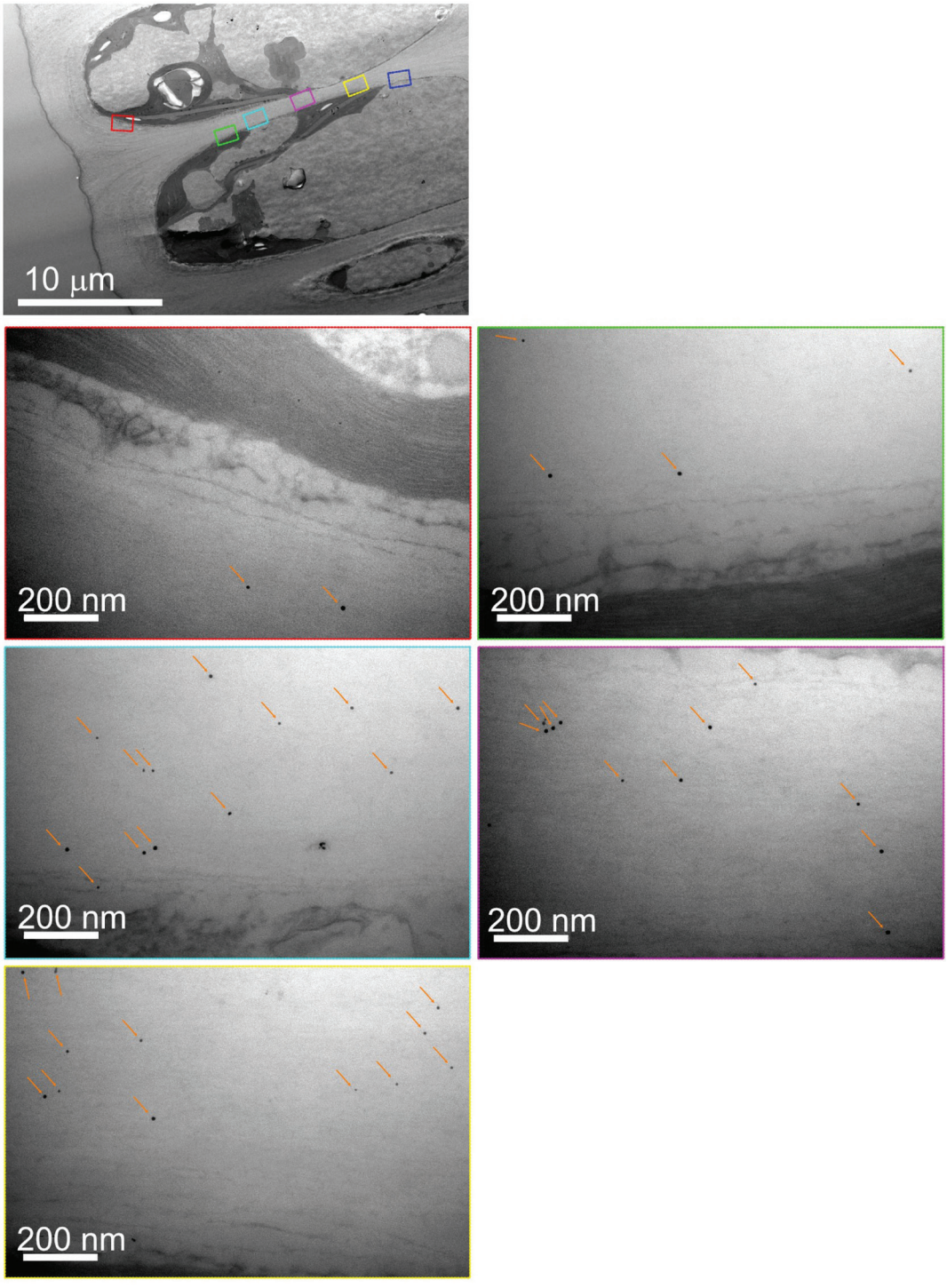

Figure 20. Biodistribution of PVP-15nm Ag NPs in *U. fenestrata* after 14 days of exposure. The different color squares in the lower magnification TEM image indicate the portions of tissue analyzed at higher magnification. Orange arrows indicated the position of Ag NPs.

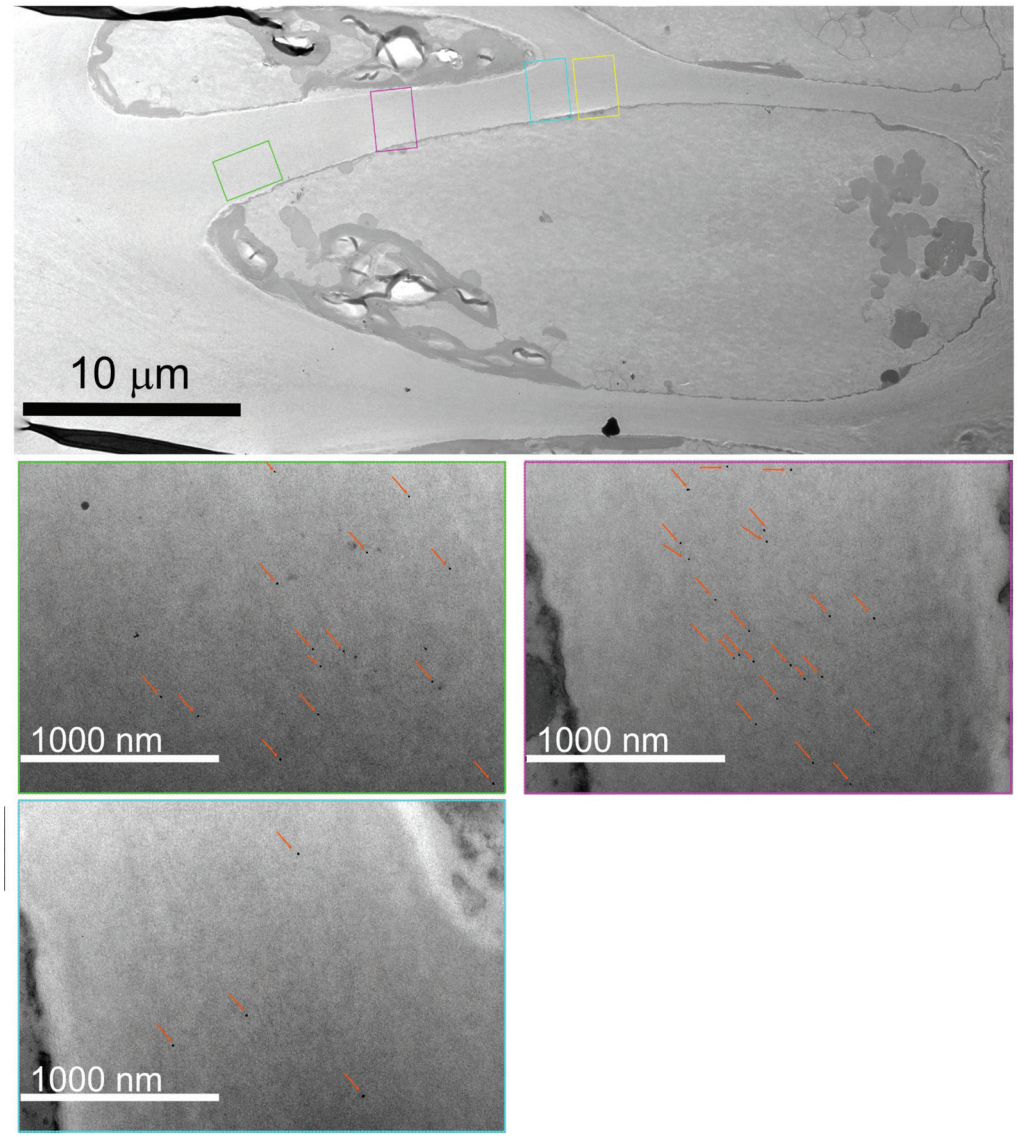

Figure 21. Biodistribution of PVP-15nm Ag NPs in *U. fenestrata* after 21 days of exposure. The different color squares in the lower magnification TEM image indicate the portions of tissue analyzed at higher magnification. Orange arrows indicated the position of Ag NPs.

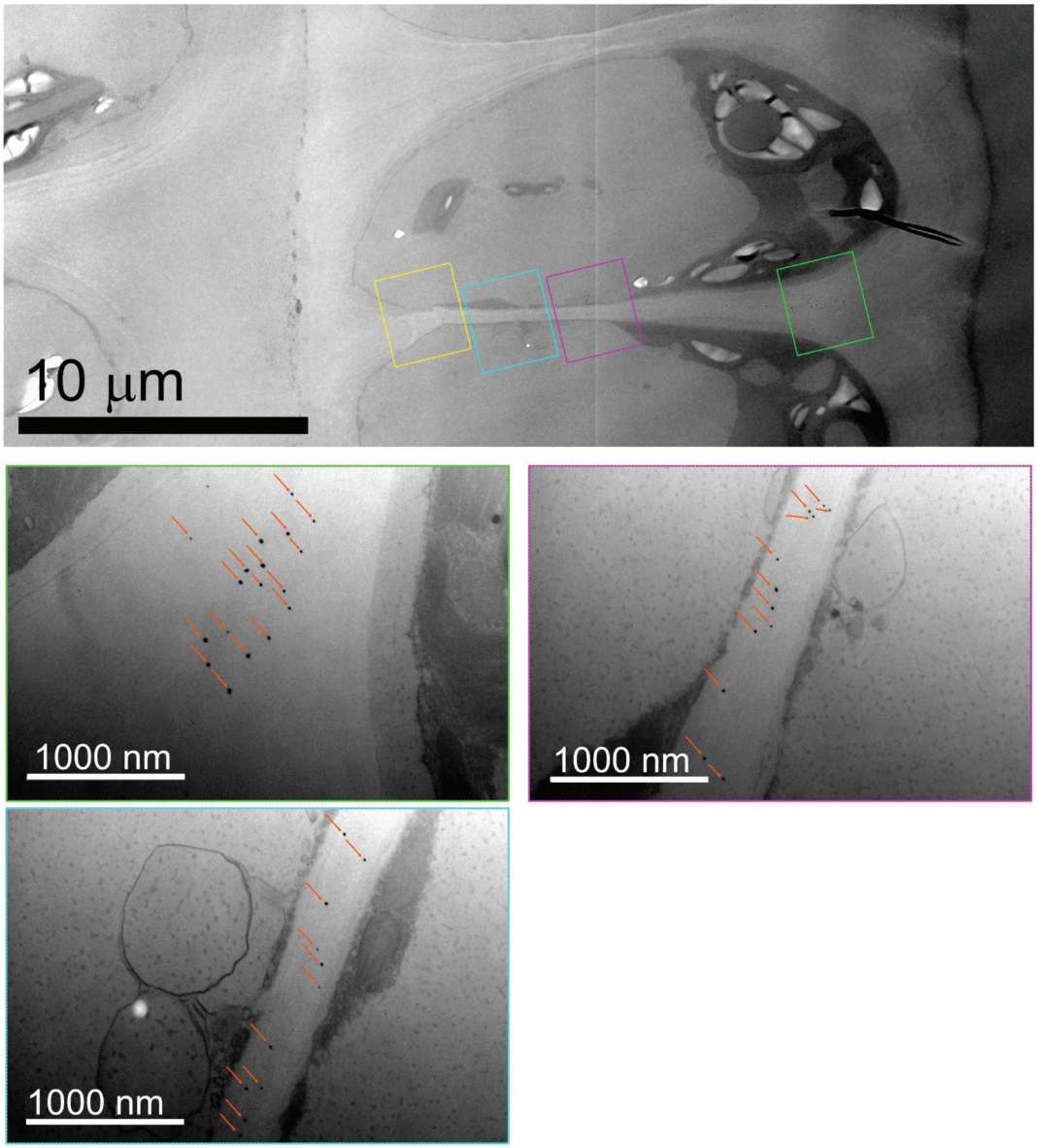

Figure 22. Biodistribution of PVP-15nm Ag NPs in *U. fenestrata* after 28 days of exposure. The different color squares in the lower magnification of TEM image indicate the portions of tissue analyzed at higher magnification. Orange arrows indicated the position of Ag NPs.

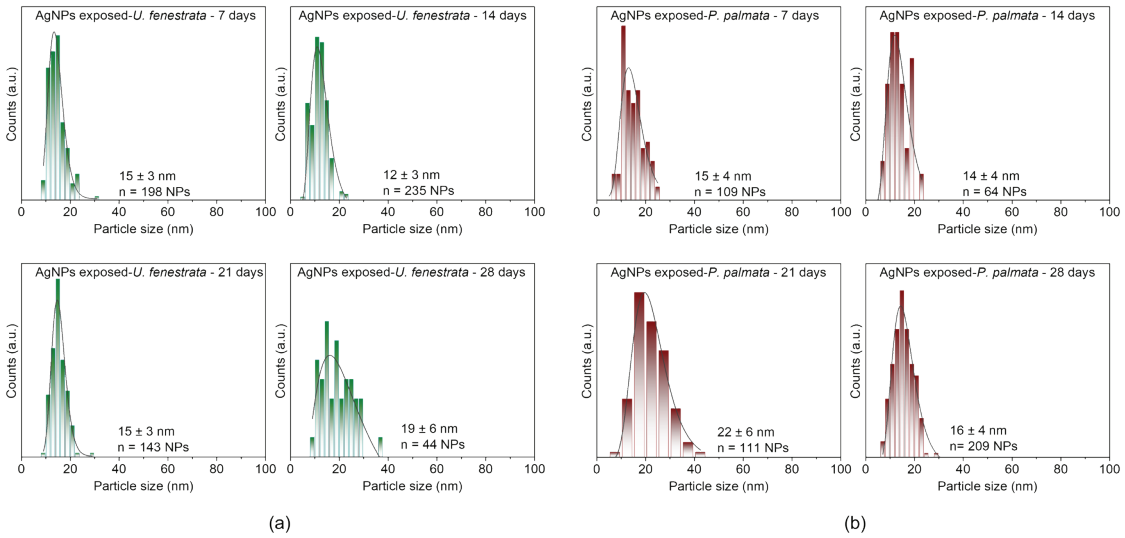

Figure 23. Size distribution histograms of PVP-15nm Ag NPs measured within seaweed tissue after 7, 14, 21 and 28 days of exposure.

In contrast to the results obtained for *U. fenestrata*, PVP-15nm Ag NPs biodistribution in *P. palmata* showed a different behavior. After 7 days of exposure, all particles in *P. palmata* were confined between the cuticle and the mucilage with some exceptions that begin to get in closer proximity to the first line of cortical cells, as shown in Figure 24 and Figure 25. At 14 days, the NPs were already channeled through the extracellular space, reaching deeper location of the tissue (Figure 24, and Figure 26). Also, in some cases, a possible cellular internalization could be suggested (Figure 26, cyan square). Similar behavior was observed in the NPs distribution after 21 (Figure 24, and Figure 27) and 28 days (Figure 24, and Figure 28) of exposure, where the particles tended to accumulate all along the cell wall close to the cell membrane and do not pass the second line of cells that belong to the cortex. The number of NPs accumulated increased as a function of the exposure time: < 10 NPs counted after 7 days in any of the sections analyzed, > 15 NPs found after both 21 and 28 days. Moreover, as in the case of *U. fenestrata*, NPs size also decreased inside of *P. palmata* if correlated to the initial size (Figure 23): 15 – 22 nm internalized Ag NPs VS 24 nm Ag NPs, confirming that some dissolution occurred during internalization.

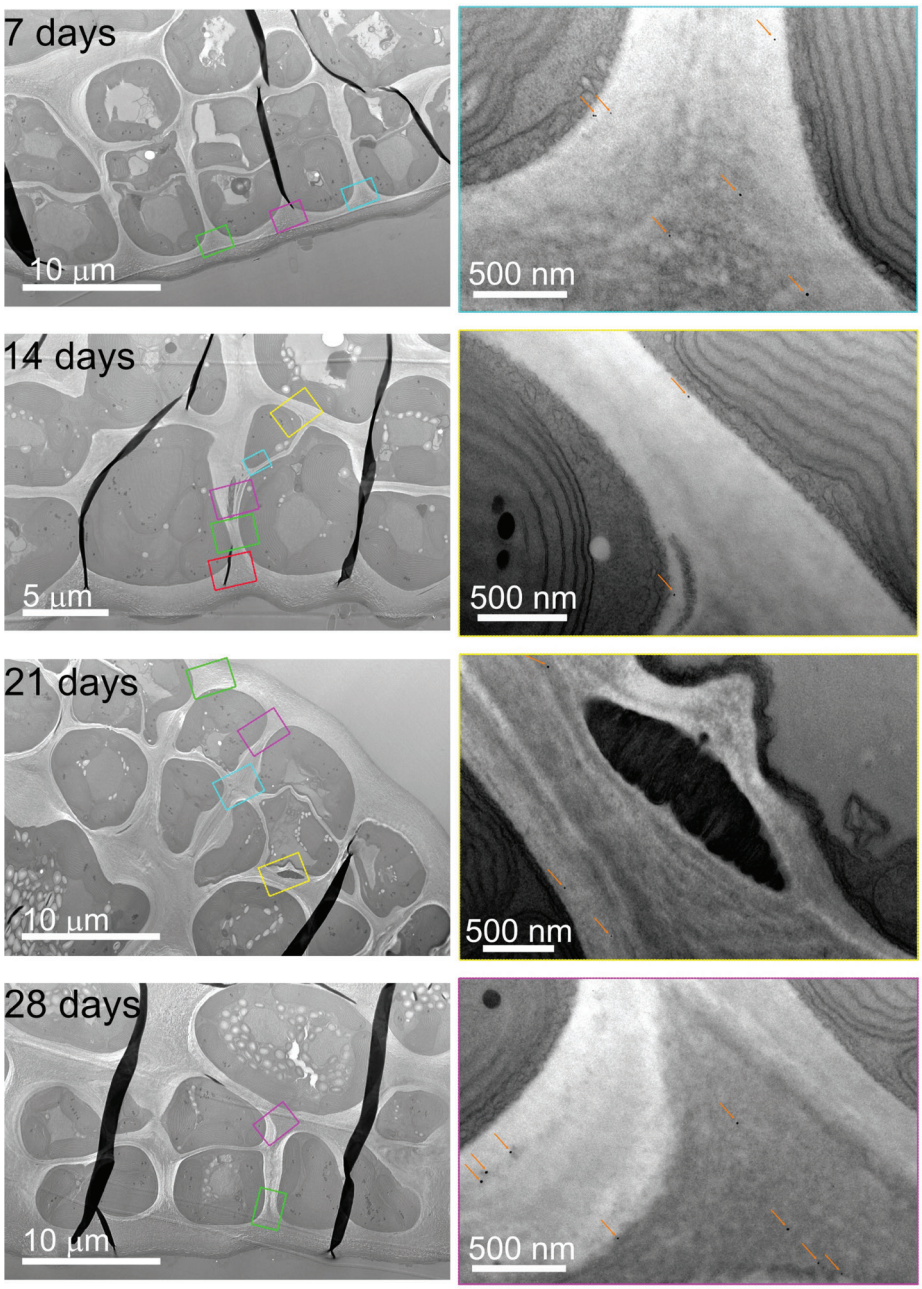

Figure 24. Biodistribution of PVP-15nm Ag NPs in *P. palmata* after 7, 14, 21 and 28 days of exposure. The different color squares in the lower magnification TEM images (left) indicate the tissue positions analyzed at higher magnification. TEM images on the right show Ag NPs localized in the deeper location of the tissue. The remaining color squares analyzed at higher magnification after 7, 14, 21 and 28 days of exposure can be found in Figure 25, Figure 26, Figure 27 Figure 28, respectively. The orange arrows indicate Ag NPs.

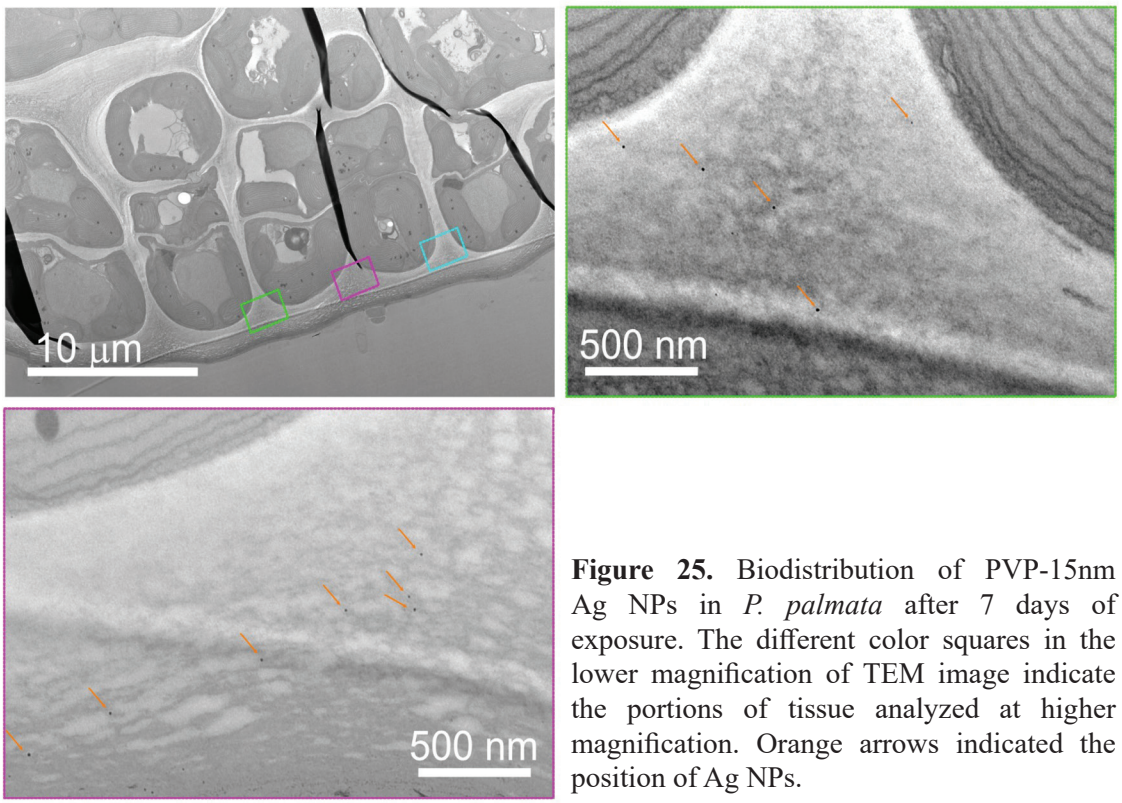

Figure 25. Biodistribution of PVP-15nm Ag NPs in *P. palmata* after 7 days of exposure. The different color squares in the lower magnification of TEM image indicate the portions of tissue analyzed at higher magnification. Orange arrows indicated the position of Ag NPs.

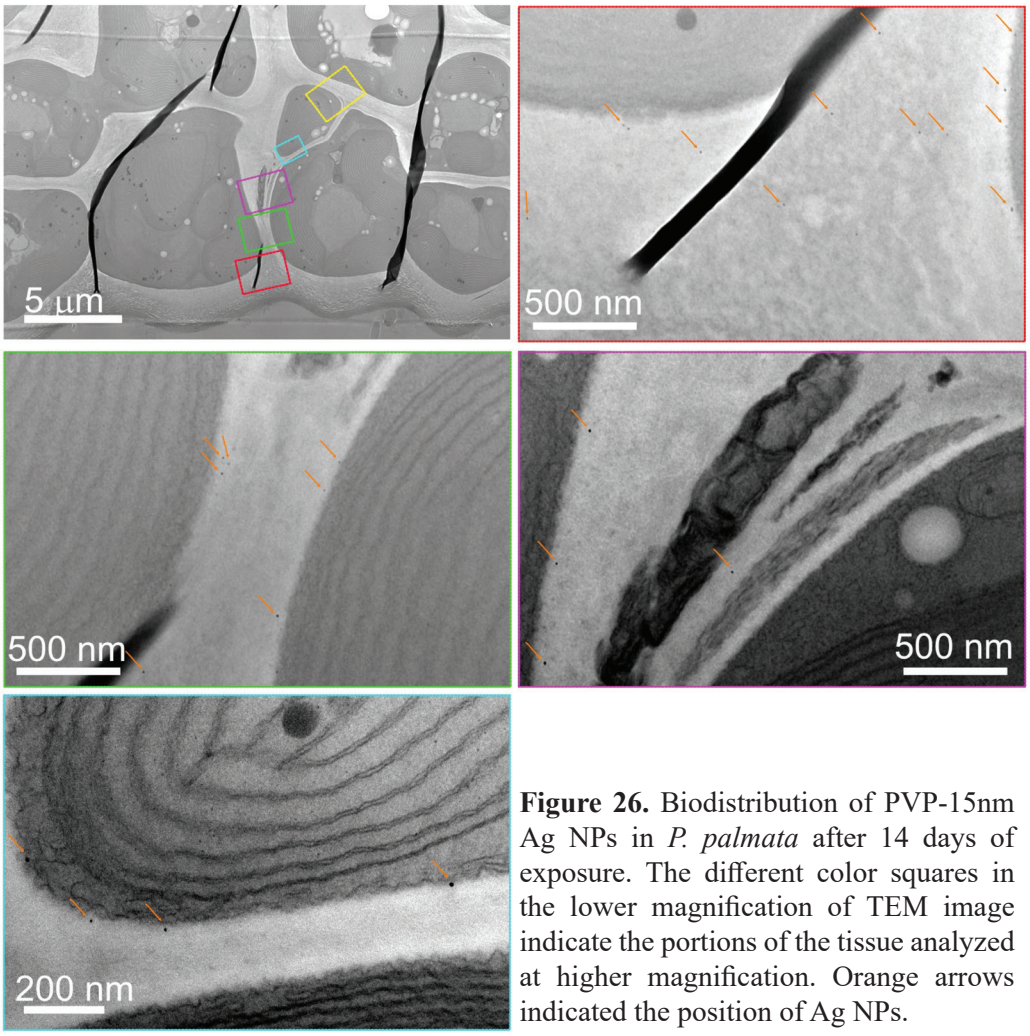

Figure 26. Biodistribution of PVP-15nm Ag NPs in *P. palmata* after 14 days of exposure. The different color squares in the lower magnification of TEM image indicate the portions of the tissue analyzed at higher magnification. Orange arrows indicated the position of Ag NPs.

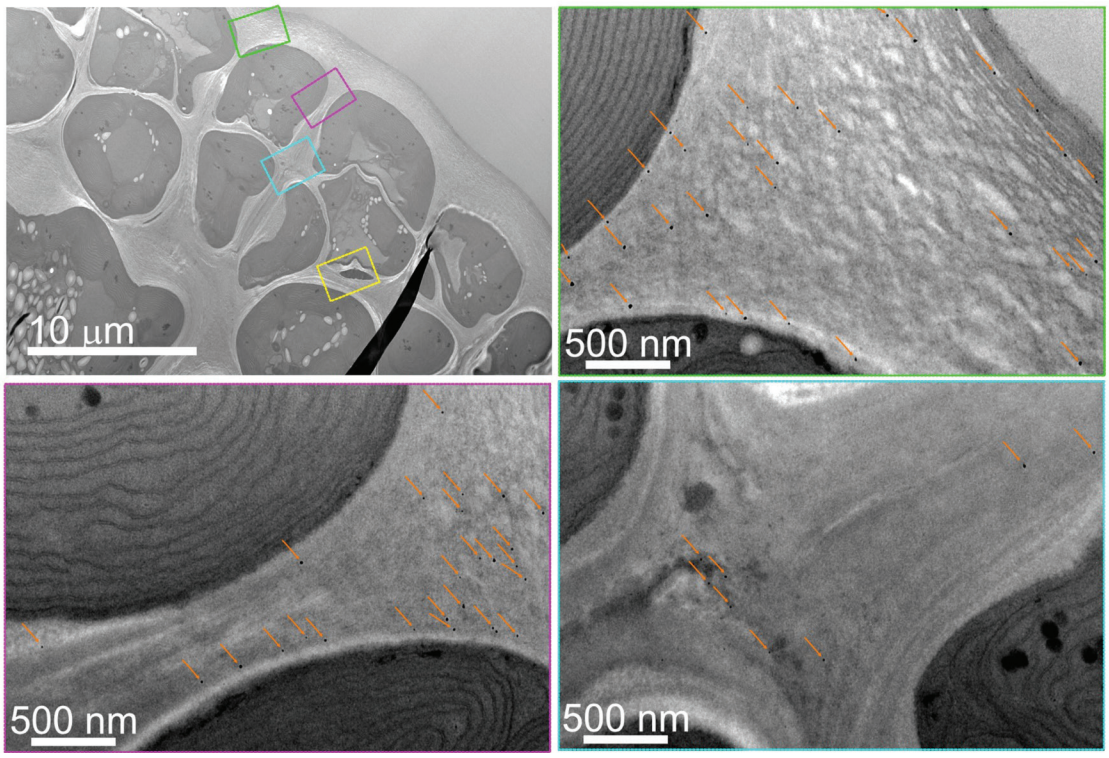

Figure 27. Biodistribution of PVP-15nm Ag NPs in *P. palmata* after 21 days of exposure. The different color squares in the lower magnification of TEM image indicate the portions of the tissue analyzed at higher magnification. Orange arrows indicated the position of Ag NPs.

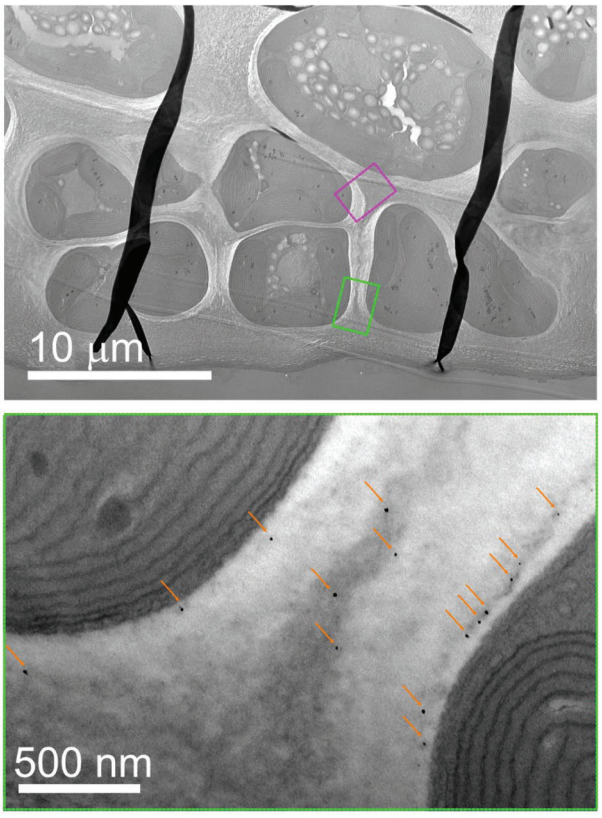

Figure 28. Biodistribution of PVP-15nm Ag NPs in *P. palmata* after 28 days of exposure. The different color squares in the lower magnification of TEM image indicate the portions of the tissue analyzed at higher magnification. Orange arrows indicated the position of Ag NPs.

The biodistribution was also investigated using STEM, taking advantage of the microscope integration with an EDX detector to deeply study the transformation of PVP-15nm Ag NPs after internalization. STEM images confirmed the same particles fate observed by TEM: at 7 days of exposure, *P. palmaria*, found the NPs accumulate outside the cuticle or start to be in the mucilage and polysaccharides intercellular matrix right before the beginning of the first line of cells, with some NPs inside the chloroplasts, trespassing the cell membrane (Figure 29); while in *U. fenestrata*, no NPs were found close to the cell membrane, but appear canalized in the intercellular matrix and cell walls (Figure 30). No NP were observed in the organelles or cytoplasm in this condition. In both seaweeds, going through the different time points, it was possible to follow the particles gradually reaching the inner areas of the tissue. EDX mapping identifies the silver element in the spherical electron-dense NPs with a diameter between 8 – 20 nm, confirming the bioaccumulation of Ag NPs. Several electron-dense NPs were found with different shapes and sizes in *U. fenestrata*, which were identified as other inorganic nanoparticles (Figure 31).

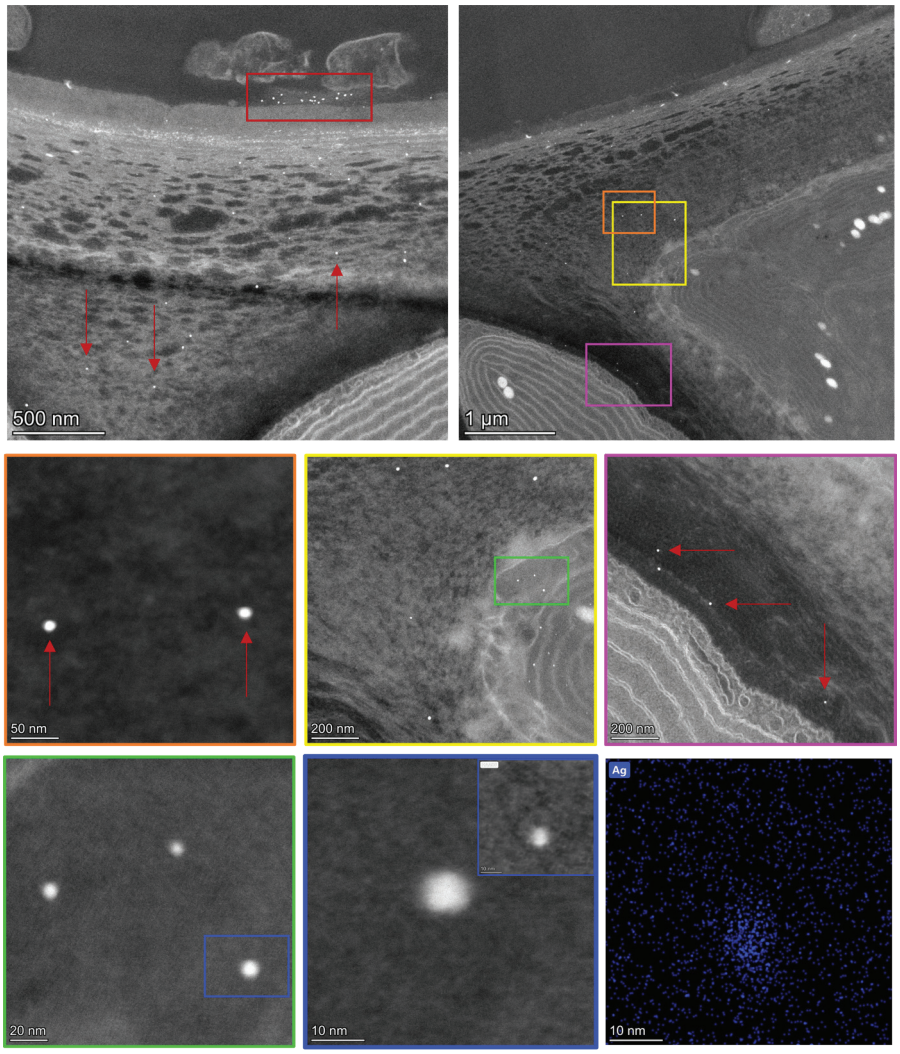

(a)

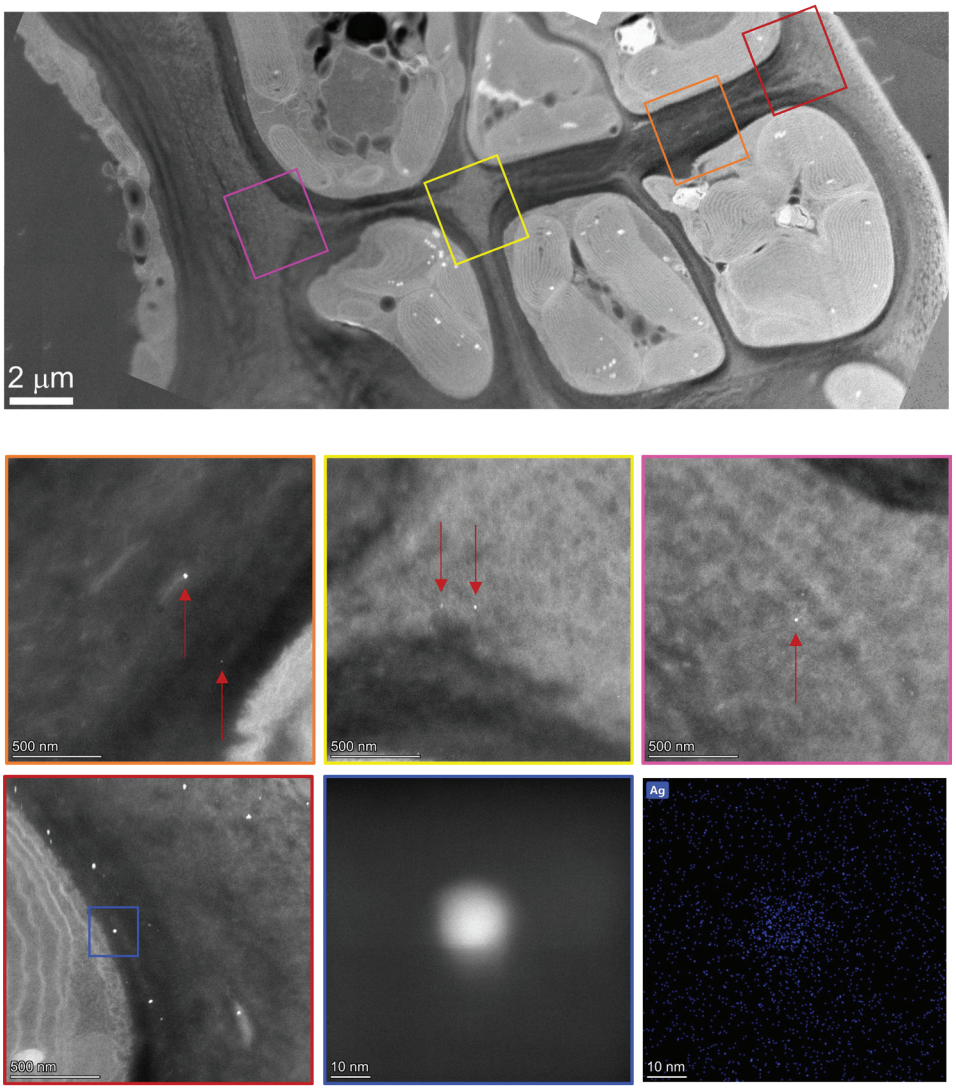

(b)

Figure 29. Distribution of PVP-15nm Ag NPs in *P. palmata* after 7 (a) and 28 (b) days of exposure. From the top, high angle annular dark field (HAADF) low mag images of cells organization. High mag images where Ag NPs (bright dots) are pointed by red arrows and squared. At the bottom, STEM-EDX elemental mapping of the area of interest, confirming the presence of Ag.

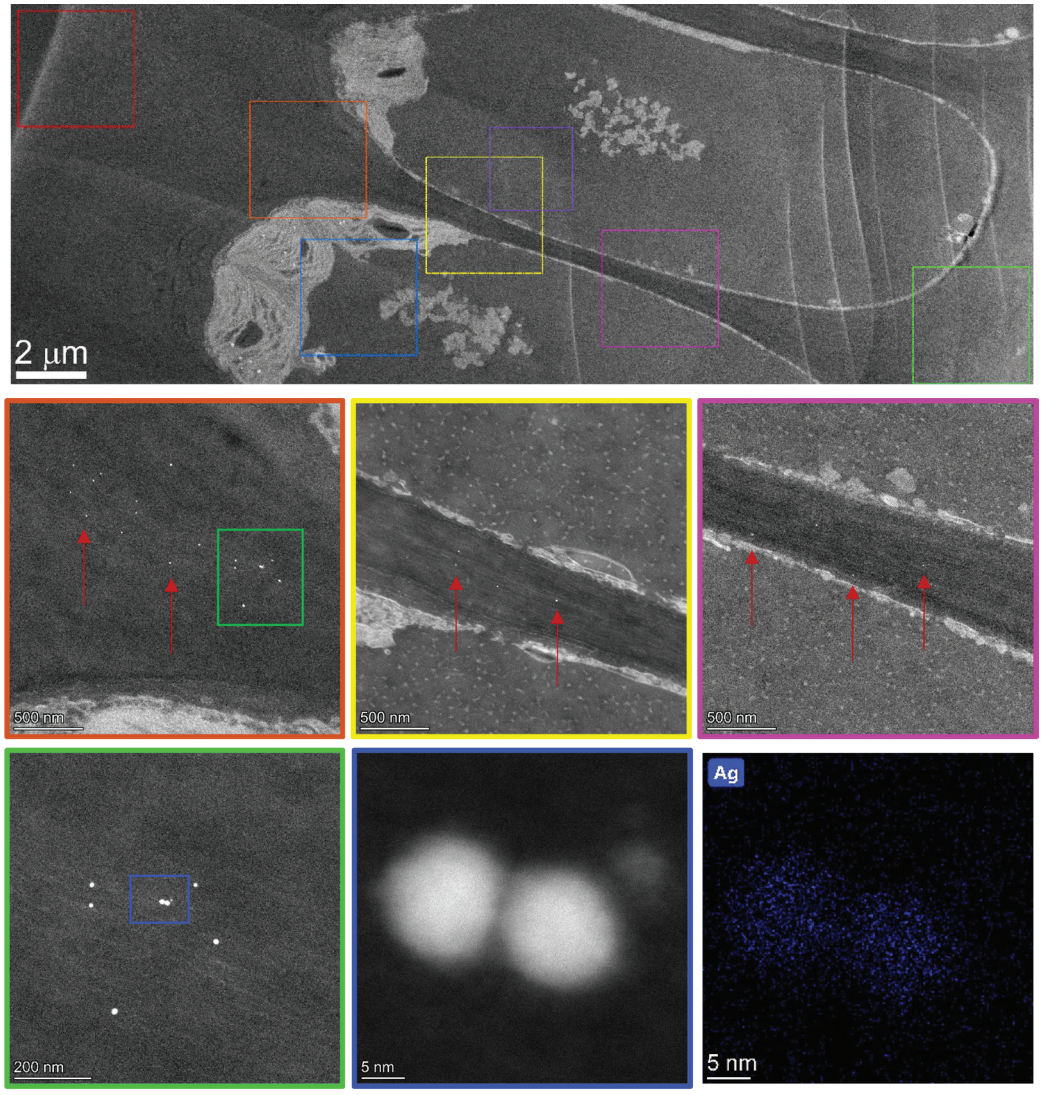

(a)

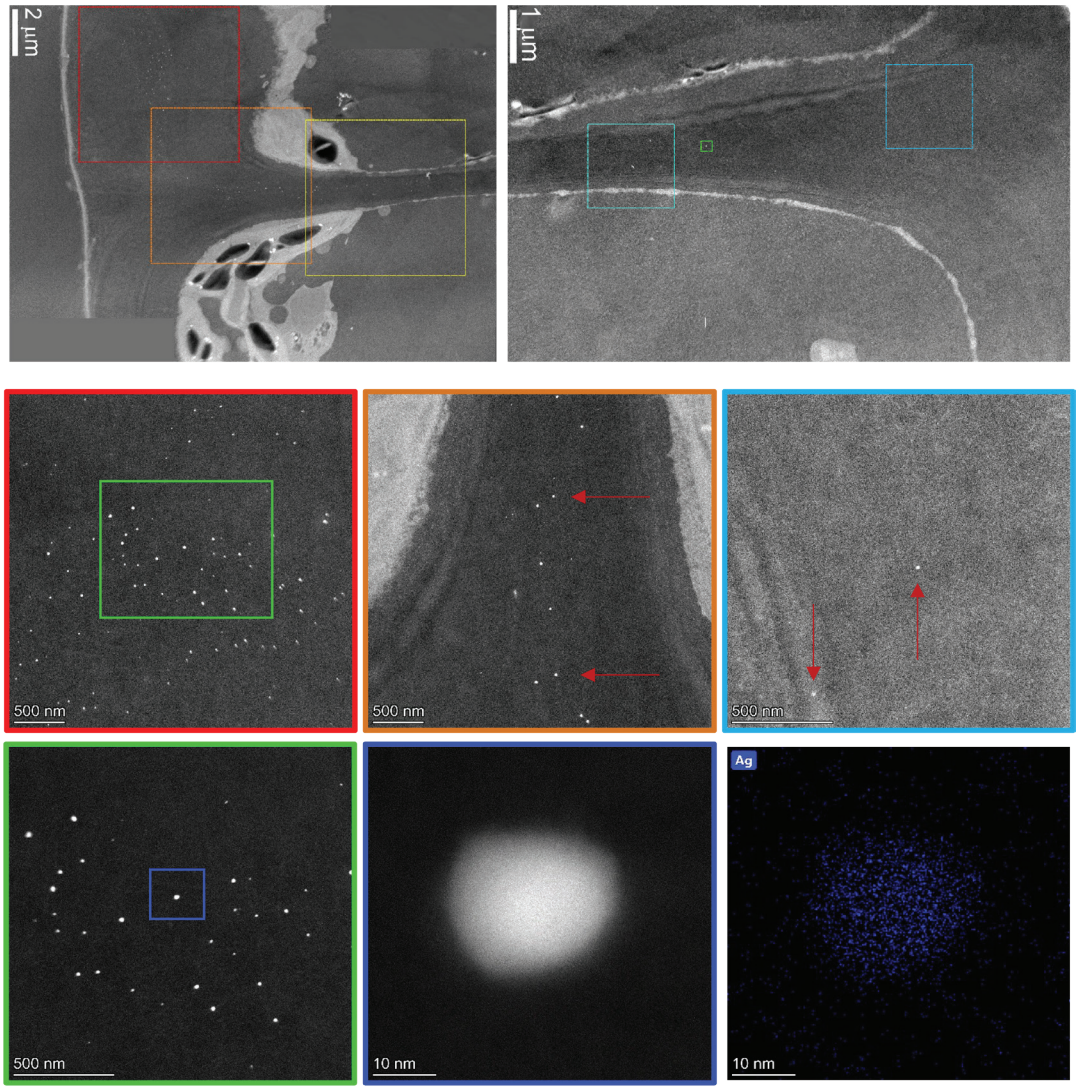

(b)

Figure 30. Distribution of PVP-15nm Ag NPs in *U. fenestrata* after 7 (a) and 28 (b) days of exposure. From the top, high angle annular dark field (HAADF) low mag images of cells organization. High mag images where Ag NPs (bright dots) are pointed by red arrows and squared. At the bottom, STEM-EDX elemental mapping of the area of interest, confirming the presence of Ag.

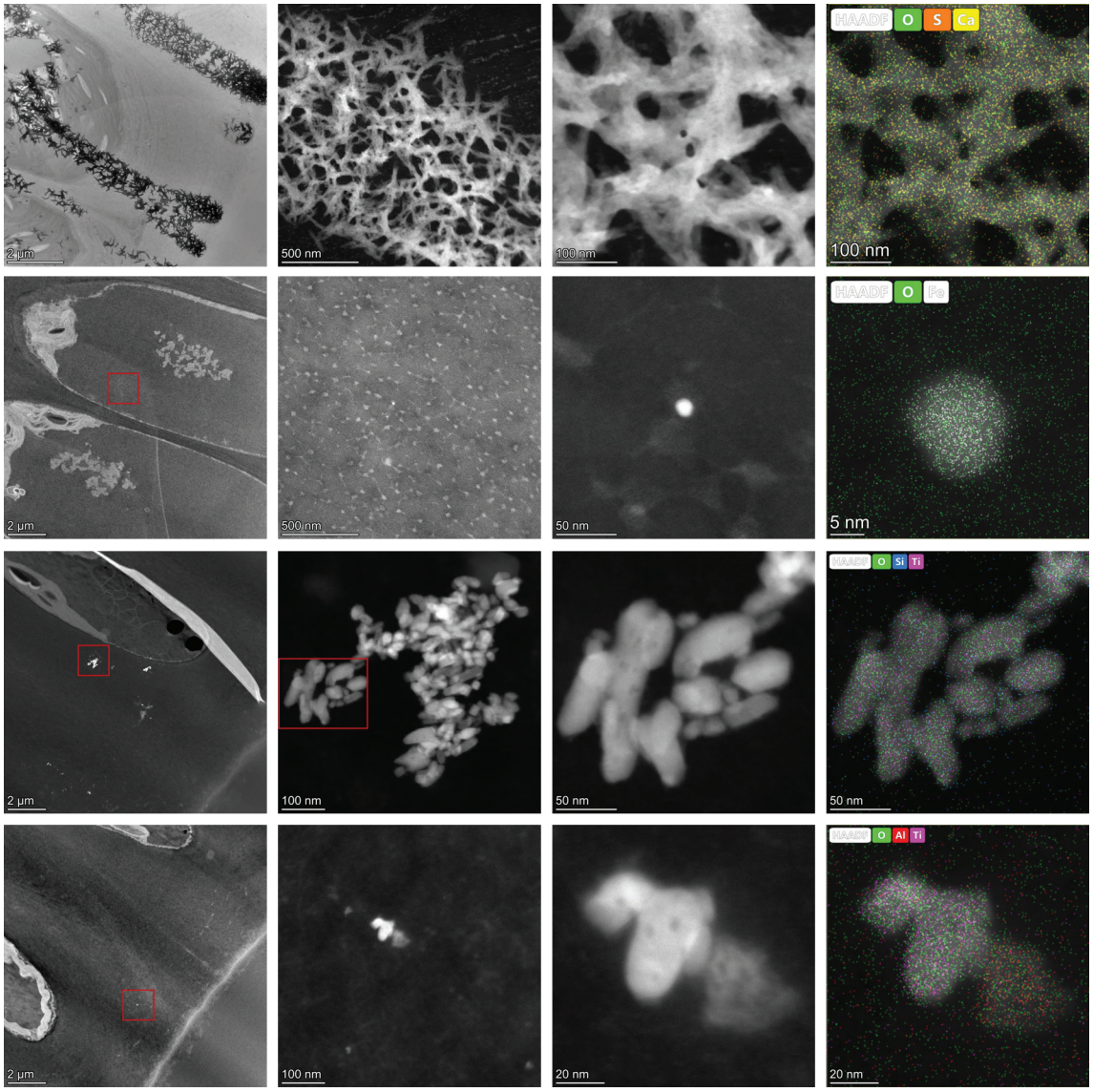

Figure 31. STEM-EDX images of different elements found in *U. fenestrata* tissue during the analysis. The mapping shows the presence of $CaSO_4$, Fe_2O_3, TiO_2 and Al_2O_3.

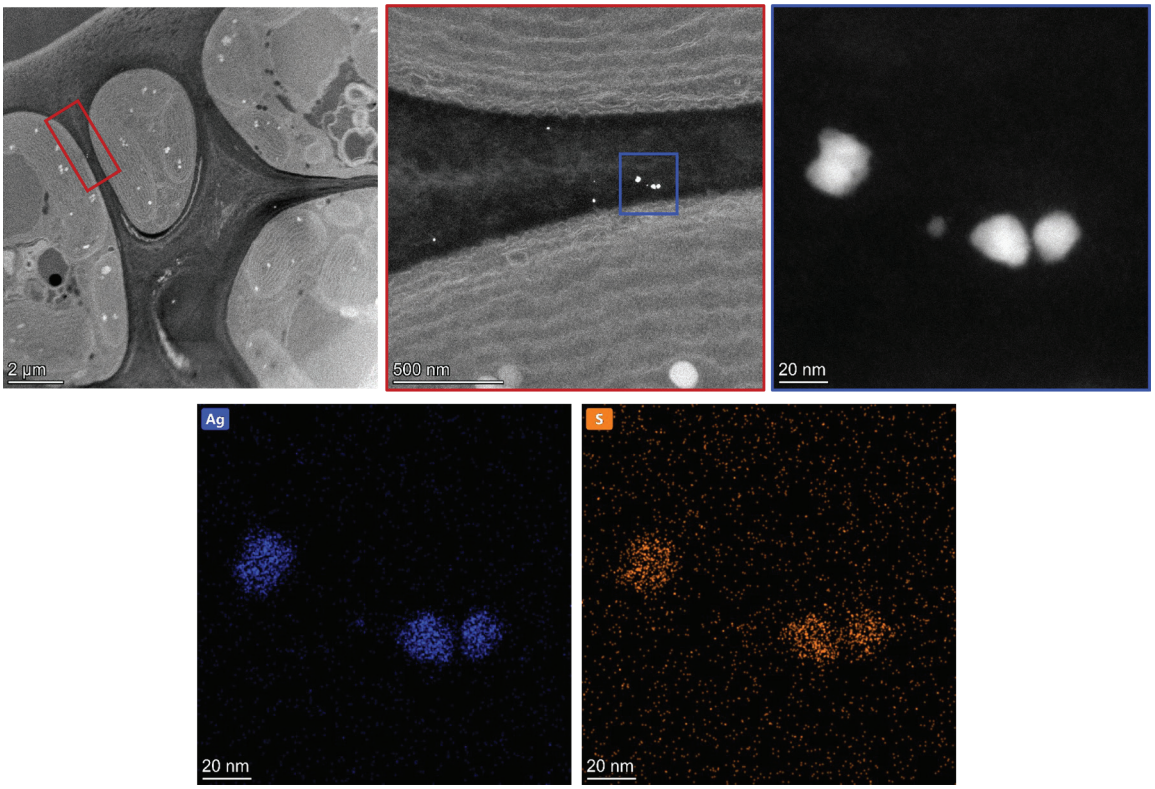

Figure 32. STEM-EDX images showing sulfidation process of Ag NPs after internalization. Images related to 21 days of exposure are shown.

Taking into account the decrease in size of the Ag NPs during the internalization in the tissues and their possible interactions with the matrix, the potential transformation of Ag NPs happening inside the seaweed tissue was investigated since chemical speciation of the NPs could modify the potential risk associated to their accumulation. STEM-EDX analysis was performed in the tissues as a function of time of exposure. The most possible transformations of Ag NPs are oxidative dissolution, sulfidation and chlorination.[27,28] Therefore, the peaks related to Cl, S and O plus Ag in the EDX spectra were analyzed and only S and Ag were clearly identified in all the analyzed cases. It is well-known that seaweeds contain sulfur-rich polysaccharides and they synthesize and store more sulfur-containing compounds than terrestrial plants.[29,30] Therefore, it could be assumed that the main transformation of PVP-15nm Ag NPs would be the sulfidation. The Figure 32 shows an example of the procedure followed in this study. After localizing Ag NPs inside the seaweed tissue by STEM, the acquisition of EDX maps of Ag and S, from 3 to 7 NPs per time of exposure, was performed. By following the Ag/S ratio associated to the particles located in different region of the tissue, the degree of sulfidation was assessed as a function of tissue penetration and exposure time. Figure 33 shows that *U. fenestrata*,

has an almost stable Ag/S ratio over all exposure times, while *P. palmata*, shows an increase of sulfidation with the longer exposure times. Interestingly, the sulfidation after 28 days of exposure in *P. palmata* present higher heterogeneity. The localization of each Ag NPs in the STEM image was analyzed and it was observed that higher sulfidation was directly proportional to higher penetration of the NPs as shown in Figure 34.

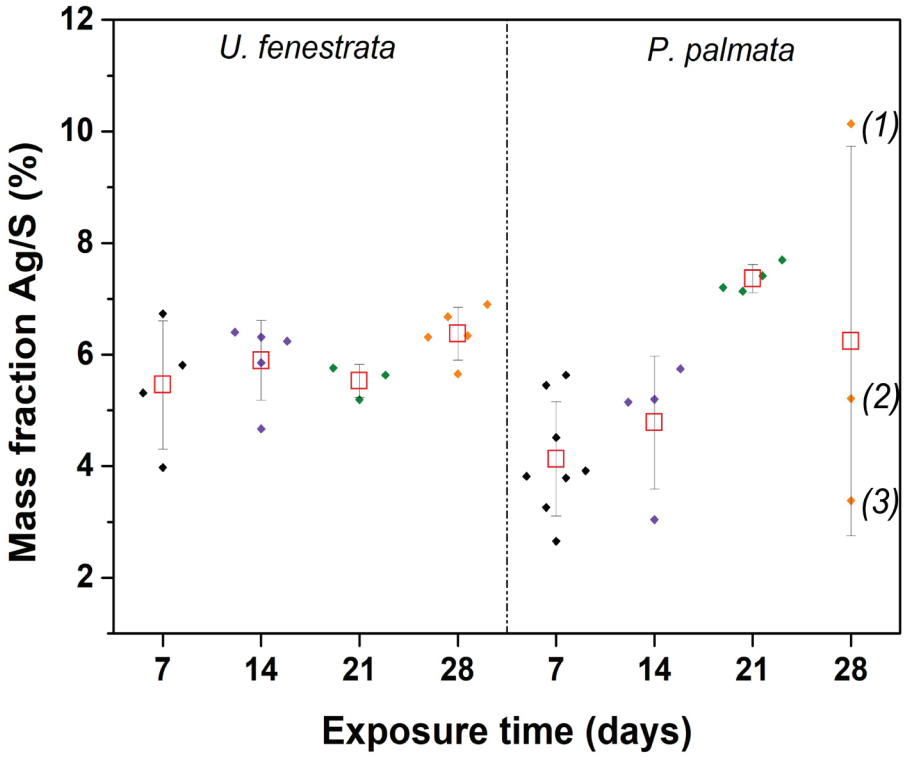

Figure 33. Mass fraction percentage of Ag/S ratio among different time points in *U. fenestrata* and *P. palmata* respectively.

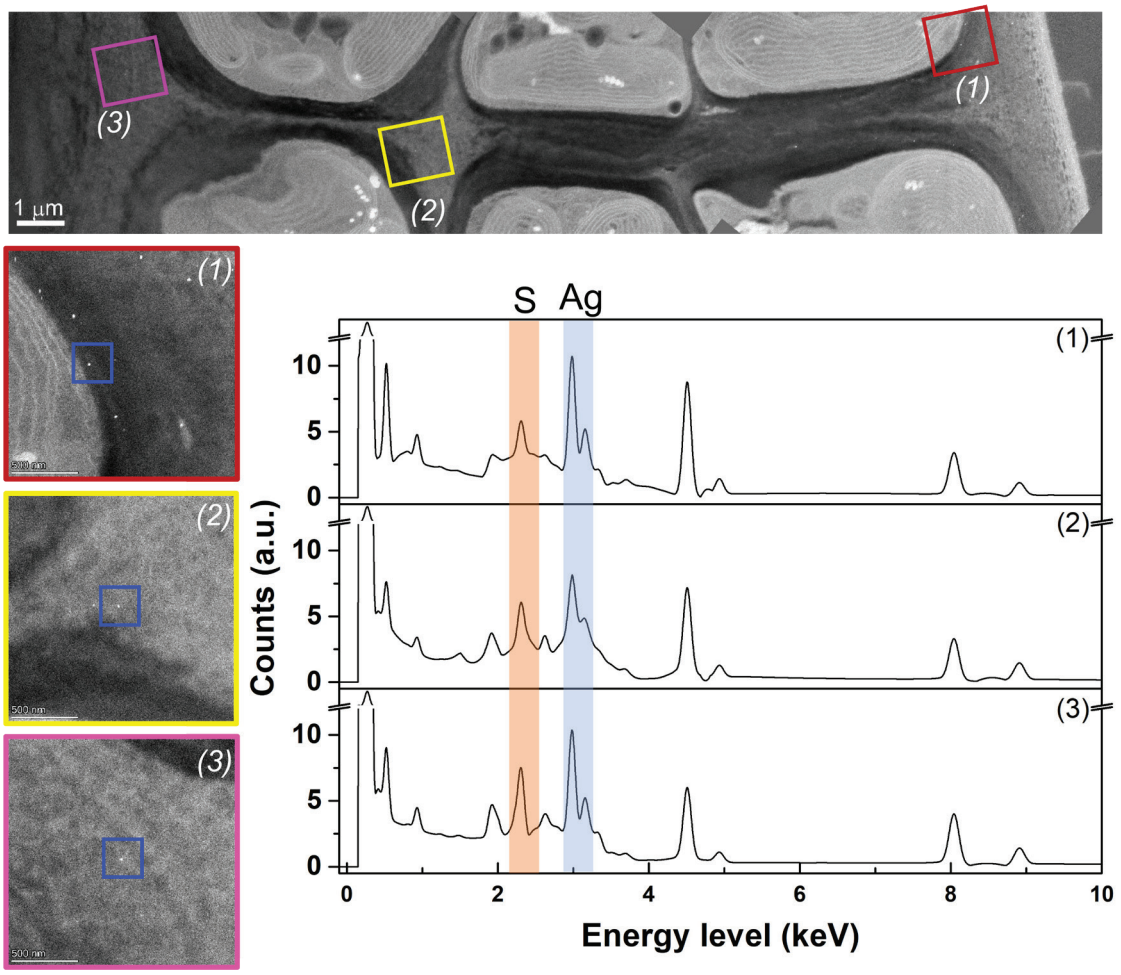

Figure 34. Low mag STEM image showing Ag NPs different localization within the *P. palmata* tissue after 28 days of exposure. (1), (2) and (3) represent the NPs analysed by EDX whose spectra is reported.

The explanation to the difference in the biodistribution and the transformation level that the particles are subjected to, could be found in the different cell wall composition that the two seaweeds species present. In the case of *Ulva*, the cell walls are mainly composed by cellulose, xyloglucan and ulvan. Attention was given to ulvan, which is mainly composed by repeating units of sulphated disaccharides involving β-d-glucuronic acid (1 → 4)-α-1-rhamnose-3-sulfate, and α-l-iduronic acid (1 → 4)-α-l-rhamnose-3-sulfate.[31] While the main component of cell walls in *P. palmata* is β-(1→4)- and β-(1→3)-linked D-xylose units in a proportion of about 4:1.[32] Interestingly, these partly acidic units are essentially held in the cell wall by hydrogen bonds. In addition, this acidity of the xylans is produced by covalent linking with sulphated and/or phosphorylated xylogalactoprotein complexes.[33] This could allow hypothesizing about the difference in the Ag NPs transportation and their sulfidation between both seaweeds. The presence of these hydrogen bonds may produce a more compact and rigid cross-linked polysaccharides which would hinder the NP

transportation through the cell wall of *P. palmata*. Therefore, this could explain the fact that the biodistribution of Ag NPs in *P. palmata* is time-dependent, while in *U. fenestrata* the distribution is homogeneous in all exposure times studied (Figure 18 for *Ulva* and Figure 24 for *Palmaria*).

The variation of sulfidation of Ag NPs could be also attributed to the difference in the cell wall composition. Water-soluble sulphated polysaccharides ulvan in green seaweed are homogeneously distributed into the cell wall allowing an "easier" interaction of the sulphate groups with Ag surface, favoring Ag-SO3-R complexation.[34] In the case of red seaweed, the sulphated xylogalactoproteins are linked to the xylans, affecting Ag-SO3-R complexation.

3.3 Conclusions

In summary, PVP-100nm Ag NPs were localized and identified mainly in the digestive gland of clams, while the scarce bioaccumulation of citrate-45nm TiO_2 NPs prevented their analysis by EM. Clearly, PVP-100nm Ag NPs underwent a transformation related to dissolution when they were uptaken by clams. Moreover, it was demonstrated the effect of the size in the biodistribution of MNPs in seaweeds. None of the citrate-TiO_2 NPs studied here were internalized by seaweed, but they were localized on the surface forming big aggregates; while well-dispersed PVP-15nm Ag NPs were uptaken and their biodistribution was dependent to the seaweed type and time of exposure. It was reported for the first time, to the best of our knowledge, not only the localization of bioaccumulated PVP-15nm Ag NPs but also their transformation into two seaweeds: *P. palmata* and *U. fenestrata*. There are some questions that remain open yet and should be explored in subsequent studies. One of them is to elucidate the oxidation state of both Ag and S observed by EDX analysis, which would allow to understand the complex compound formed and to better predict the potential response of the seaweed against the exposure to these NPs. Sulfidation significantly decreases the solubility and availability of Ag ions and consequently, toxicity. However, because of the potential accumulation and long-term stability of Ag_2S NPs in the environment, it is necessary to evaluate chronic exposure effects. Additionally, it is important to take into account that sulphate groups do not avoid dissolution of Ag as efficiently as sulphides.[35]

References

1. Zhou, K., Hu, Y., Zhang, L., Yang, K. & Lin, D. The role of exopolymeric substances in the bioaccumulation and toxicity of Ag nanoparticles to algae. Sci. Rep. 6, 32998 (2016).
2. Huq, M. A. & Akter, S. Bacterial Mediated Rapid and Facile Synthesis of Silver Nanoparticles and Their Antimicrobial Efficacy against Pathogenic Microorganisms. Materials (Basel). 14, 2615 (2021).
3. Huq, M. A. Green Synthesis of Silver Nanoparticles Using Pseudoduganella eburnea MAHUQ-39 and Their Antimicrobial Mechanisms Investigation against Drug Resistant Human Pathogens. Int. J. Mol. Sci. 21, 1510 (2020).
4. Wang, X. et al. A novel approach towards high-performance composite photocatalyst of TiO2 deposited on activated carbon. Appl. Surf. Sci. 255, 3953–3958 (2009).
5. Blinova, I. et al. Toxicity of two types of silver nanoparticles to aquatic crustaceans Daphnia magna and Thamnocephalus platyurus. Environ. Sci. Pollut. Res. 20, 3456–3463 (2013).
6. Li, Y. & Cummins, E. A semi-quantitative risk ranking of potential human exposure to engineered nanoparticles (ENPs) in Europe. Sci. Total Environ. 778, 146232 (2021).
7. Xu, L., Cai, J., Gao, T. & Ma, A. Shellfish consumption and health: A comprehensive review of human studies and recommendations for enhanced public policy. Crit. Rev. Food Sci. Nutr. 62, 4656–4668 (2022).
8. Parodi, A. et al. The potential of future foods for sustainable and healthy diets. Nat. Sustain. 1, 782–789 (2018).
9. El-Naggar, N. E.-A., Hussein, M. H., Shaaban-Dessuuki, S. A. & Dalal, S. R. Production, extraction and characterization of Chlorella vulgaris soluble polysaccharides and their applications in AgNPs biosynthesis and biostimulation of plant growth. Sci. Rep. 10, 3011 (2020).
10. Hahn, J. L. et al. Chemical contaminant levels in edible seaweeds of the Salish Sea and implications for their consumption. PLoS One 17, e0269269 (2022).
11. Gökçe, D. Algae as an Indicator of Water Quality. in Algae - Organisms for Imminent Biotechnology (InTech, 2016). doi:10.5772/62916.
12. Dhargalkar, V. K. & Verlecar, X. N. Southern Ocean seaweeds: A resource for exploration in food and drugs. Aquaculture 287, 229–242 (2009).
13. Peng, Z. et al. Species-specific bioaccumulation and health risk assessment of heavy metal in seaweeds in tropic coasts of South China Sea. Sci. Total Environ. 832, 155031 (2022).
14. Giusti, L. Heavy metal contamination of brown seaweed and sediments from the UK coastline between the Wear river and the Tees river. Environ. Int. 26, 275–286 (2001).
15. Turner, A., Brice, D. & Brown, M. T. Interactions of silver nanoparticles with the marine macroalga, Ulva lactuca. Ecotoxicology 21, 148–154 (2012).
16. Miao, A.-J. et al. The algal toxicity of silver engineered nanoparticles and detoxification by exopolymeric substances. Environ. Pollut. 157, 3034–3041 (2009).
17. Grasso, A. et al. Chemical Characterization and Quantification of Titanium Dioxide

Nanoparticles (TiO2-NPs) in Seafood by Single-Particle ICP-MS: Assessment of Dietary Exposure. Int. J. Environ. Res. Public Health 17, 9547 (2020).
18. Zhou, Q. et al. Determination and characterization of metal nanoparticles in clams and oysters. Ecotoxicol. Environ. Saf. 198, 110670 (2020).
19. Siddiqui, S. & Bielmyer-Fraser, G. Accumulation and Effects of Dissolved and Nanoparticle Silver and Copper in Two Marine Seaweed Species. Georg. J. Sci. 77, 1 (2019).
20. García-Negrete, C. A., Jiménez de Haro, M. C., Blasco, J., Soto, M. & Fernández, A. STEM-in-SEM high resolution imaging of gold nanoparticles and bivalve tissues in bioaccumulation experiments. Analyst 140, 3082–3089 (2015).
21. Jorge de Souza, T. A., Rosa Souza, L. R. & Franchi, L. P. Silver nanoparticles: An integrated view of green synthesis methods, transformation in the environment, and toxicity. Ecotoxicol. Environ. Saf. 171, 691–700 (2019).
22. Plascencia-Villa, G. et al. High-resolution analytical imaging and electron holography of magnetite particles in amyloid cores of Alzheimer's disease. Sci. Rep. 6, 24873 (2016).
23. Auclair, J. et al. The Influence of Surface Coatings of Silver Nanoparticles on the Bioavailability and Toxicity to Elliptio complanata Mussels. J. Nanomater. 2019, 1–10 (2019).
24. Aouini, F., Trombini, C., Sendra, M. & Blasco, J. Biochemical response of the clam Ruditapes philippinarum to silver (AgD and AgNPs) exposure and application of an integrated biomarker response approach. Mar. Environ. Res. 152, 104783 (2019).
25. Xu, Y. et al. Size Effect of Mesoporous Silica Nanoparticles on Pesticide Loading, Release, and Delivery in Cucumber Plants. Appl. Sci. 11, 575 (2021).
26. Wang et al. Effects of Nanoparticles on Algae: Adsorption, Distribution, Ecotoxicity and Fate. Appl. Sci. 9, 1534 (2019).
27. Sekine, R. et al. Speciation and Lability of Ag-, AgCl-, and Ag 2 S-Nanoparticles in Soil Determined by X-ray Absorption Spectroscopy and Diffusive Gradients in Thin Films. Environ. Sci. Technol. 49, 897–905 (2015).
28. Wang, P. et al. Silver sulfide nanoparticles (Ag 2 S-NPs) are taken up by plants and are phytotoxic. Nanotoxicology 9, 1041–1049 (2015).
29. Percival, E. The polysaccharides of green, red and brown seaweeds: Their basic structure, biosynthesis and function. Br. Phycol. J. 14, 103–117 (1979).
30. Raposo, M., De Morais, R. & Bernardo de Morais, A. Bioactivity and Applications of Sulphated Polysaccharides from Marine Microalgae. Mar. Drugs 11, 233–252 (2013).
31. Wahlström, N. et al. Composition and structure of cell wall ulvans recovered from Ulva spp. along the Swedish west coast. Carbohydr. Polym. 233, 115852 (2020).
32. Stévant, P. et al. Concise review of the red macroalga dulse, Palmaria palmata (L.) Weber & Mohr. J. Appl. Phycol. 35, 523–550 (2023).
33. Deniaud, E., Quemener, B., Fleurence, J. & Lahaye, M. Structural studies of the mix-linked β-(1→3)/β-(1→4)-d-xylans from the cell wall of Palmaria palmata (Rhodophyta). Int. J. Biol. Macromol. 33, 9–18 (2003).
34. Wang, Y.-C. et al. Pore-Confined Silver Nanoparticles in a Porphyrinic Metal–Organic Framework for Electrochemical Nitrite Detection. ACS Appl. Nano Mater. 3, 9440–9448 (2020).
35. Levard, C., Hotze, E. M., Lowry, G. V. & Brown, G. E. Environmental Transformations of Silver Nanoparticles: Impact on Stability and Toxicity. Environ. Sci. Technol. 46, 6900–6914 (2012).

Chapter 4

Surface-enhanced Raman scattering (SERS) - based portable sensor for ultratrace detection of silver nanoparticles in seawater

Marine pollution is an environmental and economic concern due to its deleterious effects on biodiversity, food chain and impact on fishing and aquaculture. Metallic nanoparticles (MNPs) have been detected in marine water bodies, such as coastal waters, which can lead to their bioaccumulation in aquatic organisms, posing a final risk to human health. Silver nanoparticles (Ag NPs) are one of the most used MNPs due to their unique physicochemical properties which make them among the top four engineered NPs prioritized for human health risk. Unfortunately, the common detection methods used to determine their presence require laborious sample preparation procedures besides being cost and time consuming. Surface-enhanced Raman Scattering (SERS) offers unique advantages as detection tool due to its high selectivity and sensitivity, providing a promising approach for the development of highly sensitive sensor platforms, cost-effective, and with the potential for on-site detection. Thus, an indirect SERS strategy for Ag NPs detection was designed here. This strategy was tested using three commercial Ag NPs coated with polyvinylpyrrolidone (PVP) to determine their relative size (PVP-15nm Ag NPs and PVP-100nm Ag NPs) and aggregation (predefined Ag aggregates, PVP-50–80nm Ag NPs) impact. Results showed that this indirect SERS-based method had the capacity to detect and quantify single NPs and aggregates in artificial seawater in the range of mg/L using a portable Raman system. However, this range was far from the predicted environmental concentration of Ag NPs (ng/L). Therefore, a portable SERS-based detection modules was developed by integrating a microfluidic chamber and

SERS substrate immobilization with the aim of improving system portability and sensor robustness in terms of reproducibility and specificity. This SERS-on-a-chip was able to detect concentration of Ag NPs and sulfidated Ag NPs in organic matter-contained seawater (i.e., water collected from aquarium in which mussels were cultured) in the ng/L range.

Chapter 4

4.1.Introduction

Nanomaterials[1]handling these nanometric systems require defining specific parameters to establish the possible advantages and disadvantages in specific applications. This review presents the fundamental factors of nanoparticles and its microenvironment that must be considered to make an appropriate design for medical applications, mainly: (i are becoming more and more prevalent as ingredients for several consumer products including paints, personal care items, food, and cosmetics.[2–4] Silver nanoparticles (Ag NPs) are, among others, one of the most used metallic nanoparticles (MNPs) mainly due to their antibacterial properties and widely used in consumer products, such as textiles, disinfectants and filtration membranes where the particles can be found in both solid or liquid (coating and spray) state.[5] Despite all the promising applications, there is a growing concern about associated risks to humans and ecosystems. The production, transport, washing, or disposal of products containing Ag NPs are only some of the steps that could lead to Ag release into the environment compromising agricultural and fishery activities with a potential impact on human health.[6–8] Therefore, there is a growing need for an analytical method to directly detect these NPs present in the environment.

At present, there are different techniques that allow the detection and quantification of Ag NPs, including spectroscopic[9] and electrochemical methods,[10] and, for the majority, single-particle inductively coupled plasma mass spectrometry (sp-ICP-MS).[11–13] Although these techniques allow both qualitative and quantitative determination of NPs, it is crucial to develop equally accurate and fast methods for their characterization and environmental risk assessment on-site. The development of port-able sensors for their detection is also necessary since those will allow

decentralized monitoring and quick implementation of measures for risk mitigation.[14]

Taking advantage of the high scattering and plasmonic properties of Ag NPs,[15,16] specific detection methods based on surface-enhanced Raman scattering (SERS) could be developed. Unlike Raman spectroscopy, SERS overcomes the limitation due to weak signals by exploiting such metal NPs properties via electromagnetic enhancement mechanism to Raman signal increase.[17] This, coupled with chemical interactions between molecular probe and plasmonic NP and with the ability of metal surfaces to quench the fluorescence background when both are in close proximity, makes SERS sensitive enough to detect trace amounts for analysis even at the single molecule level.[18] A non-overlapped spectra with a narrow bandwidth sensitive to slight changes in molecule structures and orientation is the output of this technique.[19]

The applicability of SERS in the detection of nanostructures, like Ag NPs, has been already reported, where a Raman reporter molecule, ferbam (ferric dimethyl-dithiocarbamate), allowed the detection of NPs in mg/L range in complex matrices after strong interactions were established.[20] Also, SERS detection of Ag NPs in dietary supplement products and nasal spray was reported.[21] However, higher Ag NPs concentrations were used (20 mg/L) and a microRaman spectrometer was employed for the detection. The concentration used was far from the predicted environmental concentration (PEC) for these MNPs, which is in the range of ng/L of total silver in surface water.[22] Therefore, the main aim of this chapter was to design a detection system that could be implemented in a portable Raman system, allowing its future use for point-of-care monitoring, despite the initial limitations of those systems such as less spatial resolution, less sensitivity, less reproducibility, and lower control of emission losses.

Thus, an indirect SERS strategy for Ag NPs detection in water by correlating the enhancement of SERS signal of 4-aminobenzenethiol (4ABT) attached to gold nanostars (Au NSs) with the presence of Ag NPs in seawater was developed. Seawater was selected as an environmentally relevant medium since coastal waters are one of the main sinks at the end-of-life of Ag NPs-containing products, mainly through treated and untreated wastewater discharges.[23] Au NSs were selected as a highly efficient SERS substrate due to the high localization of the electromagnetic field at their tips and their consequent behavior as individual hot spots allowing zeptomole detection of molecules attached to their surface.[24–26] 4ABT was chosen as Raman reporter due to both, its aromatic nature that confers a high Raman cross-section and its functional groups, -SH and -NH_2, which strongly interact with Au and Ag. In fact, 4ABT has been already used as Raman reporter molecule to detect Ag

NPs in dietary supplement products as commented above. In this case, 4ABT interacted with Ag surface via the formation of S-Ag bond.[27] In this work, a different approach was carried out: first, 4ABT was conjugated to the Au NSs and, as a consequence, its free amino group was available to bind Ag NPs.[28] The enhancement of SERS signal produced in presence of Ag NPs can be thus explained by inter-particles AgNPs-AuNSs interaction via 4ABT generating hot spots, which increases the concentration of electromagnetic field at these sites and, as a consequence, the enhancement of SERS signal also occurs.[29] This enhancement depends on the plasmonic properties of Ag NPs, which in turn depend on the physicochemical properties of the NPs such as size, shape, aggregation state, and surface coating. To investigate the effect of these parameters, three commercially available Ag NPs coated with polyvinylpyrrolidone (PVP) were selected. PVP is a widely used water-soluble polymer whose role as stabilizing agent is well known.[30,31] The molar ratio between silver and macromolecule (i.e., polymer) is usually enough to prevent or at least slow down aggregation and dissolution processes over time.[32] Having similar surface properties due to the presence of PVP, the effect of the size on SERS enhancement, using two Ag NPs with a diameter of 15 (PVP-15nm Ag NPs) and 100 nm (PVP-100nm Ag NPs), and the effect of the aggregation, including a predefined product formed by Ag aggregates coated with PVP with a primary NP size of 50–80 nm (PVP-50–80 Ag NPs), was studied. The colloidal stability of the selected Ag NPs in seawater was already assessed in chapter 2.

Ag NPs interaction with 4ABT-coated Au NSs was characterized by transmission electron microscopy (TEM) and the colloidal stability of Au NSs in seawater by UV-Vis spectroscopy. Calibration curves for all Ag NPs, were made in seawater using a portable Raman system. Using this approach, the limits of detection (LoDs) obtained with a portable Raman system were similar to the ones obtained using a Raman confocal microscope despite having lower spatial resolution and detector sensitivity.[33,34]powerful instruments for laboratory experiments or handheld instruments for in situ point detection. We have chosen to examine the performance of certain benchtop Raman probe systems with the goal of developing an inexpensive, portable system that could be used to operate in a field forensics laboratory to examine explosives-related residues or samples. To this end, a rugged, low distortion line imaging dispersive Raman spectrograph was configured to work at 830 nm laser excitation and was used to determine whether the composition of thin films of plastic explosives or small (e.g., ≤10 μ m However, the LoDs obtained were in the mg/L range, far behind from the PEC stated to be in the ng/L range for Ag NPs in surface water compartments.[35] For this reason, after verifying the ability of the indirect SERS strategy in detecting Ag NPs in seawater, a further approach was also developed, where plasmonic

nanostructures, 4ABT-functionalized Au NSs, were immobilized onto solid substrates and integrated into microfluidic platforms, with the aim of gaining sensitivity, efficiency and system portability. Integrated solid phase substrates together with metallic nanostructures were already investigated and reported for their SERS enhancement efficiency,[36,37] as well as microfluidic devices are currently used for the detection of trace substances, environmental monitoring, medical diagnosis, food safety and organ chips among many other applications.[38–42]

Here, a flexible, cost-effective, and easy sample preparation solid substrate, based on the abovementioned approach, was combined with a re-usable microfluidic chip to achieve Ag NPs trace detection in seawater ensuring a rapid on-site monitoring system. This time, detection levels in the ng/L range were achieved by using more realistic media (i.e., synthetic seawater containing organic particulate released from mussels cultured in aquarium, named here as mussel seawater), as well as the ability of the sensor in detecting Ag NPs after environmental transformation processes.

4.2. Results and discussion

4.2.1. Detection of Ag NPs in artificial seawater using in-suspension SERS approach: a proof of concept

Au NSs were selected as SERS active substrate because they offer an enhancement factor of the Raman signal up to 10^{12} thanks to the lowest-energy, localized surface plasmon mode highly concentrated at the apex of the tips.[43,44] In addition, the core of the Au NSs acts as an electron reservoir due to strong plasmonic coupling effects, contributing significantly to the enhancement of SERS signal. Au NSs were synthesized by reducing a gold (III) salt in N,N-dimethylformamide (DMF) in the presence of a high concentration of PVP and preformed 13 nm-spherical PVP-coated Au seeds (Figure 1) (Synthesis details in Annex I, section 5.1).

TEM analysis of Au NSs reveals a particle size diameter of 63 ± 7 nm (Figure 2, a – b). The UV-Vis spectrum of Au NSs showed two LSPR modes, one of them showing a maximum wavelength in the near infrared region (NIR) at 753 nm, related to a plasmon mode localized at the NSs tips and, a second lower mode, at 540 nm, associated with the internal core. Therefore,

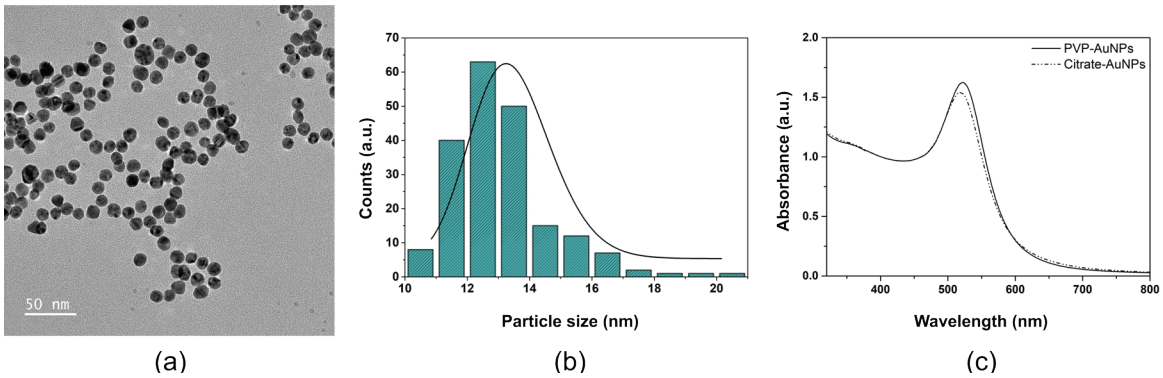

Figure 1. (a) Representative TEM images of spherical Au NPs used as seed in the Au NSs synthesis and (b) the relative histogram. TEM analysis relevels a diameter of 13 ± 2 nm. (c) UV-Vis spectrum before and after PVP coating of AuNPs.

785 nm laser was selected as excitation source adopted for the SERS measurements, because this laser overlaps with the LSPR mode at the tips (Figure 2, c). In addition, this laser was selected to avoid any photodegradation of the probe molecule (4-aminobenzenethiol, 4ABT) used and reduce the possible matrix interference suppressing the fluorescence background and absorption from organic matter dissolved in real water samples.

Before performing SERS experiments, the colloidal stability of Au NSs was assessed in order to confirm that the chosen SERS substrate was not affected by the influence of the surrounding environment. As explained before, level of aggregation, formation of hot-spot regions, and modification of the involved particles could modify the SERS sensitivity also affecting the system reproducibility.[45] Au NSs were tested for their colloidal stability in both, ultrapure water and synthetic seawater, for a period of time of 30 min, which would be the maximum analysis time for Ag NPs detection. Recorded spectra showed that Au NSs were not affected by the surrounding media and the presence of high ionic strength was not able to modify their initial colloidal stability (Figure 2, c – d).

SERS is a surface-sensitive technique and, by coupling metallic surfaces with a reporter molecule, it is possible to increase not only the sensitivity but also the specificity toward the interested analyte. Au NSs were then functionalized with 4ABT, which is able to form a self-assembled monolayer (SAM) on the Au surface by forming S-Au bond. As a consequence, a strong SERS signal in-suspension (i.e., average SERS) was recorded (Figure 2, e, black spectrum).[46]

This average SERS spectrum displays three peaks at 1589, 1077, and 390 cm^{-1}, which correspond to ring stretching vibrations.[47] The amine group of 4ABT, in para-substitution, has a strong interaction with Ag surface, allowing a specific detection of Ag NPs. This

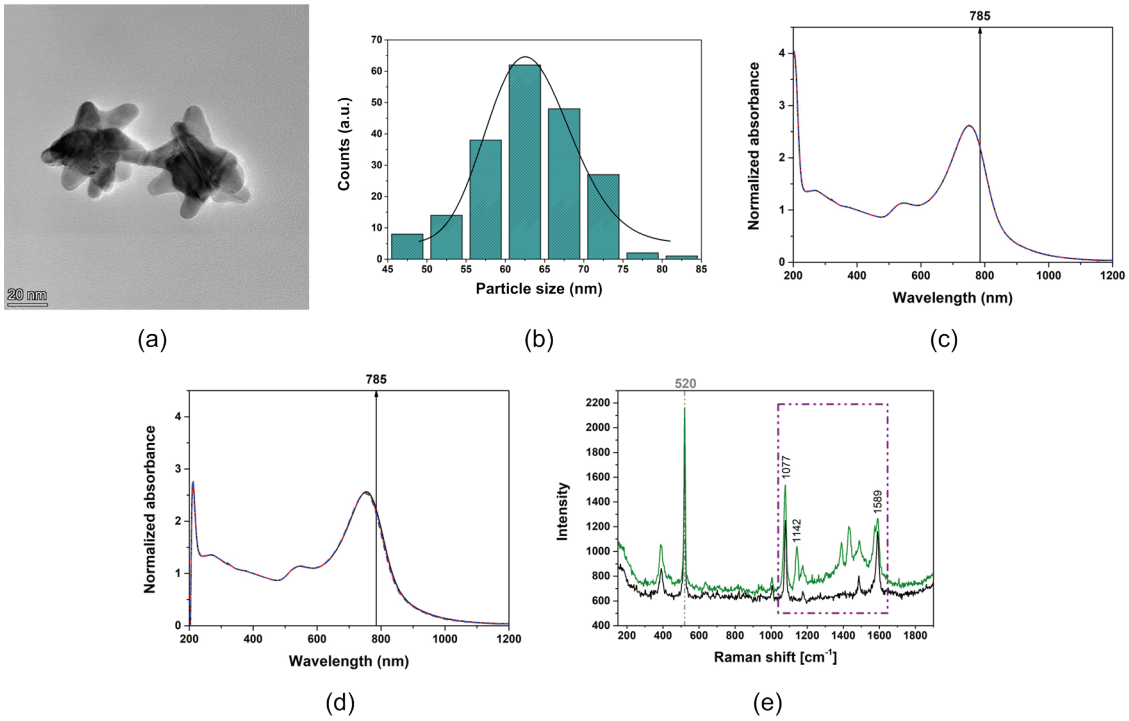

Figure 2. (a) TEM image of Au NSs and (b) relative particles size distribution and Gaussian fitting estimated on an average of 200 particles analyzed. Scale bar of 100 nm. (c) Average SERS spectra of 4ABT-functionalized Au NSs (1 mM of Au NSs, black line) and sandwich-like configuration of AgNPs-4ABT-AuNSs (0.5 mM of Au NSs in the presence of 25 mg/L of PVP-100nm Ag NPs, green line). The characteristic peaks of 4ABT (purple dashed rectangle, C-H ring bending 1142 cm^{-1} and ring stretching 1077 and 1589 cm^{-1}) are shown. The light-grey dashed line indicates the characteristic peak of silicon (520 cm^{-1}) that was used as internal standard. Au NSs stability in (c) ultrapure water and (d) artificial seawater is shown. Times of 0, 15, and 30 min are represented by black, red, and blue lines, respectively. Black arrows show the wavelength excitation source at 785 nm used for SERS analysis.

interaction between the amine group and Ag NPs generated very clear changes in the SERS spectrum of 4ABT (Figure 2, e, green spectrum). Apart from the obvious enhancement of the SERS intensity, four additional peaks are observed: 1142, 1175, 1390, and 1431 cm^{-1} that correspond to C-H ring bending vibrations. Despite its extensive use in SERS, it is common to consider p-ABT as a molecule with an abnormal enhancement mechanism depending on both substrates (i.e., Au and Ag) and used experimental conditions.[48,49] In this case, the system could be considered to form a sandwich-like configuration of AuNSs-4ABT-AgNPs (Figure 3, a) and the selective enhancement of those peaks can be associated with the charge transfer mechanism (i.e., charge transfer between both metal NPs coupled with the vibrations of 4ABT), as reported by Zhou et al.[46]

In this work, it is proposed an indirect detection method based on changes in the 4ABT SERS signal in presence of Ag NPs. The choice was made due to the increase in

the selectivity by covalent interaction of the amino group with the Ag surface and the enhancement of SERS signal produced by the formation of sandwich-like configuration AgNPs-4ABT-AuNSs that could be correlated with the Ag NPs concentration. The correlation among different Ag concentrations was determined by the analysis of the band at ~ 1080 cm^{-1}, the one supposed to arise from electromagnetic field enhancement coupled with chemical enhancement.[50] The in-suspension SERS analysis was performed (i.e., the measurements were done in liquid) and all integrated areas under the 1080 cm^{-1} peak were normalized with respect to those of silicon wafers (520 cm^{-1}) used for support and internal standard. Thus, average SERS spectra of 4ABT on Au NSs in the presence of different concentration of PVP-15nm Ag NPs with a portable Raman system and a confocal Raman system with a 10× objective were acquired to compare the performance. SERS measurements were carried out both in ultrapure water, as a control medium, and artificial seawater. A detailed analysis about Ag NPs behavior in both, ultrapure water and artificial seawater, is addressed in chapter 2 (section 2.3.1, 2.2.2), which demonstrated that PVP-15nm Ag NPs were colloidally stable in both media during at least 1 month.

Figure 4, a – b show representative SERS spectra acquired in both, ultrapure water and artificial seawater, as well as the relative calibration curves where the error bars indicate standard deviations of three independent experiments, obtained in both media (ultrapure water, in green, and artificial seawater, in red) and using both Raman systems. For both ultrapure water and seawater, the plot of the ratio between the areas under the peaks at 1080 (4ABT) and 520 (Si) cm^{-1} against Ag NPs concentration showed a good linear correlation with r^2 values of 0.8464 (ultrapure water) and 0.9403 (seawater) for the portable Raman system and 0.9162 and 0.9137 for the confocal Raman system, when PVP-15nm Ag NPs were analyzed. The limit of detection (LoD) was calculated from the sensitivity of the

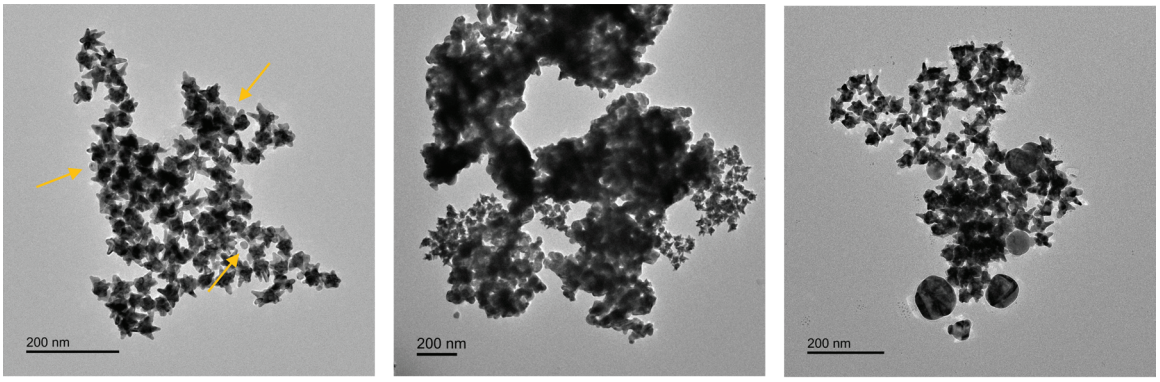

Figure 3. TEM images of AgNPs-4ABT-AuNSs interaction. (a) PVP-15nm Ag NPs, (b) PVP-50-80nm Ag NPs, and (c) PVP-100nm Ag NPs in ultrapure water. Scale bar of 200 nm. Yellow arrows pointing at Ag NPs.

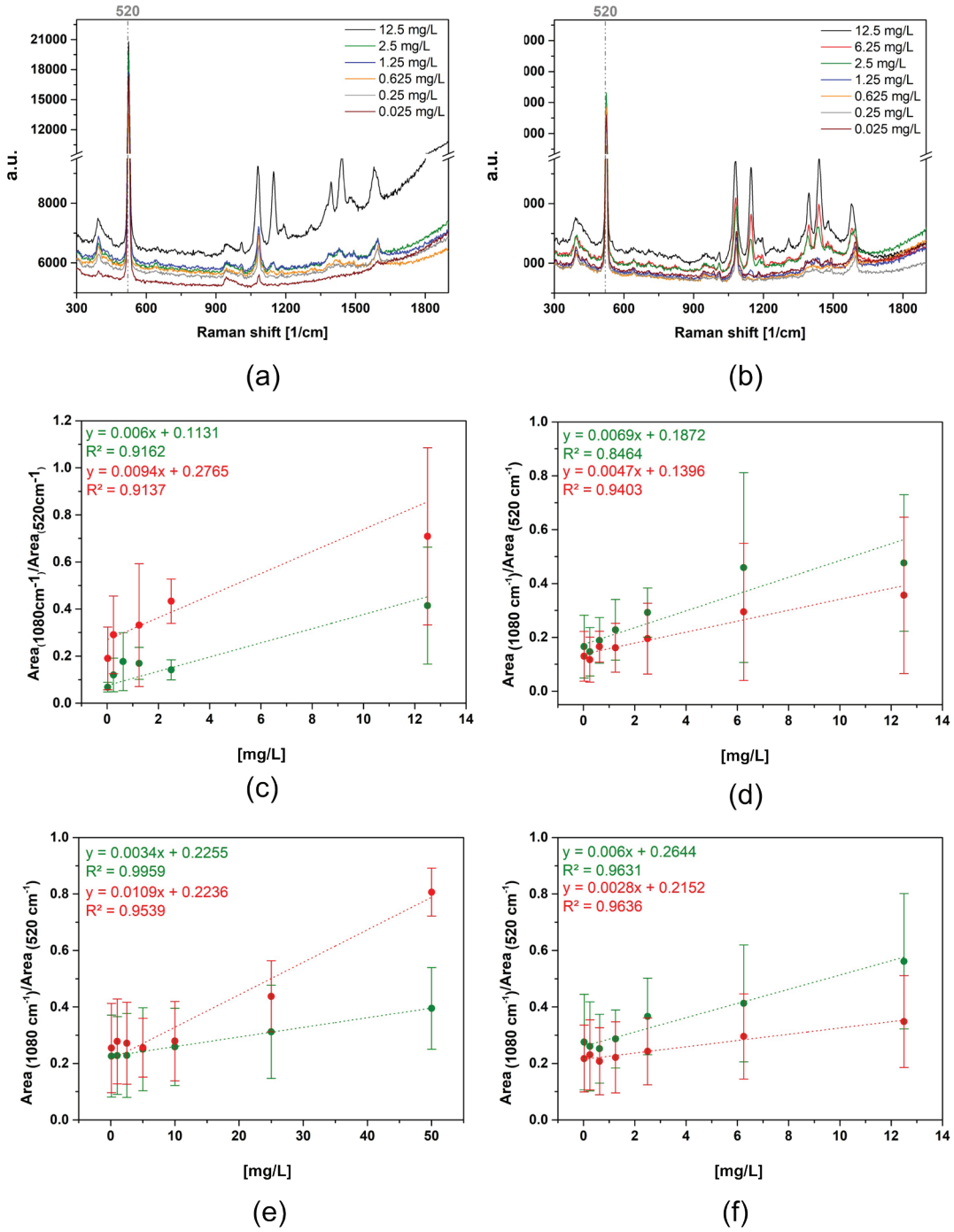

Figure 4. Calibration curve of PVP-15nm Ag NPs acquired by (a, c) Confocal Raman and (b, d) portable Raman system. (e) PVP-50-80nm Ag NPs and (f) PVP-100nm Ag NPs detection obtained by portable Raman system in ultrapure water (green line) and artificial seawater (red line).

calibration curve using the equation 3.3SDy/a, where SDy is the standard deviation of the response of the curve and a is the slope of the calibration curve. LoD values were similar for both media and the two Raman systems: 3.08 ± 1.47 (ultrapure water) and 2.15 ± 1.22 mg/L (seawater) for the portable Raman system and 3.12 ± 2.28 (ultrapure water) and 2.17 ± 0.93 mg/L for the confocal Raman system. The similar performance shown for both

systems can be explained by the fact that an average SERS strategy (i.e., in liquid) for Ag NPs detection was selected, and therefore no advantage has been taken from the better spatial resolution of the confocal Raman system.

SERS analysis about the possible effect of the particle size and aggregation degree of Ag NPs was performed using only the portable Raman system. Thus, a set of SERS measurements using the same conditions as before for PVP-15nm Ag NPs, PVP-50-80nm Ag NPs, and PVP-100nm Ag NPs were carried out. The analysis of the colloidal stability of PVP-50-80nm Ag NPs, and PVP-100nm Ag NPs (chapter 2, section 2.3.1, 2.2.2) demonstrating that both PVP-15nm and PVP-100nm NPs remained colloidally stable in artificial seawater while PVP-50-80nm Ag NPs formed bigger aggregates in seawater but keeping the size stable over time, allowing to study the effect of size and aggregates in SERS performance. Figure 4 shows the calibration curves for PVP-50-80nm Ag NPs (e) and PVP-100nm Ag NPs (f) obtained in both ultrapure water and artificial seawater. A better fit was obtained in relation to PVP-100nm Ag NPs (r^2 of 0.9631 in ultrapure water and 0.9636 in seawater) and PVP-50-80nm Ag NPs (r^2 of 0.9959 in ultrapure water and 0.9539 in seawater) in comparison with PVP-15nm Ag NPs. This is probably due to the better coupling of the LSPR band (Chapter 2, Figure 4) to the 785 nm excitation wavelength and the higher local electromagnetic field generated from NPs with bigger size.[47] However, similar LoD values were obtained in ultrapure water: 2.28 ± 1.46 mg/L for PVP-100nm Ag NPs and 3.75 ± 1.00 mg/L for PVP-50-80nm Ag NPs, which may be related to AgNPs-4ABT-AuNSs sandwich-like configuration (Figure 3, b and c). The enhancement is produced in the gap between Au NSs and Ag NPs and not all the surface area of Ag NPs is covered by 4ABT. Interestingly, it was observed a different behavior of the detection in seawater. The LoD values were similar for Ag NPs that remained colloidally stable in seawater, i.e., PVP-15nm Ag NPs (LoD = 2.15 ± 1.22 mg/L) and PVP-100nm Ag NPs 1.51 ± 0.71 mg/L), while LoD for Ag aggregates increased 4-fold (6.08 ± 1.21 mg/L), demonstrating that aggregation has an extremely high impact on the sensitivity of our average SERS approach. This can be explained in terms of decreasing the available surface area that interacts with 4ABT-AuNSs (Figure 3, b). Nonetheless, a pre-concentration step should be a considerable improvement to bring the detection level down to an order of magnitude relevant to environmental concentrations, i.e., ng/L range. In the next section, the use of titanates nanowires (Ti NWs) films as optical accumulators will be explored.

4.2.2. *Microfluidic device development for in-situ detection of Ag NPs in seawater using SERS*

From the preliminary results obtained, 4ABT functionalized Au NSs revealed to be an efficient detection strategy to monitor the presence of Ag NPs in seawater. However, the technique showed some limitations. Firstly, the limit of detection was still too far from the PEC, stated to be in the ng/L range. Secondly, performing the measurement in liquid, the aggregation degree of NPs was not controllable, resulting in poor reproducibility of the detection measurements. In addition, despite a portable Raman was used, the overall portability of the system was compromised due to the need to prepare the substrate solution every time before analysis, affecting the ease of use of a ready-to-use device.

In light of this, the previous developed indirect SERS strategy was implemented by supporting the 4ABT-coated Au NSs on the porous structure of titanates nanowires (Ti NWs) film and subsequently their integration with a microfluidic device. This configuration allows the filtration of larger volumes of water, while retaining Ag NPs on 4ABT-coated Au NSs so that their SERS signal variation could be monitored. Thus, this hybrid composite involving negatively charged Au NSs attached to positively charged polyallylamine hydrochloride (PAH)-coated Ti NWs was supported on a 0.45 μm nylon membrane. This configuration provided a dense network of active SERS substrate without blocking the filter pores, allowing a relatively fast flow of the water sample and the accumulation of Ag NPs in a specific area defined for the size of the microfluidic device. This SERS-on-a-chip system acts as an optical accumulator for Ag NPs quantification in seawater, improving its stability and reproducibility.

The fabrication of this SERS-on-a-chip involved several steps. The Ti NWs were prepared as previously described by Negrín-Montecelo et al.,[51] (more details in Material and methods). After cleaning the Ti NWs to reach a neutral pH, the Ti NWs were coated with PAH and subsequently with Au NSs by electrostatic interaction since PAH coating gives a positive surface charge to Ti NWs and Au NSs display a negative surface charge (Zeta potential is -14 ± 7 mV).

The Au NSs-coated Ti NWs were then functionalized with 4ABT, which acted as Raman reporter in this approach (Figure 5a). Thus, the SERS active hybrid substrate was ready to integrate in the lab-made polymethyl methacrylate (PMMA) chamber. To do so, the chamber had to be first assembled. Figure 5, b – c show a schematic representation and real pictures of the components and dimensions of the PMMA chamber. Two PMMA square

parts with a dimension of 4.7 x 4.7 cm and 0.3 cm of thickness were screwed together, while holding in between two polydimethylsiloxane (PDMS)-made O'-rings and a nylon membrane, guaranteeing the perfect sealing of the system. The chamber contained one inlet and two outlets, providing lateral and vertical flow. Importantly, the top PMMA part involved a sensing window of 0.5 cm of diameter and covered with a glass coverslip.

The microfluidic device was then connected to a syringe pump using the inlet, filled with water using the outlet that offered the lateral flow and subsequently the active hybrid substrate dispersion was injected using the outlet that offered the vertical flow. The control over the flow allowed the solution to gradually penetrate the nylon membrane providing a uniform substrate distribution on the sensing window. 3 mL of water were then passed through the filter to remove the unbounded moieties.

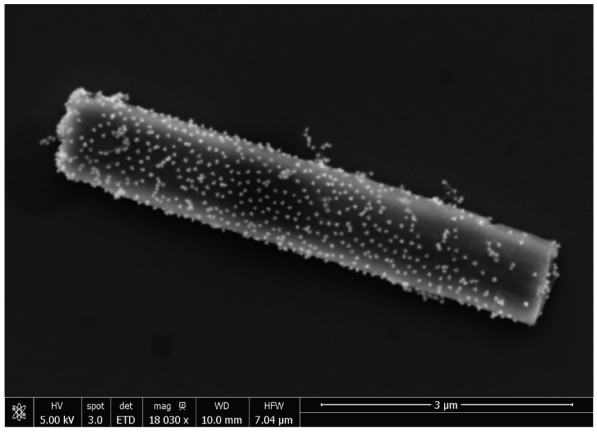

(a)

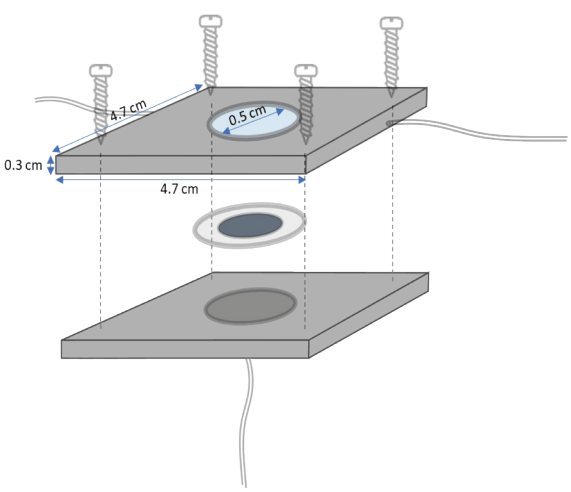

(b)

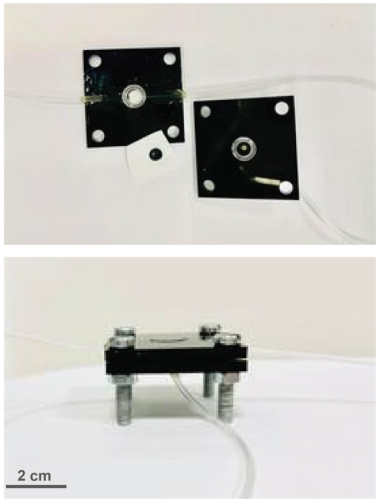

(c)

Figure 5. (a) SEM analysis of Ti NWs functionalized with Au NSs. (b) Schematic representation and (c) real images of the lab-made fabricated microfluidic chamber.

In figure 6a a representative SEM image of 4ABT-AuNSs-coated Ti NWs after immobilization onto the nylon membrane is shown.

At this point, the analyte containing suspension was injected, the pre-concentration of Ag NPs by filtering the dispersion occurred and their detection using SERS following the characteristic peak of 4ABT centered at 1080 cm-1 was performed. Figure 6b shows a SEM image of the active SERS hybrid substrate after its interaction with PVP-50-80nm Ag NPs. EDX analysis confirmed the presence of the NPs after filtering the dispersion using the lab-made PMMA chamber (Figure 6c). Thus, a set of SERS spectra of 4ABT using the active SERS hybrid substrate film, which acted as an optical accumulator inside the microfluidic chamber in the presence of different Ag NPs concentrations, were acquired using a portable Raman system. Considering the previous results, this time, the measurements were performed in mussel seawater (i.e., seawater containing organic matter released from cultured mussels in aquarium), considered a more realistic medium given the final application of the device.

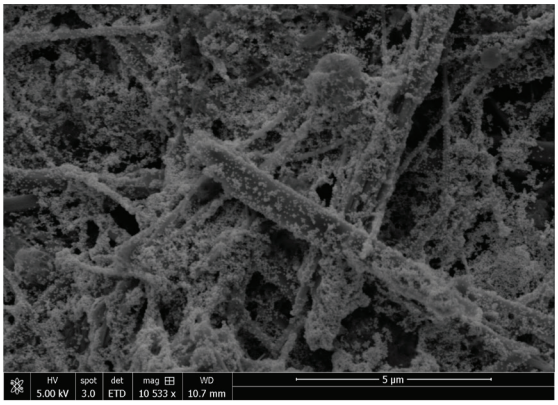

(a)

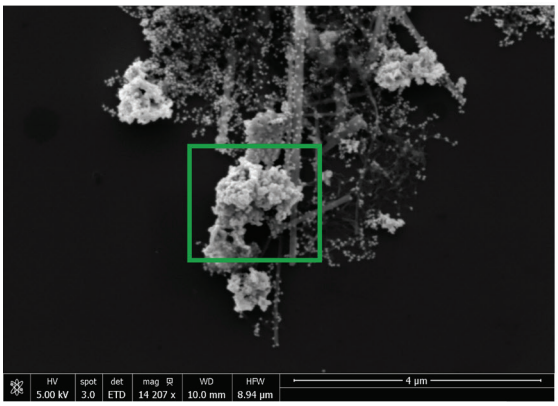

(b)

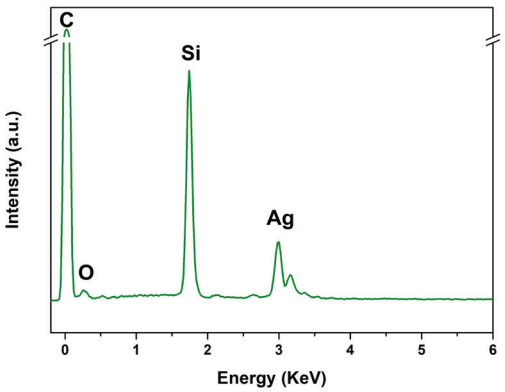

(c)

Figure 6. (a) TiNWs-AuNSs after immobilization onto the solid substrate. (b) TiNWs-AuNSs after interaction with PVP-Ag NPs and (c) related EDX spectra confirming the presence of Ag NPs.

Correlation among Ag concentrations was determined following the previous analysis, where changes in the intensity of the band at 1080 cm^{-1} were analyzed by integrating the area under the peak. However, in this case the integrated area was normalized respect to the one recorded in absence of Ag NPs (initial value of 4ABT attached to Au NSs).

Figure 7 shows the calibration curves built for PVP-15nm Ag NPs, PVP-50-80nm Ag NPs and PVP-100nm Ag NPs dispersed in mussel seawater in 0 – 100 ng/L range. Error bars indicate standard deviations from three independent experiments, showing more reproducibility between replicates than in-suspension SERS approach. Good linear correlation with r^2 values of 0.981 for PVP-15nm Ag NPs, 0.994 for PVP-50-80nm Ag NPs and 0.996 for PVP-100nm Ag NPs were respectively recorded. LoDs were calculated followed the abovementioned method and values of 11.49 ± 2.55 ng/L, 16.56 ± 8.25 ng/L and 8.89 ± 1.44 ng/L were obtained for PVP-15nm Ag NPs, PVP-50-80nm Ag NPs and PVP-100nm Ag NPs respectively. Spectra were recorded until saturation of the detection area was reached, which was achieved first for smaller particles, at 80 ng/L and later, at higher concentrations, for bigger particles or particles-forming aggregates, at 100 ng/L. This can be attributed to the fact that at equal mass concentrations, 15nm Ag NPs contain ≈6-fold higher number of NPs than 100nm Ag NPs and, therefore, the saturation of the sensing area was reached at lower mass concentration for smaller NPs. Interestingly, the aggregation of the particles shows to have a lower impact on the sensitivity of the technique than in the previous in-suspension SERS strategy, since only a slightly increased of LoD was recorded for PVP-50-80nm Ag NPs. This is likely due to the fact that the interaction was produced on a supported SERS substrate instead of having the Au NSs in-suspension.

As discussed in Chapter 3, Ag NPs can undergo transformation processes (i.e., dissolution, sulfidation, chlorination) while in the environment or after internalization into living organisms. Results showed that the main transformation involving PVP-15nm Ag NPs after cellular uptake was the sulfidation, transformation considered important in seawater compartments.[52] The formation of Ag_2S from the sulfidation of Ag NPs in seawater would have an important impact on SERS enhancement, which does not mean "a decrease in the signal". The contribution of charge-transfer in the SERS effect of Ag and Ag_2S NPs are different, being higher in the case of Ag_2S as reported by Fu et al.[53] For this reason, to understand the impact of the sulfidation on the SERS-based sensor developed here, Ag_2S-coated Ag NPs were prepared using sodium sulfide as sulfur source and PVP-15nm Ag NPs as reference NP.

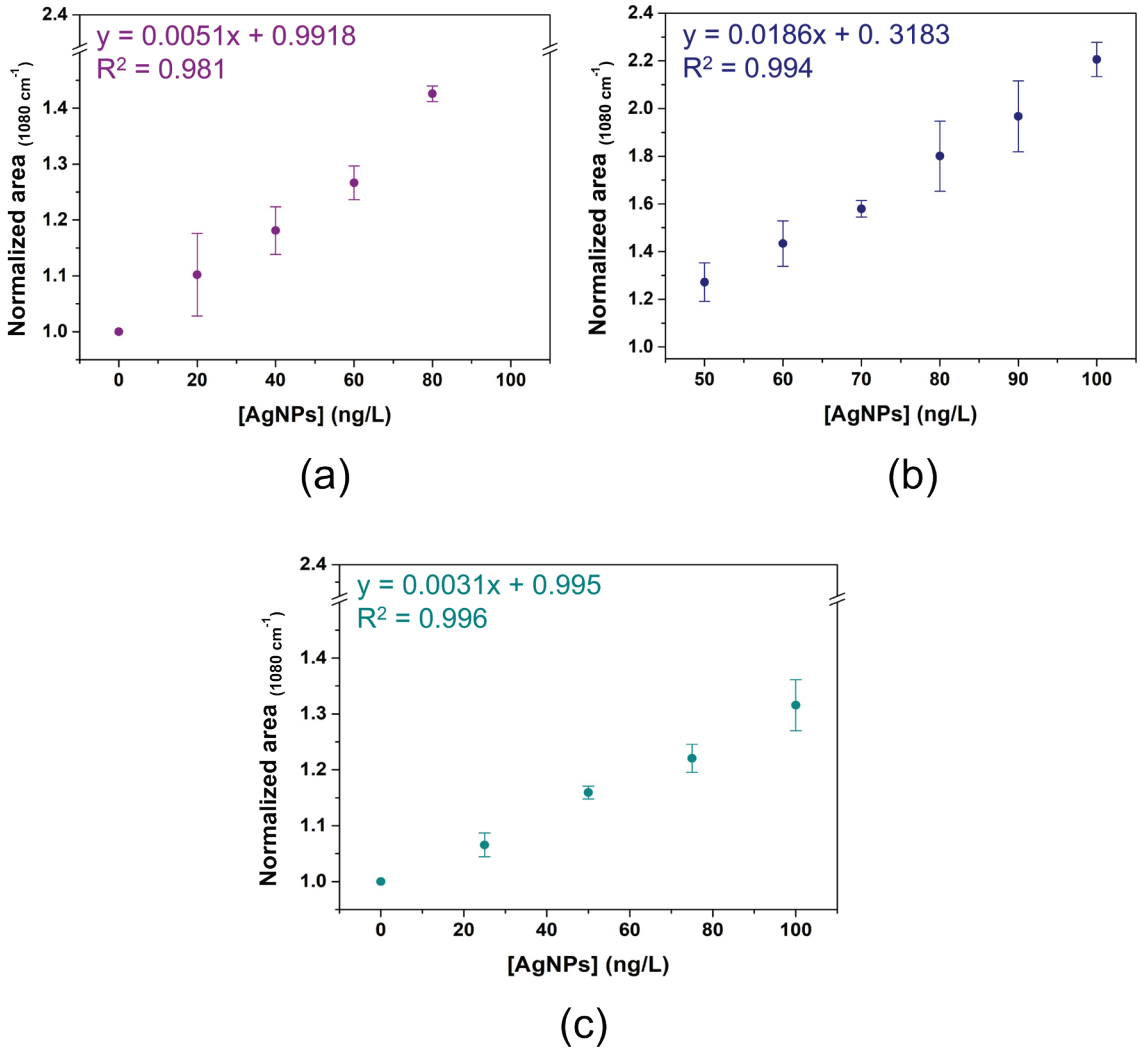

Figure 7. Calibration curve of (a) PVP-15nm Ag NPs (b) PVP-50-80nm Ag NPs and (c) PVP-100nm Ag NPs detection in mussel water obtained after substrate immobilization, microfluidic integration and using the portable Raman system for the detection.

Different concentrations of sodium sulfide, from 0 to 10 mM, were added to PVP-15nm Ag NPs as previously described.[54] The formation of Ag_2S layer on Ag NPs were characterized by UV-Vis spectroscopy. Figure 8a shows the UV-Vis spectra acquired of pure Ag NPs and Ag NPs after sodium sulfide addition at different concentrations. A variation in LSPR band of Ag NPs was clearly observed. The LSPR band underwent a blue-shift at concentration of Na_2S below 250 µM, which may be attributed to the decrease in size of the pure Ag core and the formation of non-uniform Ag_2S shell.[55] As showed in Figure 8, already at 2.5 mM there was an acute damping of the LSPR band, which occurs when complete Ag_2S shell is formed.[55] Among all the sulfur ions concentrations used, from 0.005 to 10 mM range, only five concentrations were selected to perform further tests, discarding

the highest concentrations of Na_2S since they displayed the same optical properties that the one obtained with 2.5 mM of Na_2S. The selected NPs were characterized also by DLS (Table 1), showing that they remained colloidally stable after the sulfidation process. The original Ag NPs, Ag@Ag_2S NPs (0.25 mM Na_2S) and Ag@Ag_2S NPs (2.5 mM Na2S) were also analyzed by HRTEM and an estimation about Ag/S ratio was also calculated by performing EDX analysis (Figure 9).

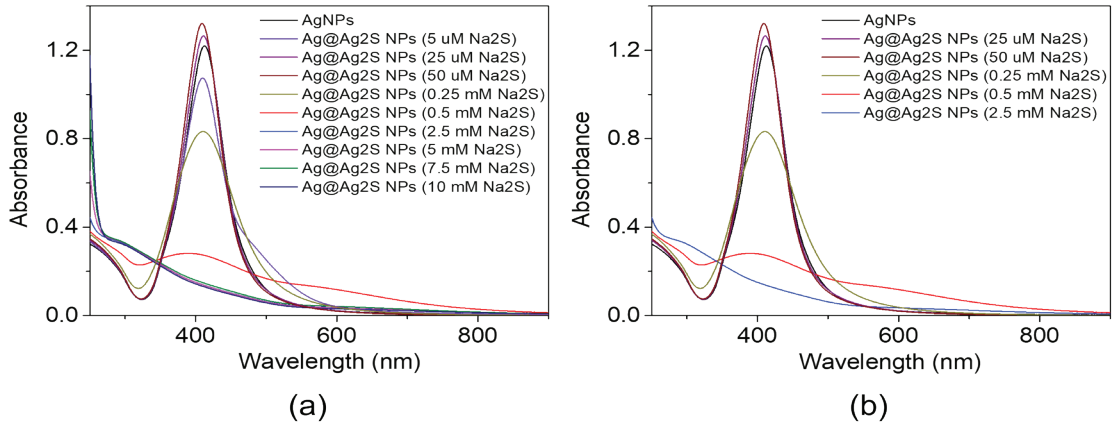

Figure 8. (a) UV-Vis extinction spectra of Ag@Ag_2S NPs from 0.005 to 10 mM range and (b) extinction spectra of the selected concentrations.

	Ag@Ag2S NPs	
Sample	***Hydrodynamic diameter[1] (nm)***	***PDI (%)[2]***
PVP-15 nm Ag NPs	47.84 ± 1.45	0.36 ± 0.05
Ag@Ag2S NPs (25 uM Na2S)	61.82 ± 1.49	0.40 ± 0.05
Ag@Ag2S NPs (50 uM Na2S)	60.88 ± 0.69	0.38 ± 0.02
Ag@Ag2S NPs (250 uM Na2S)	46.44 ± 0.40	0.34 ± 0.01
Ag@Ag2S NPs (500 uM Na2S)	45.14 ± 0.87	0.35 ± 0.06
Ag@Ag2S NPs (2.5 mM Na2S)	52.92 ± 0.47	0.19 ± 0.03

[1] Mean hydrodynamic diameter and [2] polydispersity index obtained by DLS at a scattering angle of 173° and 25 °C. DLS measurements were carried by quintupled: mean ± standard deviation (SD).
[3] Zeta potentials were measured in 5 runs (mean ± SD).

Table 1. Hydrodynamic size distribution of Ag@Ag_2S NPs at different sulfur ions concentrations.

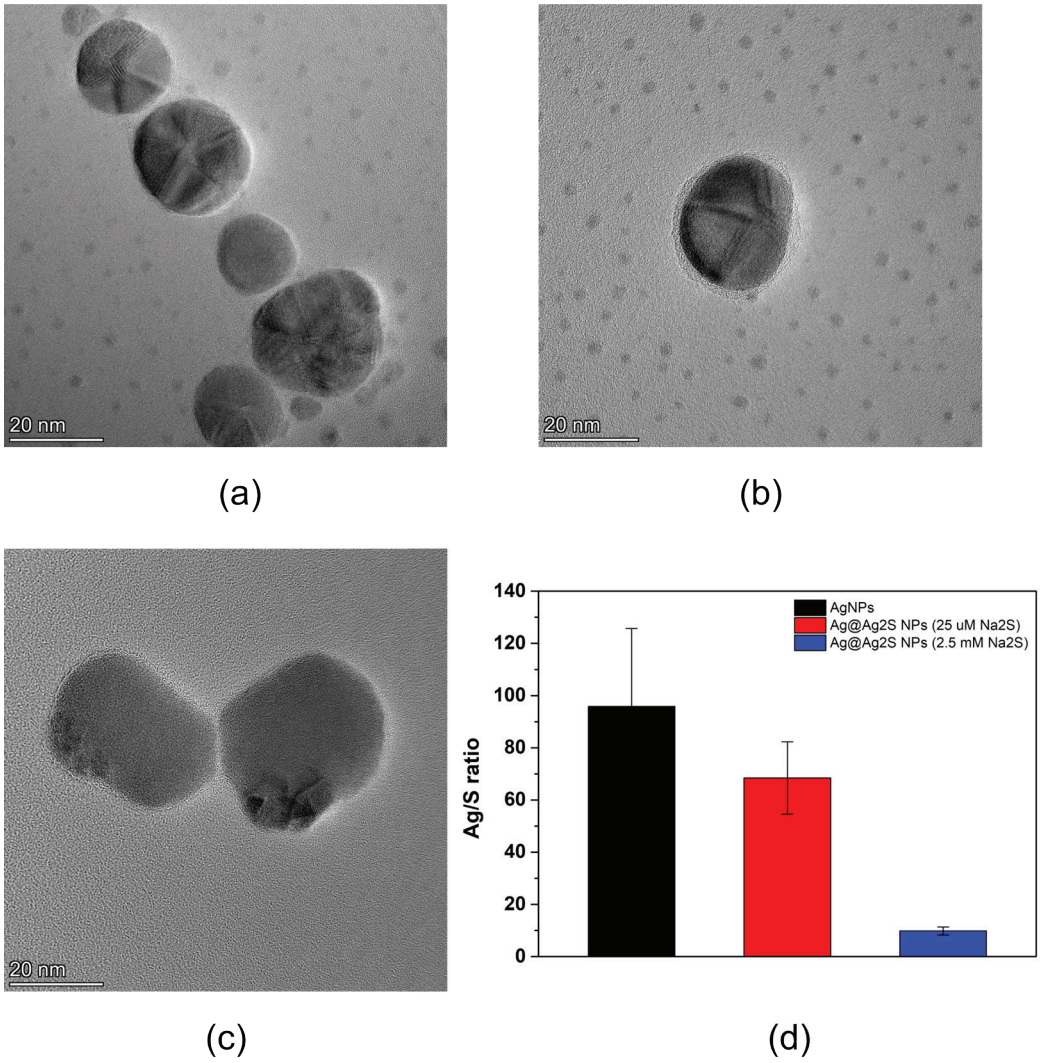

Figure 9. HRTEM of (a) PVP-15nm Ag NP and Ag@Ag2S NPs at (a) 0.025 mM and (b) 2.5 mM. (d) Histograms representing an estimation of Ag/S ratio at different concentration. Scale bars of 20 nm.

An estimation of the Ag/S ratio was determined by calculating the percentage of the mass fraction of Ag and sulfur (S) in the examined particles. More particles needed to be analyzed to have more precise results, but preliminary tests demonstrated how the Ag/S ratio decreased when the sulfur ions concentration in the particles increased, confirming the formation of Ag_2S onto Ag surface.

The selected particles, besides PVP-15nm Ag NPs used as control, were tested for their detection by using both approaches presented here, in-suspension SERS detection (i.e., a liquid dispersion placed on Si wafer) and SERS-on-a-chip (i.e., the integration with the microfluidic device). Based on the calibration curves obtained before (Figure 4, Figure 7), Ag concentrations of 4 mg/L for in-suspension SERS detection and 50 ng/L for SERS-

on-a-chip were selected to study the effect of sulfidation in Ag NPs detection. This time, for a system simplification, ultrapure water was the medium selected for particles dispersion (Figure 10).

Figure 10 shows the correlation between SERS signal and Ag_2S formation on Ag surface. It can be noticed that at 25 and 50 µM concentration of Na_2S, the SERS signal from the in-suspension method remained unchanged from the signal obtained with the original Ag NPs, being also the concentrations that provoked less change on the plasmonic properties of Ag NPs (Figure 8). For the SERS-on-a-chip, and for lower concentration of the in-suspension method, the signal decreases with the increase of Na_2S concentration added, except for Ag@Ag_2S NPs (2.5 mM Na_2S) detected using the SERS-on-chip system. Further studies are necessary to completely understand the behavior at higher sulfidation, since the contributions of charge-transfer in the SERS effect of Ag and Ag_2S NPs are different as previously reported.[53]

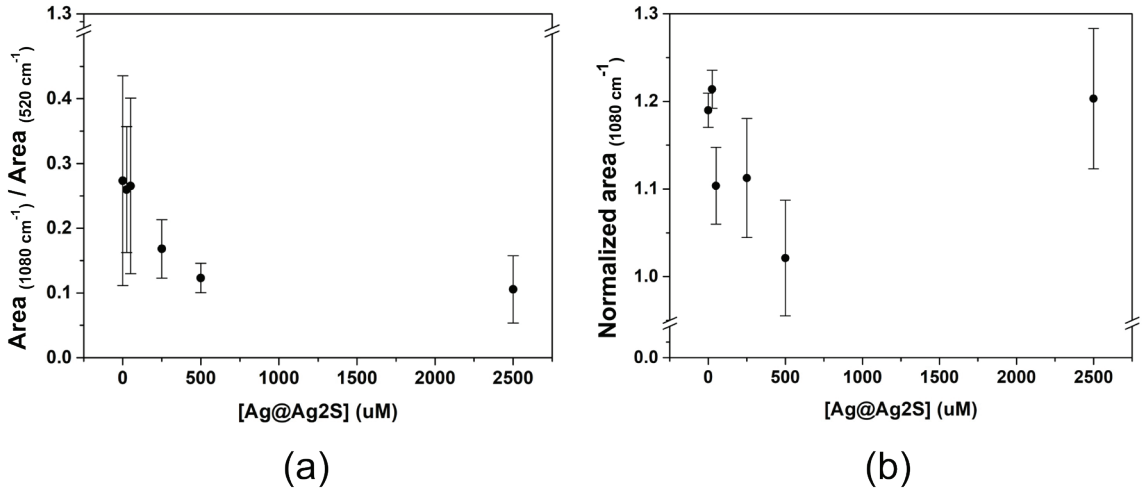

Figure 10. SERS detection of PVP-15nm Ag NPs at different concentration of Na_2S on Ag surface using (a) in-suspension method normalized against the Si wafer integrated area and by (b) SERS-on-a-chip where the integrated areas were normalized toward the blank condition (i.e., initial NPs suspension).

4.3. Conclusions

An indirect in-suspension SERS strategy for the detection of PVP-coated Ag NPs in artificial seawater using a portable Raman system was designed. Within this in-suspension SERS strategy, it was possible to detect a concentration of Ag NPs down to 1.51 ± 0.71 mg/L. The sensitivity was affected by the aggregation of Ag NPs, increasing of almost 4-fold in the LoD when NPs were aggregated. However, the size of Ag NPs had a minimal impact on the sensitivity of the method: LoD of 2.15 ± 1.22 mg/L and 1.51 ± 0.71 mg/L for PVP-15nm Ag NPs and PVP-100nm Ag NPs respectively. Clearly, the in-suspension SERS strategy was able to detect and quantify single NPs and aggregates in artificial seawater; however, the LoDs obtained were far from the predicted environmental concentration (PEC) of Ag NPs (i.e., ng/L of total silver).

Considering the PEC for Ag NPs, a system involving SERS and a microfluidic technology was developed. This system involved the pre-concentration of Ag NPs by filtration through a SERS-substrate supported on a nylon membrane and placed into a lab-made polymethyl methacrylate (PMMA) chamber, followed by their detection using SERS. With this SERS-on-a-chip system, the linear range obtained was 0 – 80 ng/L for PVP-15nm Ag NPs and 0 – 100 ng/L for PVP-50-80nm Ag NPs and PVP-100nm Ag NPs, in seawater collected from mussels tanks, being able to detect environmentally relevant concentrations of Ag NPs in presence of organic matter. In this case, both aggregation and size had a minimum effect on the sensitivity of the method: LoD of 8.89 ± 1.44 ng/L, 11.49 ± 2.55 ng/L, 16.56 ± 8.25 ng/L for PVP-100nmAg NPs, PVP-15nm Ag NPs and PVP-50-80nm Ag NPs, respectively.

PVP-15nm Ag NPs were also sulfidized at different degree to study the impact of the transformation on the SERS-based method. Results showed that the sulfidation had a higher effect on the sensitivity and variability when the plasmonic properties were strongly modified.

Therefore, this SERS-on-a-chip sensor can overcome intrinsic difficulties related to conventional detection methods and prove to be a fast and sensitive monitoring not only for Ag NPs but also for other plasmonic NPs, being able to reduce time and cost of on-site detection systems.

However, something to keep in mind is that not only the Ag NPs transformation but also the presence of other plasmonic NPs (e.g., Pt, Pd, and Cu NPs from the catalysis and wood preservation industries) could have an impact on this analytical method. Therefore, it is not possible to rule out their interference in the detection system and calibration curves for Ag NPs detection must be performed also in the presence of these NPs (including Ag_2S). It is then possible that mixed signals will be obtained with the added contribution of several types of plasmonic NPs, preventing the exact identification; however, in this case, it was possible to extract a correlation in terms of "Ag NPs equivalents", which would nevertheless have high impact as an early warning system.

References

1. Auría-Soro, C. et al. Interactions of nanoparticles and biosystems: Microenvironment of nanoparticles and biomolecules in nanomedicine. Nanomaterials 9, (2019).
2. Sarfraz, J., Gulin-Sarfraz, T., Nilsen-Nygaard, J. & Pettersen, M. K. Nanocomposites for Food Packaging Applications: An Overview. Nanomaterials 11, 10 (2020).
3. Wang, H. et al. Diagnostic imaging and therapeutic application of nanoparticles targeting the liver. J. Mater. Chem. B 3, 939–958 (2015).
4. Otsuka, H., Nagasaki, Y. & Kataoka, K. PEGylated nanoparticles for biological and pharmaceutical applications. Adv. Drug Deliv. Rev. 55, 403–419 (2003).
5. Fabrega, J., Luoma, S. N., Tyler, C. R., Galloway, T. S. & Lead, J. R. Silver nanoparticles: Behaviour and effects in the aquatic environment. Environ. Int. 37, 517–531 (2011).
6. Benn, T. M. & Westerhoff, P. Nanoparticle Silver Released into Water from Commercially Available Sock Fabrics. Environ. Sci. Technol. 42, 4133–4139 (2008).
7. Geranio, L., Heuberger, M. & Nowack, B. The Behavior of Silver Nanotextiles during Washing. Environ. Sci. Technol. 43, 8113–8118 (2009).
8. Tortella, G. R. et al. Silver nanoparticles: Toxicity in model organisms as an overview of its hazard for human health and the environment. J. Hazard. Mater. 390, 121974 (2020).
9. Corps Ricardo, A. I., Rodríguez Fariñas, N., Guzmán Bernardo, F. J., Rodríguez Martín-Doimeadios, R. C. & Ríos, Á. Screening-confirmation strategy for nanomaterials involving spectroscopic analytical techniques and its application to the control of silver nanoparticles in pastry samples. Spectrochim. Acta Part A Mol. Biomol. Spectrosc. 246, 119015 (2021).
10. Culková, E. et al. Voltammetric detection of silver in commercial products on boron doped diamond electrode: stripping at lowered potential in the presence of thiosulfate ions. Monatshefte für Chemie - Chem. Mon. 151, 1009–1017 (2020).
11. Mahdi, K. N. M. et al. Silver nanoparticles in soil: Aqueous extraction combined with single-particle ICP-MS for detection and characterization. Environ. Nanotechnology, Monit. Manag. 7, 24–33 (2017).
12. Yang, Y., Long, C.-L., Li, H.-P., Wang, Q. & Yang, Z.-G. Analysis of silver and gold nanoparticles in environmental water using single particle-inductively coupled plasma-mass spectrometry. Sci. Total Environ. 563–564, 996–1007 (2016).
13. Ramos, K., Gómez-Gómez, M. M., Cámara, C. & Ramos, L. Silver speciation and characterization of nanoparticles released from plastic food containers by single particle ICPMS. Talanta 151, 83–90 (2016).
14. Asamoah, B. O., Kanyathare, B., Roussey, M. & Peiponen, K.-E. A prototype of a portable optical sensor for the detection of transparent and translucent microplastics in freshwater. Chemosphere 231, 161–167 (2019).
15. Wu, M. et al. 3D Ultrasensitive Polymers-Plasmonic Hybrid Flexible Platform for In-Situ Detection. Polymers (Basel). 12, 392 (2020).
16. Willner, M. R. & Vikesland, P. J. Nanomaterial enabled sensors for environmental contaminants. J. Nanobiotechnology 16, 95 (2018).
17. Demirel, G. et al. Surface-enhanced Raman spectroscopy (SERS): an adventure from

plasmonic metals to organic semiconductors as SERS platforms. J. Mater. Chem. C 6, 5314–5335 (2018).
18. Hankus, M. E., Li, H., Gibson, G. J. & Cullum, B. M. Surface-Enhanced Raman Scattering-Based Nanoprobe for High-Resolution, Non-Scanning Chemical Imaging. Anal. Chem. 78, 7535–7546 (2006).
19. Culha, M., Cullum, B., Lavrik, N. & Klutse, C. K. Surface-Enhanced Raman Scattering as an Emerging Characterization and Detection Technique. J. Nanotechnol. 2012, 1–15 (2012).
20. Guo, H. et al. Analysis of silver nanoparticles in antimicrobial products using surface-enhanced raman spectroscopy (SERS). Environ. Sci. Technol. 49, 4317–4324 (2015).
21. Nguyen, T. H. D., Zhou, P., Mustapha, A. & Lin, M. Use of aminothiophenol as an indicator for the analysis of silver nanoparticles in consumer products by surface-enhanced Raman spectroscopy. Analyst 141, 5382–5389 (2016).
22. McGillicuddy, E. et al. Silver nanoparticles in the environment: Sources, detection and ecotoxicology. Sci. Total Environ. 575, 231–246 (2017).
23. Shi, W. et al. Ocean acidification increases the accumulation of titanium dioxide nanoparticles (nTiO 2) in edible bivalve mollusks and poses a potential threat to seafood safety. Sci. Rep. 9, 1–10 (2019).
24. Park, S., Lee, J. & Ko, H. Transparent and Flexible Surface-Enhanced Raman Scattering (SERS) Sensors Based on Gold Nanostar Arrays Embedded in Silicon Rubber Film. ACS Appl. Mater. Interfaces 9, 44088–44095 (2017).
25. Rodríguez-Lorenzo, L. et al. Gold Nanostars for the Detection of Foodborne Pathogens via Surface-Enhanced Raman Scattering Combined with Microfluidics. ACS Appl. Nano Mater. 2, 6081–6086 (2019).
26. Rodríguez-Lorenzo, L. et al. Zeptomol Detection Through Controlled Ultrasensitive Surface-Enhanced Raman Scattering. J. Am. Chem. Soc. 131, 4616–4618 (2009).
27. Kim, K., Kim, K. L., Shin, D., Choi, J. Y. & Shin, K. S. Surface-enhanced Raman scattering of 4-aminobenzenethiol on Ag and Au: PH dependence of b 2-type bands. J. Phys. Chem. C 116, 4774–4779 (2012).
28. Wu, D. Y. et al. Surface catalytic coupling reaction of p-mercaptoaniline linking to silver nanostructures responsible for abnormal SERS enhancement: A DFT study. J. Phys. Chem. C 113, 18212–18222 (2009).
29. Rycenga, M., Camargo, P. H. C., Li, W., Moran, C. H. & Xia, Y. Understanding the SERS Effects of Single Silver Nanoparticles and Their Dimers, One at a Time. J. Phys. Chem. Lett. 1, 696–703 (2010).
30. Mirzaei, A. et al. Characterization and optical studies of PVP-capped silver nanoparticles. J. Nanostructure Chem. 7, 37–46 (2017).
31. Tejamaya, M., Römer, I., Merrifield, R. C. & Lead, J. R. Stability of Citrate, PVP, and PEG Coated Silver Nanoparticles in Ecotoxicology Media. Environ. Sci. Technol. 46, 7011–7017 (2012).
32. Jiménez-Lamana, J. & Slaveykova, V. I. Silver nanoparticle behaviour in lake water depends on their surface coating. Sci. Total Environ. 573, 946–953 (2016).
33. Kelly, J. F., Blake, T. A., Bernacki, B. E. & Johnson, T. J. Design Considerations for a Portable Raman Probe Spectrometer for Field Forensics. Int. J. Spectrosc. 2012, 1–15 (2012).
34. Barone, G. et al. A portable versus micro-Raman equipment comparison for gemmological purposes: the case of sapphires and their imitations. J. Raman Spectrosc. 45, 1309–1317 (2014).
35. Wimmer, A., Markus, A. A. & Schuster, M. Silver Nanoparticle Levels in River Wa-

ter: Real Environmental Measurements and Modeling Approaches—A Comparative Study. Environ. Sci. Technol. Lett. 6, 353–358 (2019).
36. Lee, C. H., Hankus, M. E., Tian, L., Pellegrino, P. M. & Singamaneni, S. Highly Sensitive Surface Enhanced Raman Scattering Substrates Based on Filter Paper Loaded with Plasmonic Nanostructures. Anal. Chem. 83, 8953–8958 (2011).
37. Zhang, R. et al. Highly efficient SERS test strips. Chem. Commun. 48, 5913 (2012).
38. Zhang, Y. S. et al. Multisensor-integrated organs-on-chips platform for automated and continual in situ monitoring of organoid behaviors. Proc. Natl. Acad. Sci. 114, (2017).
39. Medina-Sánchez, M. et al. Microfluidic platform for environmental contaminants sensing and degradation based on boron-doped diamond electrodes. Biosens. Bioelectron. 75, 365–374 (2016).
40. Freitas, C. B., Moreira, R. C., de Oliveira Tavares, M. G. & Coltro, W. K. T. Monitoring of nitrite, nitrate, chloride and sulfate in environmental samples using electrophoresis microchips coupled with contactless conductivity detection. Talanta 147, 335–341 (2016).
41. An, X., Zuo, P. & Ye, B.-C. A single cell droplet microfluidic system for quantitative determination of food-borne pathogens. Talanta 209, 120571 (2020).
42. Seo, M. et al. Continuous Microfluidic Reactors for Polymer Particles. Langmuir 21, 11614–11622 (2005).
43. Pazos-perez, N., Guerrini, L. & Alvarez-puebla, R. A. Plasmon Tunability of Gold Nanostars at the Tip Apexes. (2018) doi:10.1021/acsomega.8b02686.
44. Rodríguez-Lorenzo, L., Álvarez-Puebla, R. A., de Abajo, F. J. G. & Liz-Marzán, L. M. Surface Enhanced Raman Scattering Using Star-Shaped Gold Colloidal Nanoparticles. J. Phys. Chem. C 114, 7336–7340 (2010).
45. Bell, S. E. J. & McCourt, M. R. SERS enhancement by aggregated Au colloids: effect of particle size. Phys. Chem. Chem. Phys. 11, 7455 (2009).
46. Zhou, Q., Li, X., Fan, Q., Zhang, X. & Zheng, J. Charge transfer between metal nanoparticles interconnected with a functionalized molecule probed by surface-enhanced Raman spectroscopy. Angew. Chemie - Int. Ed. 45, 3970–3973 (2006).
47. Hong, S. & Li, X. Optimal Size of Gold Nanoparticles for Surface-Enhanced Raman Spectroscopy under Different Conditions. J. Nanomater. 2013, 1–9 (2013).
48. Kim, K., Kim, K. L., Shin, D., Choi, J.-Y. & Shin, K. S. Surface-Enhanced Raman Scattering of 4-Aminobenzenethiol on Ag and Au: pH Dependence of b 2 -Type Bands. J. Phys. Chem. C 116, 4774–4779 (2012).
49. Wu, D.-Y. et al. Surface Catalytic Coupling Reaction of p -Mercaptoaniline Linking to Silver Nanostructures Responsible for Abnormal SERS Enhancement: A DFT Study. J. Phys. Chem. C 113, 18212–18222 (2009).
50. Kim, K., Choi, J.-Y., Lee, H. B. & Shin, K. S. Raman scattering of 4-aminobenzenethiol sandwiched between Ag nanoparticle and macroscopically smooth Au substrate: Effects of size of Ag nanoparticles and the excitation wavelength. J. Chem. Phys. 135, 124705 (2011).
51. Negrín-Montecelo, Y. et al. Titanate Nanowires as One-Dimensional Hot Spot Generators for Broadband Au–TiO2 Photocatalysis. Nanomaterials 9, 990 (2019).
52. Khaksar, M. et al. In Situ Chemical Transformations of Silver Nanoparticles along the Water–Sediment Continuum. Environ. Sci. Technol. 49, 318–325 (2015).
53. Fu, X., Jiang, T., Zhao, Q. & Yin, H. Charge-transfer contributions in surface-enhanced Raman scattering from Ag, Ag 2 S and Ag 2 Se substrates. J. Raman Spectrosc. 43, 1191–1195 (2012).
54. Ansari, J. R. et al. Enhanced near infrared luminescence in Ag@Ag2S core-shell

nanoparticles. Appl. Surf. Sci. 463, 573–580 (2019).
55. Mehrdel, B., Aziz, A. A., Yoon, T. L. & Lee, S. C. Effect of chemical interface damping and aggregation size of bare gold nanoparticles in NaCl on the plasmon resonance damping. Opt. Mater. Express 7, 955 (2017).

Chapter 5

General Conclusions

Even though specific conclusions have been presented at the end of each chapter, the most relevant, global conclusions of the research described in this thesis are summarised in the present chapter.

Chapter 5

General conclusions

As the production of MNPs is in rapid expansion, there is an urgent need to understand and predict the potential toxic effect related to it. Many factors such as NPs composition, dispersion medium, size and coatings can have an impact on the development of general regulations for NPs risk assessment in the environment.

This thesis work focused to bridge the gap between existence knowledge and future developments in relation to detection, identification and quantification of MNPs in marine species and water relevant to aquaculture. In this line, sample treatments were investigated to allow a more accurate particles analysis, as well as alternatives method based on electron microscopy and chemical analysis for NPs monitoring and identification upon living organism interaction. In addition, the development of a portable sensor based on surface-enhanced Raman scattering (SERS) for the detection of one of the most used MNPs, i.e., Ag NPs, was achieved allowing decentralized monitoring and implementation of risk mitigation measures.

More in detail, the main conclusions of this work can be summarized as follow:

- Surface functionalization plays a strong role in affecting MNPs stability in seawater: PVP coating kept colloidally stable the Ag NPs over a period of 28 days, where no aggregation or severe dissolution were recorded. The use of sodium citrate as stabilizer or the absence of coating, as in the case of TiO_2 NPs and ATO NPs respectively, led to aggregation phenomena right after media dispersion.

- TMAH digestion can be considered a valuable sample preparation technique to allow a reliable and reproducible NPs analysis after extraction from complex matrices (i.e., bivalve mussels). This sample preparation method was tested for the extraction of ATO NPs from mussels and no evident modifications on the ATO NPs were observed, in term of size or aggregation level. This allowed a good elemental recovery during the quantification. In addition, due to the only slight bioaccumulation of ATO NPs observed in bivalve mussels, they do not seem to pose concern to human health by seafood consumption.

- CPE proves to be an efficient technique for MNPs (i.e., TiO_2 and Ag NPs) pre-concentration in seawater. Clearly size, aggregation level and dispersion media played an important role in determining the success of the CPE. Increasing efficiencies were obtained going from smaller to bigger particles as well as from PVP-coated to citrate-coated NPs in presence of particulate organic matter, which makes the technique promising for environmental applications.

- The use of a set of electron microscopy techniques in combination with elemental analysis is a promising alternative tool to assess the bioaccumulation, biodistribution and transformation of MNPs in biota without the need of extracting them from the tissue. Results showed that monodispersed PVP-coated Ag NPs of 15 nm were internalized by edible seaweed already at early stage of exposure, while citrate-coated TiO_2 NPs, with the tendency to form aggregates, were not able to cross the external

cell wall and their interaction within seaweed surface was confirmed by SEM analysis. Ag NPs underwent sulfidation process after internalization, which was assessed using STEM-EDX analysis. Thus, the combination of different EM techniques and EDX analysis allows to obtain a more complete picture about NPs-organisms interaction, discriminating between surface interaction, particles internalization and NPs transformation processes.

- A SERS-on-a-chip portable sensor for a fast and sensitive monitoring of commercially available PVP-coated Ag NPs in real seawater samples was developed. The detection of environmentally relevant concentrations of Ag NPs in surface water (ng/L range) was reached by combining a sandwich-like configuration involving AuNSs-4ABT-AgNPs with the integration of a microfluidic device upon substrate immobilization. Results showed that aggregation and size have a minimum effect on the sensitivity of the system. However, further studies are required to assess the detection efficiency when other plasmonic NPs are present in the system.

In conclusion, this work provides reliable and reproducible tools for NPs extraction from complex matrices, including biota and water samples, as well as for their assessment in edible organisms. In addition, the development of a portable sensor to monitor the presence of NPs in seawater could be a valuable tool especially when water monitoring is needed for commercial purposes and could lead to a final potential toxicity to humans.

Appendix I

Matherials and Methods

In this Appendix experimental details used throughout the thesis are presented, including NPs characterization, bioaccumulation assays and preparation of SERS substrates.

Appendix 1

1. Nanoparticles characterization

1.1. *Antimony Tin Oxide Nanoparticles (ATO NPs) – Chapter 2*

ATO nanopowder, NanoArc®, 100% crystalline, was purchased from Alfa Aesar (Kandel, Germany). The powder was dispersed in different media (ultrapure water and synthetic seawater) by using an ultrasonic probe (Ultrasonics Digital Sonifier Model 450, Branson, USA) to reduce particles aggregation/agglomeration and then fully characterized. Hydrodynamic size and surface net charge was assessed by using a Zetasizer (SZ-100 device, Horiba, ABX SAS, Amadora, Portugal), while the primary size distribution was obtained by transmission electron microscopy (TEM) analysis (Tecnai F20 FEI), operating at 200 kV.

1.2. *Silver nanoparticles (Ag NPs) – Chapter 2, 3 and 4*

The three different Ag NPs used among this thesis work, have been characterized as follow. Ag NPs powders with a core diameter of 15 nm (PVP-15nm Ag NPs) and 50–80 nm (PVP-50–80nm Ag NPs) were supplied by SSNano (Houston, TX, USA; product code: 0127SH) and US Research Nanomaterials, Inc (Houston, TX, USA; product code: US1018), respectively, and used without any further purification. The powder composition was 25% wt silver and 75% wt polyvinylpyrrolidone (PVP) for PVP-15nm Ag NPs and 0.2% of PVP for PVP-50–80nm Ag NPs. Further, 1 g/L of Ag NPs dispersion was prepared in ultrapure water with a resistivity of 18.2 MW at 25 °C (Millipore apparatus, MQ Aquantage A10, Merck, Algés, Portugal) and sonicated for 15 min using a bath sonicator (Elmasonic P, Elma, VWR, Amadora, Portugal) (37 kHz, 100% at 25 ºC). The dispersion was stored at 4 ºC until further use.

An Ag NPs ink containing 30% wt Ag NPs dispersed in ethylene glycol was purchased from Sigma-Aldrich (Merck Life Science-Sigma Aldrich, Algés, Portugal; product code: 798738). In order to remove the ethylene glycol due to its toxicity[1], 4 g of Ag NPs ink were diluted with ultrapure water to reach a concentration of ethylene glycol of 0.15 – 0.3 M (30 – 15 mL final volume). The diluted ink was then dialyzed using a 12 kDa cellulose membrane (Merck Life Science Sigma-Aldrich, Algés, Portugal; product code: D6191) against ultrapure water for 6 h. After dialysis, Ag NPs were mixed with 24 mL of 150 g/L PVP solution, reaching an Ag:PVP ratio of 1:3 wt. The PVP-100nm Ag NPs dispersion was stored at 4 ºC until further use. The purification process and PVP coating of these Ag NPs were characterized by DLS (SZ-100 device, Horiba, ABX SAS, Amadora, Portugal) and UV-Vis spectroscopy (Perkin-Elmer LAMBDA 950 spectrophotometer, Scientific Laboratory Supplies, Wilford, Nottingham, UK).

Optical, colloidal stability and morphological particles characterization was carried out using UV-Vis-NIR spectroscopy (Perkin-Elmer LAMBDA 950 spectrophotometer, Scientific Laboratory Suppliers, Wilford, Nottingham, UK), size/zeta potential analyzer (SZ-100 device, Horiba, ABX SAS, Amadora, Portugal) and transmission electron microscopy (JEOL 2100 200 kV TEM, Izasa Scientific, Carnaxide, Portugal and JEOL JEM 1010 transmission electron microscope operating at 100 kV, Izasa Scientific, Madrid, Spain). Sample concentration of 12.5 mg/L for PVP-15nm Ag NPs and PVP-100nm Ag NPs and 50 mg/L for PVP-50–80nm Ag NPs was loaded into a quartz cuvette, 10 mm optical path, to perform dynamic light scattering (DLS) and UV-Vis analysis. A scattering angle of 90º and a working temperature of 25 ºC was used for hydrodynamic size determination. For TEM analysis, the particles were subjected to several centrifugation cycles (3 cycles of 60 min at 8960 g for PVP-15nm Ag NPs; 3 cycles of 15 min at 2500 g for PVP-100nm Ag NPs and 1 cycle of 10 min at 1500 g for PVP-50–80nm Ag NPs) to remove the excess of PVP that could interfere with the analysis. To prevent particles aggregation, several drops of the suspension were placed onto pure carbon 400 Ti mesh grids and an acceleration voltage of 200 kV was used.

1.3. *Titanium dioxide nanoparticles (TiO_2 NPs) – Chapter 2 and 3*

Commercially available 5 nm TiO_2 NPs, 25 nm TiO_2 NPs and 45 nm TiO_2 NPs were supplied by Nanostructured & Amorphous Materials, Inc. (Katy, TX, USA; anatase, 5 nm size, 99%) and Sigma-Aldrich (Merk Life science, products code: 718467 and 634662; 99.5% purity, mixture of rutile and anatase), and used without any further purification.

The NPs stock dispersions were prepared in ultrapure water (Millipore apparatus). Citrate-5nm TiO_2 NPs, citrate-25nm TiO_2 NPs and citrate-45nm TiO_2 NPs dispersions were prepared by dispersing a mixture of trisodium citrate dihydrate (Sigma-Aldrich) and TiO_2 powder at weight ratio of TiO_2:citrate 1:1.5 wt:wt for 5 and 45 nm NPs and 1:0.8 wt:wt for 25 nm NPs using an ultrasonic probe (Branson Desintegrator Ultrasonic Mod. 450) for 30 min, with 30 sec pulse on / 5 sec pulse off, and 50 % amplitude. The final concentration of all citrate-TiO_2 NPs suspensions was 15.5 g/L. The particles were stored at 4 ºC until further use.

The analysis of TiO_2 NPs stocks, size and shape, was performed using the JEOL 2100 TEM operating at 200 kV (Izasa Scientific, Carnaxide, Portugal) for 25 nm TiO_2 NPs, the JEOL JEM 1010 TEM operating at 100 kV (Izasa Scientific, Madrid, Spain) for 45 nm TiO_2 NPs and the FEI Titan Cubed Themis 60-300 kV operating at 200 kV (Thermo Fisher Scientific, Portugal) for 5 nm TiO_2 NPs. A formvar/carbon-coated copper grids 200 mesh were used for TEM analysis. The colloidal stability in ultrapure water and artificial seawater (35 ppm salinity) was characterized by DLS and zeta potential using the SZ-100 device (Horiba, ABX SAS, Amadora, Portugal). The nano crystallite size of 5 nm TiO_2NPs was estimated by XRD pattern using Scherrer equation. XRD pattern was collected on a X'Pert PRO diffractometer (PANalytical) set at 45 kV and 40 mA, using Cu Kα radiation (λ = 1.541874 Å) and a PIXcel detector.

1.4. *Silver based – silver sulfide nanoparticles (Ag@Ag_2S NPs) – Chapter 4*

Ag@Ag_2S NPs were synthesized following an already published protocol, where sodium sulfide (Na_2S) was used as sulfur source adsorbed onto the surface of PVP-15nm Ag NPs previously characterized (Section 1.2.)[2]. Nano-crystalline Ag@Ag_2S NPs were synthesized by soft chemical route varying the concentration of sulfur ions from 0.005 mM to 10 mM, while the concentration of Ag NPs remained constant. Briefly an aqueous solution of Na_2S was added dropwise to the Ag NPs solution under continuous shaking. The resultant dispersion was kept under shaking for 2 h at room temperature (RT) and color change of the suspension indicated the formation of Ag@Ag_2S NPs. The particles were stored at 4 ºC until further use.

Differences in absorbance and changes in hydrodynamic size were analyzed by UV-Vis-NIR spectroscopy (Perkin-Elmer LAMBDA 950 spectrophotometer, Scientific Laboratory Suppliers, Wilford, Nottingham, UK) and DLS analysis (SZ-100 device, Horiba, ABX SAS, Amadora, Portugal), respectively. TEM and EDX analysis were performed using FEI Titan Cubed Themis 60-300 kV operating at 200 kV (Thermo Fisher Scientific, Portugal).

2. Metal nanoparticles extraction methods – Chapter 2

2.1. Metal nanoparticles (MNPs) extraction from mussels using alkaline digestion

Five mussels were collected from each aquarium after 0, 7, 14, 21 and 28 days of exposure to the ATO NPs, de-shelled, the excess of water removed, and the total soft tissue frozen at –80 ºC until further processing.

Before alkaline digestion, the mussels were freeze-dried, and the dry weight recorded. The digestion approach involved the use of an aqueous solution of 10% (v/v) tetramethylammonium hydroxide (TMAH) and 2 h incubation using a bath sonicator (Elma, Elmasonic P), followed by a centrifugation step (2500 g, 20 min). The pellet obtained was subjected to a second 10% (v/v) TMAH digestion for 1 h. The mixture was centrifuged at 2500 g for 20 min and redispersed in 1% (v/v) sodium dodecyl sulphate (SDS) in order to improve the NPs separation from protein aggregates. In the last step, 15 mL of hydrogen peroxide (30% v/v H_2O_2) was gradually added to the suspension while heating at 70 ºC under stirring, reaching a final pale-yellow color, evidencing the complete organic fraction digestion. The solution was then cooled down and filtered using 5 µm pore size cellulose acetate (CA) filter. Standards were prepared by spiking the mussels with ATO NPs in the 0 – 2 mg/L range. Blanks were prepared to correct the results from the potential procedure contamination.

Total antimony (Sb) and tin (Sn) concentration was obtained using a NexIon® 2000 ICP-MS (Perkin Elmer, Waltham, MA, USA), while the quantification and size distribution of ATO NPs was assessed using the Syngistix™ Nano Application 2.5 software (Perkin Elmer) allowing to work in the single particle mode (sp-ICP-MS).

2.2 *Metal nanoparticles (MNPs) extraction and pre-concentration using Cloud Point Extraction*

Cloud point extraction (CPE) was the selected technique used to extract and pre-concentrate MNPs from water samples. Among others, commercially available PVP-15nm Ag NPs and PVP-100nm Ag NPs, as well as citrate-5nm TiO_2 NPs and citrate-45nm TiO_2

NPs were used to assess the efficiency of the CPE. Full particles characterization was addressed in Section 1 of this chapter. Synthetic seawater (35 ppm salinity) and seawater containing organic matter, referred to as "mussel seawater", were the chosen media to test the technique efficiency.

After dilution in seawater and mussel seawater, six independent NPs concentrations, in the range 0 – 5 mg/mL, were mixed with 4 mM Triton X-114 (TX-114) and 0.05 mL of hydrochloric acid (HCl, 37%), reaching a final volume of 40 mL. After vortexing for 10 sec, the dispersions were placed in a boiling water bath and incubated for 1 hour. Followed the separation of the two phases and the resuspension of the surfactant rich phase in 1 mL of ultrapure water (Figure 1).

Particles were then digested, and the total elemental quantification performed using inductively coupled plasma optical emission spectroscopy (ICPE-9000 Shimadzu).

Ag NPs digestion was performed by adding 0.75 mL of HCl (37%) and 0.25 mL of nitric acid (HNO_3, 65%) to 1 mL of both, surfactant-rich phase and aqueous solution, followed by overnight incubation at RT. The samples were diluted up to 12 mL with ultrapure water prior ICP-OES measurement.

TiO_2 NPs, instead, were subjected to microwave-assisted acid digestion by using a microwave reaction system (Anton Paar Multiwave 5000). Here, 1 mL of surfactant-rich phase and aqueous solution respectively, were transferred to the microwave Teflon vessels and mixed with 2 mL of concentrated sulfuric acid (H_2SO_4, 95-97%) and 1 mL of concentrated HNO_3 (65 %). The capped vessels were subjected to microwave irradiation after gradually reaching 200 ºC for 1 h. The digested samples were transferred to 15 mL plastic tube and diluted with ultrapure water reaching 12 mL final volume.

Internal standards of Ag and TiO_2, supplied by Sigma-Aldrich (Merk Life science, products code: 12818 and 12237), were subjected, as the related samples, to the acid or microwave digestion and used to build a nine-point calibration curve, in the 0.00 – 0.67 mg/L range. The elemental determination was obtained by monitoring the 328.068 and 337.28 nm wavelength for silver and titanium, respectively.

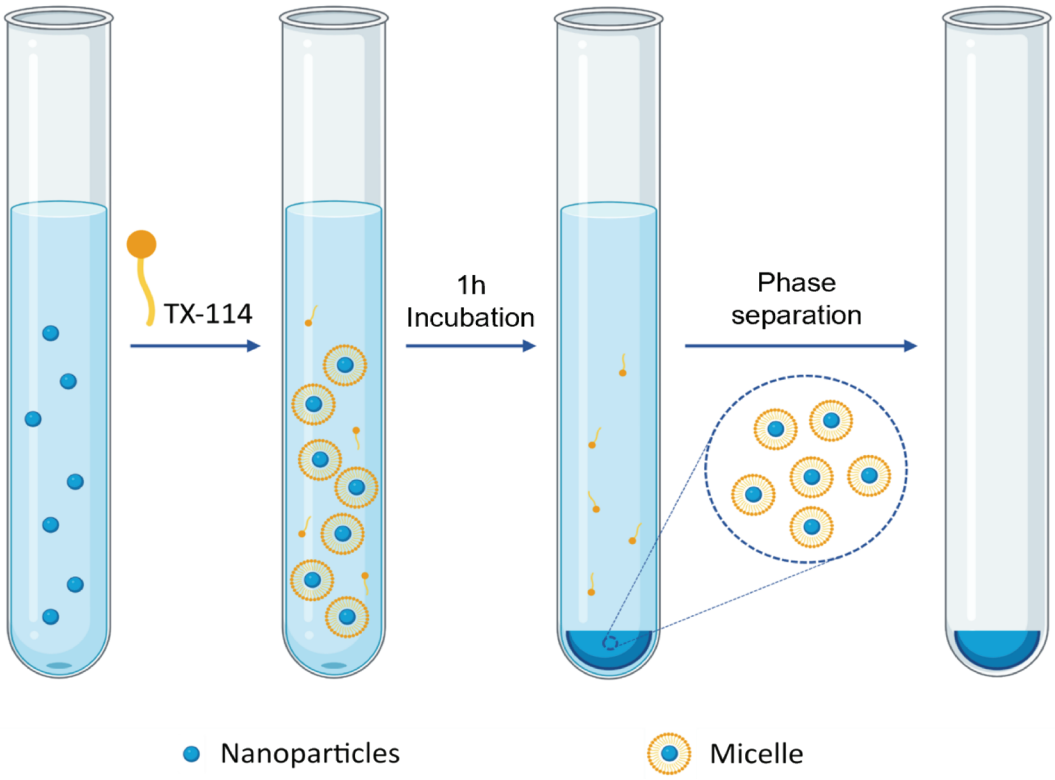

Figure 1. CPE representation scheme.

3. Bioaccumulation assays

3.1. Mussels exposure to Antimony Tin Oxide nanoparticles – Chapter 2

ATO NPs bioaccumulation assays were performed at the International Iberian Nanotechnology Laboratory (INL), using the eco-nanotoxicology facility according to the OECD test guidelines TG 305.

Adult mussels, *Mytilus galloprovincialis*, were obtained already depurated from a local company (Falcamar; Labruge, Portugal). The acclimation period to the laboratory conditions was at least one week. During this period, the water was periodically renewed and, temperature, salinity, conductivity, pH and oxygen saturation checked using a multiparametric probe (model HI98194, Hanna Instruments®). The temperature was kept

at 18 ± 2 ºC while alternating 14 hours of light to 10 hours of darkness. The animals were fed every other day with commercial food for filter feeders (NT Labs, United Kingdom). Forty-six mussels were randomly distributed into aquarium, filled with synthetic seawater, and individually aerated. For 28 days mussels were exposed, in triplicates, to ATO NPs at the nominal concentrations of 0 mg/L as control, 0.1 mg/L and 1 mg/L. Once per week, the total water from the aquarium was renewed and the NPs exposure was repeated by pre-mixing freshly prepared ATO NPs suspensions with microalgae, and subsequently poured into each aquarium. Two additional water renovations of 25% were performed every week. The sampling, occurring every 7 days, at 0, 7, 14, 21 and 28 days respectively, involved the collection of 5 mussels in total, 3 for ICP-MS analysis and 2 for electron microscopy investigation. Followed a washing step with ultrapure water for salts and contaminants removal. The samples were then frozen until further analysis.

Total and NPs quantification were performed at University of Santiago de Compostela (USC, Spain), while electron microscopy analysis was carried out at INL and UVigo.

3.2 *Seaweed exposure to Silver and Titanium dioxide nanoparticles – Chapter 3*

Seaweed bioaccumulation assays were performed at Indigo Rock Marine Research Station (Cork, Ireland).

Two different edible seaweed species, red Palmaria palmata and green Ulva fenestrata, were farmed for 28 days and exposed to two different sizes of Ag NPs, PVP-15nm and PVP-100nm and two different sizes of TiO_2 NPs, citrate-5nm and citrate-25nm. 0.1 and 1 mg/L were the tested concentrations, besides 0 mg/L, used as control condition where no NPs were added, and three additional replicates with the only citrate administration, used to evaluate the effect of NPs coating. Microalgae were fed with the cell-Hi F2P medium, a soluble nutrient blend commonly used for the production of marine microalgae, by adding twice a week, 30 mL (0.1 g/mL) of F2 media containing phytoplankton. Seaweeds were cultured in 40 L tanks, at 16 ± 1 ºC, alternating 2 hours of light to 12 hours of darkness. Temperature, salinity, pH and oxygen saturation were daily measured, while conductivity, ammonium, and nitrites were tested twice a week. 50% of the water was replaced twice per week, two days before and two days after NPs addition. The particles were added once per week to the F2 medium by micro pipetting and manual shaking to obtain the final concentration of 0.1 and 1.0 mg/L in the 40 L tanks.

The sampling, occurring every 7 days, at 0, 7, 14, 21 and 28 days respectively, involved the collection of 5 seaweed in total, 3 for ICP-MS analysis and 2 for electron microscopy investigation. Followed a washing step with ultrapure water for salts and contaminants removal. The samples were then frozen and ready to be shipped for further analysis.

Total and NPs quantification were performed at University of Santiago de Compostela (USC, Spain) (data not shown), while electron microscopy analysis was carried out at INL and UVigo.

3.3. *Clams exposure to Silver and Titanium Dioxide nanoparticles – Chapter 3*

Clams bioaccumulation assays were performed at the facilities of the Centro Tecnológico del Cluster de la Acuicultura (CETGA, Spain).

For the assays, Asiatic clams (*Ruditapes philippinarum*) were obtained already depurated from the local fish market. The acclimation period to the laboratory conditions was at least one week. During this period, running water was supplied, previously filtered through 5 µm cartridge filter. Temperature, salinity, pH, and oxygen saturation were recorded daily. The temperature was kept at 19,9 ± 0,8 ºC while alternating 14 hours of light to 10 hours of darkness. Clams were fed every other day with microalgae cultured onsite with strains supplied from IGAFA (Instituto Galego de Formación en Acuicultura, Spain) (50:50 ratio of diatoms and flagellates).

Forty clams were randomly distributed into aquarium and filled with 40 L of filtered seawater, using 5 µm cartridge filter and individual aeration stones. Clams were exposed for 28 days, in triplicates, to PVP-100nm Ag NPs at the nominal concentrations of 0 mg/L as control, 0.1 mg/L and 1 mg/L. Once per week, the total water from the aquarium was renewed and the NPs exposure was repeated by pre-mixing the freshly sonicated PVP-100nm Ag NPs suspensions with the microalgae, and subsequently poured into each aquarium. Two additional water renovations of 25% were performed every week.

The sampling, occurring every 7 days, at 0, 7, 14, 21 and 28 days respectively, involved the collection of 5 clams in total, 3 for ICP-MS analysis and 2 for electron microscopy investigation. Followed a washing step with ultrapure water for salts and contaminants removal. The samples were then frozen and ready to be shipped for further analysis.

Total and NPs quantification were performed at University of Santiago de Compostela (USC, Spain) (data not shown), while electron microscopy analysis was carried out at INL and UVigo.

4. Sample preparation for electron microscopy analysis – Chapter 2 and 3

A set of electron microscopy (EM) techniques were used to assess the presence and monitor the distribution of MNPs within biological samples, such as mussels, clams, and seaweed.

A conventional TEM preparation protocol, based on chemical fixation, sample dehydration and resin embedded, was followed here to make samples suitable for microscopy techniques, prior imaging.

Regarding seaweed exposure, the first steps for EM analysis were performed at Indigo Rock. Right after sampling, two seaweed per each specie from each treatment group were collected and 0.7 square cm fragments of algae blade leaf cut. When mussels or clams were collected at CETGA, instead, mantel, gills and digestive glands were isolated and cut into smaller fragments. The fragments were then fixated overnight at 4 ºC using the Karnovsky fixative solution, which involves a mixture of 2% paraformaldehyde and 2.5% glutaraldehyde in 0.1 M sodium cacodylate buffer, for organelles preservation. These fragments were stored at 4 ºC under shaking for later use. Bigger fragments of seaweed (around 2 square cm) for SEM analysis were fixated in 10% neutral buffered formalin for 48 hours (replacing the formalin solution every 24 hours) and subsequently stored in 70% ethanol at room temperature until further use. At this point, the sample were ready for shipping.

Sample preparation continued at INL by following the same steps for all the analyzed samples, using a EM TP Tissue processor (Leica microsystems). Followed a post-fixation process in which the fragments were post-fixated in 1% (v/v) osmium tetroxide (OsO_4) solution, dehydrated with increased ethanol concentration (from 50 to 100%) and subjected to a final resin infiltration. The infiltration was made with a mixture of propylene oxide and epoxy resin (EMBed-812 kit) at different proportion, gradually increasing the amount of resin to finally have the fragments completely embedded in it. The cure of the blocks was performed at 60 ºC for three days.

To obtain a semi-transparent sample, ultrathin sections (~70 nm thickness) were cut using a PowerTome PC ultramicrotome (RMC Boeckeler,USA) coupled with a diamond knife (Diatome) and collected onto TEM grids, according to sample requirements: formavar/carbon 200 mesh copper grids were used for ATO and TiO_2 NPs contained-sections and

100 mesh titanium grids for Ag NPs contained-sections. Once the grids were ready, a conventional TEM analysis at low magnification was performed using JEOL 2100 200 kV operating at 80 kV (Izasa Scientific, Carnaxide, Portugal) and JEOL JEM 1010 TEM operating at 100 kV, Izasa Scientific, Madrid, Spain) to study cellular ultrastructures and possible NPs-cell interactions. For further analysis of NPs internalization, their identification and their transformation were carried out by high-resolution scanning transmission electron microscopy (HR-STEM) coupled with energy-dispersive X-ray spectroscopy (EDS) using FEI Titan (G3) Cubed Themis 60-300 kV, operating at 60 kV and, a Probe-Corrected FEI Titan G2 ChemiSTEM TEM operating at an acceleration voltage of 80 kV.

In addition, scanning electron microscopy (SEM) in combination with an EDS detector, was employed to characterize the external tissue morphology and the possible NPs-tissue interaction for citrate-5nm TiO_2 NPs using a FEI Quanta 650 FEG SEM with an Everhart-Thornley secondary electron (ETD) operating at high vacuum, at an acceleration voltage of 10 kV and spot size of 3.0 (FEI Europe B.V.). SEM images for 25 nm TiO_2 NPs were acquired using a Helios G2 NanoLab 450S dual-beam focused ion beam SEM in combination with EDX, with an Everhart-Thornley secondary electron (ETD) operating at high vacuum, at an acceleration voltage of 10 kV (FEI Europe B.V). In this case, a very limited sample preparation was required: the sample was only cut and mounted onto aluminum stubs. The SEM samples were coated with conductive carbon using an EM ACE600 coating system (Leica microsystems). The obtained data form EDX were treated using Origin 9.0.

5. Surface-enhanced Raman spectroscopy-based sensor development – Chapter 4

5.1. Synthesis and functionalization of Gold Nanostars (Au NSs)

The synthesis of Au NSs followed the seed-mediated growth method, in which gold spherical nanoparticles (Au NPs) with a diameter of 13 nm work as seeds for the following star-shaped particles formation. Au NPs were obtained by in-house synthesis according to the reduction method developed by Turkevich et al.[3] where a small amount of gold salt is reduced by the presence of sodium citrate. Briefly, 250 mL of 0.5 mM of an aqueous solution of $HAuCl_4$ (Merck Life Science Sigma-Aldrich, Algés, Portugal) was brought to boil for 5 – 10 min while being kept under vigorous stirring. Then, 12.5 mL of a warm sodium citrate solution (1% wt/V; Merck Life Science, Sigma-Aldrich, Algés, Portugal) was quickly added. The formation of

Au NPs was confirmed by the color change of the dispersion from light yellow to dark red.

Once the synthesis was over, the suspension was cooled down until room temperature was reached and kept in the dark at 4 ºC until further use. For the coating, an aqueous solution containing 530 mg of polyvinylpyrrolidone (PVP) with a molecular weight (MW) of 10K (TCI Europe, Zwinjdrecht, Belgium) was prepared and added to the Au NPs solution to provide a ratio of 60 PVP molecules per nm^2. The reaction was left overnight under magnetic stirring and the PVP excess was then removed, performing a centrifugation step at 7000 g for 90 min. PVP-coated Au NPs were re-dispersed in ethanol and stored in dark condition at 4 ºC until further use. The formation of Au NSs took place by mixing 20 g of PVP-10K with 200 mL of N-dimethylformamide (DMF, Merck Life Science, Sigma-Aldrich, Algés, Portugal) in the presence of 0.5 mM of $HAuCl_4$ and 0.023 mM of preformed Au NPs seeds. After 20 min of reaction, the solution became dark blue, and 3 cycles of 60 min centrifugation were performed to finally re-disperse the solution in water.

The functionalization occurred by the conjugation of Au NSs with a Raman reporter molecule, 4- aminobenzenthiol (4-ABT; Merck Life Science, Sigma-Aldrich, Algés, Portugal), using 1:1 molar ratio. If freshly prepared, the reaction took place in 10 min, followed by 3 centrifugation steps in order to remove the 4-ABT excess (3300 g, 4 min).

5.2. Substrate immobilization

Au NSs previously synthesized were re-arranged and adopted as substrate for the integration with a microfluidic module. This time, the Au NSs were supported on titanates nanowires (Ti NWs) and retained onto a solid nylon filter. The negatively charged Ti NWs having a mean length >20 μm and a mean diameter of 57 nm were synthesized by the University of Vigo, Spain, following a previous reported protocol.[4] To allow the interaction with equally negatively charged PVP-coated Au NSs, the Ti NWs were subsequently coated with a layer of a positively charged poly(allylamine hydrochloride) (PAH) polyelectrolyte, dissolved in a 0.5 M solution of NaCl at pH 5 and reaching a final concentration of 1 mg/mL. After 15 min sonication, 5 mg of Ti NWs were added to 10 mL of the PAH solution and stirred for 30 min at room temperature. Three centrifugation steps (4000 g, 20 min) were performed to remove the reagent excess and reach the final concentration of 1 mg/mL. For the conjugation of PAH-Ti NWs with the Au NSs, 1 mL of the Ti NWs final solution was added to 30 mL of 0.14 mM Au NSs, previously prepared and incubated for one hour. A centrifugation step (2500 g, 15 min)

was performed redispersing the particles in 5 mL of water final volume. Before substrate immobilization, the Au NSs-PAH-Ti NWs- composite, was further functionalized with the Raman reporter, 4-ABT, using 1:1 molar ratio. At this point, the whole linked molecules were passed through a 0.45 μm pore size nylon membrane, held between a microfluidic device. A washing step with water was performed to remove the unbound moieties.

5.3. Microfluidic device

The sensing chamber was composed of two polymethyl methacrylate (PMMA) components (4.7x4.7x0.3 cm), assembled one on top of each other and held together by normal screws, and two O'-rings, made of polydimethylsiloxane (PDMS), that guarantee the tightness of the system. A lateral and vertical flow were ensured by the presence of two outlets, besides the presence of an inlet, while a glass sensing window placed on the top part of the chamber, having a diameter of 0.5 cm, allowed the detection. The nylon filter disc was placed in between the two O'-rings, acting as a support for the active substrate and a syringe pump was used to keep a steady flow, by setting 100 μL/min as flow rate. 1 mL of sample was injected each time.

The microfluidic device was lab-made, where the PMMA components and the O'-ring mould were designed in ArtCAM and fabricated using a Computer Numerical Control (CNC) - High Speed Milling System (FlexiCam Viper, Germany). Using the PMMA mould, O'-rings were fabricated by replica molding.

5.4. Surface-enhanced Raman spectroscopy (SERS)

For SERS average experiments, 4-ABT functionalized Au NSs were chosen as SERS substrate for the detection of different concentration of Ag NPs, in 12.5 – 0.025 mg/L range for single particles and 50 – 0.1 mg/L range for aggregates. Different concentrations of Ag NPs were added to the Au NSs suspension (1:1, v/v) and 20 μL of the suspension was then placed on a silicon wafer. The SERS measurements were carried out in liquid. Standards were prepared by diluting the testing Ag NPs in ultrapure water or synthetic seawater. The artificial seawater was prepared by dissolving a commercial salt (ICA Sal Marinho Basic Plus, Aqualovers, Portugal) in DI water (35 ppm salinity) in order to assess salt interference during detection.

SERS spectra were acquired using a 300 Alpha Confocal Raman (WiTEC, Ulm, Germany) using 10x objective and a portable Raman spectrometer (B&Wtek, ILC-Inst. De Lab. E Cientificos, Lisboa, Portugal) with an optical fiber configuration,

where 785 nm was the excitation laser line used. The spectra acquisition was performed for 3 seconds and with 1 scan per measurement and collected using a laser power of 70 mW and 50 mW for the Confocal and the portable Raman, respectively.

For the advanced version of the sensor, after integration with the microfluidic, only the portable Raman has been used, by performing spectra acquisitions for 10 seconds and 1 scan per measurement. 3 independent measurements were tested in order to build calibration curves in the 0 – 100 ng/L range using mussel seawater.

In both cases, the resulting SERS spectra were processed using SpectraGriph 1.2.14 software (Software for optical spectroscopy 2016-20 developed by Dr. Friedrich Menges, Oberstdorf, Germany) after being baseline corrected.

References

1. Moore, M. M., Kanekar, S. G. & Dhamija, R. Ethylene Glycol Toxicity: Chemistry, Pathogenesis, and Imaging. Radiol. Case Reports 3, 122 (2008).
2. Ansari, J. R. et al. Enhanced near infrared luminescence in Ag@ Ag2S core-shell nanoparticles. Appl. Surf. Sci. 463, 573–580 (2019).
3. Enüstün, B. V. & Turkevich, J. Coagulation of Colloidal Gold. J. Am. Chem. Soc. 85, 3317–3328 (1963).
4. Huang, J. et al. High-Temperature Formation of Titanate Nanotubes and the Transformation Mechanism of Nanotubes into Nanowires. Cryst. Growth Des. 9, 3632–3637 (2009).

Resumen

Detección, identificación y cuantificación de nanopartículas metálicas en acuicultura mediante microscopía electrónica y dispersión Raman aumentada por superficie

1. Ámbito de la tesis doctoral

Los nanomateriales artificiales (NMAs) son materiales fabricados intencionalmente con un tamaño final en un rango de 1 a 100 nm en al menos una dimensión. Los NMAs son diseñados y adaptados con el objetivo de dotarlos con propiedades fisicoquímicas específicas para mejorar características concretas de una gran variedad de productos industriales y así mejorar y/o potenciar su aplicabilidad. Debido a lo cual, ha habido un aumento exponencial en el uso de estos NMAs, y hoy en día se pueden encontrar en el mercado una gran cantidad de productos, desde cosméticos hasta productos médicos, que contienen dichos nanomateriales.

Sin embargo, el uso de NMAs puede tener un impacto negativo para el medio ambiente provocado por la liberación de estos nanomateriales al ecosistema durante todo su ciclo de vida; es decir, durante su fabricación, su uso, y al final de su vida útil. Es importante resaltar que aún se necesitan muchos estudios e investigaciones para entender el potencial efecto tóxico de estos nanomateriales una vez liberados, y más concretamente en aguas naturales. Tras su liberación, los NMAs pueden interaccionar con diferentes organismos acuáticos, así como su transferencia en cadena trófica pudiendo provocar un riesgo en la salud humana a través de la ingesta de alimentos y agua contaminada por NMAs.

El objetivo de esta tesis se ha alineado con los de dos proyectos NANOCULTURE y ACUINANO, financiados por los programas Interreg Atlantic Area e Interreg España-Portugal (POCTEP), respectivamente, y que han financiado este trabajo. Ambos proyectos, así como está tesis, estaban centrados en entender, evaluar y mitigar los riesgos asociados a la presencia de NMAs en especies de acuicultura marina, Concretamente esta tesis está enfocada en nanopartículas metálicas (NPMs) de dióxido de titanio (TiO2), plata (Ag) y óxido de antimonio estaño (ATO) por ser las más usadas en productos comerciales.

Las NPMs de TiO2, Ag, y ATO, son especialmente atractivas para aplicaciones industriales principalmente por sus peculiares propiedades fisicoquímicas, las cuales sólo ocurren a escala nanométrica y que no están presenten cuando estos materiales tienen un tamaño mayor. Las NPMs de TiO2 dispersan de manera muy eficaz la luz visible y filtran la luz ultravioleta, debido a lo cual su aplicación principal es en la industria de la pintura y los recubrimientos, así como en la industria cosmética. Por otro lado, las NPMs de Ag tienen altas propiedades antimicrobianas y una elevada conductividad eléctrica, por lo que son ampliamente utilizadas con fines farmacéuticos y electrónicos. Finalmente, las NPs de ATO se usan como retardantes de llamas en la industria textil, plástica (por ejemplo, en la fabricación de juguetes) y AUTOMOCIÓN (para las cubiertas de los asientos) y son de principal interés para la industria de los semiconductores en la producción de diodos, detectores infrarrojos y dispositivos de efecto Hall.

La alta demanda y el elevado uso de estas NPMs están directamente relacionados con su posible impacto negativo al medio ambiente, especialmente en los ecosistemas acuáticos ya que en estos son donde muy probablemente las NPMs terminen al final de su vida útil. Por esta razón, este trabajo doctoral se ha enfocado en ecosistemas acuáticos relacionados con la acuicultura marina, siendo uno de los sectores de mayor relevancia económica en la Unión Europea, especialmente aquella desarrollada en la Europa Atlántica.

Los principales objetivos de esta tesis doctoral están centrados en: 1) la interacción entre NPMs de TiO2, Ag y ATO y ciertas especies de acuicultura producidas en Irlanda y España incluyendo su bioacumulación, biodistribución y sus posibles transformaciones; y 2) el desarrollo de sensores para la identificación y cuantificación in situ de dichas NPMs en plantas de acuicultura, ya sea en tanques o bateas, permitiendo la monitorización descentralizada y la rápida implementación de medidas de mitigación de riesgos.

Los resultados obtenidos para alcanzar estos objetivos se presentan en esta tesis divididos en tres capítulos técnicos, incluyendo un capítulo introductorio (Capítulo 1) y otro capítulo donde se describen las conclusiones generales (Capítulo 5).

En el Capítulo 1 se introduce la problemática, así como las bases fundamentales e instrumentales de las técnicas usadas para la identificación, localización y cuantificación de las NPMs en organismos marinos y en agua de mar.

El Capítulo 2, siendo el primero de los capítulos técnicos, está enfocado en presentar los métodos de preparación de muestra necesarios para extraer, purificar y concentrar las NPMs que se encuentran en matrices complejas, específicamente biota y agua. Para una identificación y caracterización eficiente, las NPMs necesitan ser aisladas de los tejidos donde están adsorbidas y/o internalizadas con el objetivo de evitar las interferencias de matriz y posibles artefactos que impidan su análisis por técnicas analíticas como por ejemplo la espectroscopia de emisión atómica y la espectrometría de masas con plasma de acoplamiento inductivo (ICP-OES and ICP-MS respectivamente). Concretamente, en este capítulo 2 se ha diseñado dos métodos de preparación de muestras, uno para extraer las NPMs de tejídos y otro para extraerlas de muestras de agua. El método de preparación de muestras para tejidos se basó en una digestión alcalina acoplada con ultrasonidos siendo capaz de extraer NPMs de ATO de mejillones sin modificar su forma particulada permitiendo su posterior análisis de una sola partícula por ICP-MS (spICP-MS). Además, se desarrolló una extracción en el punto de nube, también conocida como "cloud-point extraction" (CPE), capaz de pre-concentrar y aislar tanto NPMs de TiO2 como de Ag dispersas en agua de mar sin necesidad de un paso de centrifugación para tener una mejor separación de fases. Este CPE se validó utilizando ICP-OES, teniendo el potencial de poder ser acoplado en un sistema portátil, ya que la pre-concentración se hace en un solo paso.

En el Capítulo 3 se aborda la potencial bioacumulación y biodistribución tanto de NPMs de Ag como de TiO2 en los mejillones, las almejas y las algas marinas. Mejillones, las almejas y las algas marinas han sido elegidas por ser especies destinadas al consumo humano y producidas en acuicultura. Además, tanto los mejillones como las almejas son moluscos capaces de filtrar activamente hasta cuarenta litros de agua por hora, mientras las algas marinas tienen una alta capacidad de adsorción a través de su elevada superficie. Por estos motivos, estas tres especies son excelentes modelos para evaluar posibles interacciones de las NPMs con organismos marinos, y pueden ser utilizados como sistemas de monitorización de la presencia de nanocontaminantes en aguas costeras y océanos. En este capítulo 3 se describe el uso de la microscopia electrónica de barrido (SEM) para el análisis de la interacción de las NPMs con la superficie del tejido y la microscopia electrónica de transmisión (TEM) para visualizar la distribución en las estructuras tisulares y celulares. Estas técnicas permitieron discriminar entre la mera adsorción

superficial de las NPMs usando SEM y los mecanismos de internalización usando TEM, los cuales fueron investigados en detalle en órganos específicos y de tejido vegetal. De forma similar, se utilizó la microscopía electrónica de transmisión por barrido con campo oscuro anular a ángulo grande en alta resolución (HR-HAADF-STEM) en combinación con la espectroscopia de Rayos X de dispersión de energía (EDS) para identificar las NPMs localizadas dentro del tejido y se analizaron las posibles transformaciones sufridas por las NPMs durante su internalización, específicamente las NPMs de Ag.

El Capítulo 4 se enfoca en el desarrollo de una plataforma sensórica basada en la dispersión Raman aumentada por superficie (SERS) para la detección y cuantificación de NPMs de Ag en agua de mar. Una visión general de los fundamentos y principios del SERS se aborda en el Capítulo 1. El Capítulo 4 se centra en el desarrollo de la prueba de concepto para la estrategia de detección basada en una detección indirecta por SERS, seguido de una descripción del diseño y fabricación de un cartucho de microfluidica para mejorar el rendimiento del sensor, en cuestión de límite de detección y robustez de la estrategia SERS desarrollada. Se aborda en detalle la elección del sustrato SERS basado en nanoestrellas de oro funcionalizadas con una etiqueta molecular, parte fundamental para que la detección funcione. El sistema fue testado en agua ultrapura, agua de mar sintética y agua de mar que contiene materia orgánica liberada por mejillones cultivados en tanques. La especificidad y la robustez del sistema sensóricos basado en SERS fueron establecidas usando NPMs de Ag con diferente tamaño y diferente grado de agregación, así como partículas con diferente grado de sulfidación, mimetizando los procesos que puede ocurrir naturalmente cuando dichas NPMs son liberadas a medios acuáticos.

Finalmente, se presenta de forma resumida en un Capítulo 5 las conclusiones generales obtenidas durante la realización de la tesis, así como las ideas que se llevarán a cabo en trabajos futuros para explotar todo el potencial de las metodologías analíticas desarrolladas para la extracción, detección y localización de NPMs presentes en mejillones, almejas y algas marinas así como en aguas. Al final de esta tesis, se incluye un resumen en español de los capítulos técnicos (Capítulo 2, 3 y 4), en línea con la regulación actual de la Universidade de Vigo.

2. Resumen del Capítulo 2 – Métodos de preparación de la muestra para la extracción, preconcentración y detección de las nanopartículas metálicas en las muestras de biota y agua

Las NPMs son introducidas al medioambiente de manera intencionada o por accidente y pueden ser liberadas de los productos donde están integradas terminando en las masas de agua. Esto incrementa la posibilidad de una interacción con la biota, tanto microorganisms y plantas como animales marinos, provocando un incremento en el riesgo de exposición human a dichas MNPs a través de la cadena trófica. Una gran variedad de técnicas de detección han sido investigadas hasta el momento, y a pesar de su gran sensibilidad y especificidad, la posible malinterpretación de los resultados incrementa con la complejidad de la matriz donde las NPMs se encuentran dispersadas. Como consecuencia, hay una creciente necesidad de desarrollar métodos analíticos que permitan la extracción, purificación y detección de NPMs presentes en matrices complejas de forma fiable pero salvaguardando las propiedades fisicoquímicas de dichas NPMs.

Este capítulo está centrado en el desarrollo de metodologías capaces de extraer y pre-concentrar NPMs presentes en biota y en muestras de agua, cruciales para la cuantificación reproducible y fiable de estas partículas en medios complejos. Para ello, inicialmente se realizó una caracterización fisicoquímica completa de las NPMs utilizadas en esta tesis, NPMs de ATO, TiO2 y Ag. Su tamaño primario, forma y cristalinidad fueron caracterizados por microscopía electrónica y por difracción de Rayos X en polvo. La estabilidad coloidal tanto en agua ultrapura como en agua de mar artificial fue evaluada usando la dispersión dinámica de luz (DLS), el potencial zeta y la espectroscopia ultravioleta – visible (UV-Vis). La eficiencia y rendimiento de los métodos desarrollados de preparación de muestra para biota y agua fueron medidos con el análisis de una sola partícula por espectrometría de masas con plasma de acoplamiento inductivo (spICP-MS) y la espectroscopía de emisión atómica con plasma de acoplamiento inductivo (ICP-OES). Específicamente, se utilizó spICP-MS para evaluar el método basado en la digestión alcalina asistida por ultrasonidos de diferentes tejidos, y ICP-OES se usó para el análisis del método de pre¬-concentración de NPMs en agua basado en la extracción en punto de nube (CPE). Los resultados muestran claramente que ambos métodos son técnicas prometedoras para la extracción, purificación y pre-concentración de NPMs en biota (en este caso, mejillones) y agua de mar con buenos rendimientos.

3. Resumen del Capítulo 3 – Análisis de la bioacumulación, la biodistribución y la posible biotransformación de nanopartículas de plata recubiertas por polivinilpirrolidona y de dioxido de titanio recubiertas por citrato sódico, en organismos marinos destinados a consumo humano

El estudio de la biodistribución y bioacumulación de NPMs en biota permite entender los posibles mecanismos de adsorción y/o de internalización de dichas NPMs en diferentes organismos y plantas marinos(as) tales como peces (p.ej. el rodaballo), crustáceos (p.ej. las gambas), moluscos (p.ej. los mejillones y las almejas) y las algas marinas. Es de esperar que tanto la bioacumulación como la biodistribución tengan diferentes patrones no sólo en función del tipo de NPMs sino también que sean dependientes de la especie marina a estudiar. Esto último se debe a la diferente forma en la que las NPMs están expuestas a los peces, moluscos o algas marinas. Los peces pueden estar expuestos a las NPMs a través de las branquias, así como a través de la ingesta de estas partículas por vía oral, mientras que en el caso de los moluscos su principal exposición será por ingestión de partículas presentes en el agua, que previamente hayan interaccionado o no con su alimento, ya que son organismos filtradores. En el caso de las algas marinas, en primera instancia, su exposición será a través de la adsorción de dichas NPMs en su superficie y posteriormente éstas podrían internalizarse. Para estudiar diferentes mecanismos de exposición, la almeja japónica, Ruditapes philippinarum, así como dos especies de algas marinas, Palamaria palmata y Ulva fenestrata, fueron seleccionadas por su alta producidos tanto en España como en Irlanda. El consumo de algas marinas ha aumentado potencialmente debido a que se han identificado como una fuente importante de alimentos no tradicionales debido a su alto contenido nutricional y su producción sostenible.

Para este estudio, se seleccionaron NPMs de Ag recubiertas con polivinilpirrolidona y de TiO2 recubiertas con citrato debido a su uso masivo en productos de consumo haciendo que la probabilidad de liberación a ecosistemas marinos sea mayor para éstas, como hemos comentado anteriormente (Capítulo 1 y 2). Debido a la posible presencia natural de éstas y otras partículas encontradas durante el estudio de la bioacumulación y la biodistribución en los tejidos sin previa extracción, en este capítulo se propone el uso de un conjunto de técnicas de microscopia electrónica para alcanzar la identificación de estas partículas en la superficie y/o en sus estructuras celulares, su localización en los diferentes órganos y tejidos así como las posibles transformaciones que pueden sufrir durante su internalización.

Para la cuantificación de la biacumulación se utilizó spICP-MS en colaboración con la Universidad de Santiago de Compostela observando una clara diferencia en la biacumulación entre las NPMs de Ag y de TiO2. En las tres especies estudiadas, se detectaron mayores concentraciones de NPMs de Ag que de NPMs de TiO2. En el caso de la almeja japónica, sólo se pudieron localizar las NPMs de Ag en las branquias como en el sistema digestivo, siendo la mayor acumulación en el sistema digestivo identificada por microscopía electrónica. Además, se observó que las partículas localizadas presentaron un tamaño menor al inicial (< 40 nm, siendo su tamaño inicial de 100 nm), lo cual demuestra que estas partículas se disuelven cuando son internalizadas. En el caso de las algas marinas, no sólo se observaron diferentes patrones de biacumulación y biodistribución en función de la NPMs sino también entre las dos especies de algas para la misma partícula. La mayor parte de las partículas de TiO2 se localizaron en la superficie de ambas algas en forma de agregados de tamaños mayores a 6 micras. En el caso de Ulva fenestrata, se localizaron por TEM y STEM-EDX algunos agregados de TiO2 de menor tamaño (50 – 100 nm) en la parte externa de la pared celular. En el caso de las nanopartículas de Ag, las NPMs se internalizan completamente y el patrón de distribución es diferente en cada alga marina. Además, se identificaron dos transformaciones sufridas por estas partículas: disolución y sufidación.

4. Resumen del Capítulo 4 – Sistemas sensóricos portátiles basados en la la dispersión Raman aumentada en superficie (SERS) para la detección ultrasensible de las nanopartículas de plata en agua de mar

La contaminación marina provoca una preocupación desde el punto de vista ambiental y económico debido a sus efectos nocivos sobre la biodiversidad, en la cadena alimentaria y su potencial impacto sobre la pesca y la acuicultura. En Europa, la acuicultura representa aproximadamente el 20% de la producción de pescado y da empleo directo a unas 85 000 personas. La acuicultura de la Unión Europea es conocida por su alta calidad, su sostenibilidad y su normativa sobre protección de los consumidores. Por eso, la presencia de NPMs en medios acuáticos ha despertado el interés de conocer y entender los posibles efectos tóxicos sobre la salud de los productos de acuicultura y en la salud humana. Una de las limitaciones para este conocimiento es que actualmente no hay una

tecnología desarrollada para su detección e identificación in situ cuando estás NPMs están dispersas en el agua. Además, las técnicas analíticas mencionadas anteriormente (Capítulo 1, 2 y 3), por ejemplo, spICP-MS, requieren laboriosos métodos de preparación de muestra para extraer y pre-concentrar las NPMs, son costosos y consumen mucho tiempo. La espectroscopia de dispersión Raman aumentada en superficie (SERS) ofrece unas ventajas únicas como técnica de detección gracias a sus límites de detección ultrabajos, con capacidad de detección de una sola molécula, y además nos ofrece la posibilidad de elucidación estructural y de reactividad de los sistemas moleculares bajo estudio. Así, SERS puede ser utilizada para la detección de partículas plasmónicas, tales como las NPs de Ag, en medios acuáticos seleccionando la molécula adecuada como etiqueta Raman y la nanoestructura de oro necesaria para aumentar la señal Raman en los rangos necesarios.

En este capítulo se describe la estrategia para la detección basada en SERS de NPMs de Ag basada en la detección indirecta de dichas partículas en agua de mar utilizando 4-aminobencenotiol (4-ABT), como etiqueta Raman y acoplada covalentemente a las nanostrellas de oro por un enlace Au-S. Cuando se irradia el 4-ABT con una laser 785 nm genera un espectro SERS al estar enlazada a las nanoestrellas. Dicho espectro varÍa en presencia de NPMs de Ag ya que estas a su vez tienen un efecto plásmonico y provoca un aumento de la señal SERS que se pudo correlacionar con la concentración de NPs de Ag. De esta forma fue posible no solo detectar las NPMs de Ag sino también cuantificarlas en agua de mar. Esta estrategia fue testada con tres diferentes nanopartículas de plata recubiertas con polivinilpirrolidona (PVP) para determinar el impacto relativo al tamaño (PVP-15nm Ag NPs and PVP-100nm Ag NPs) y el grado de agregación (agregados predefinidos de plata, PVP-50–80nm Ag NPs). En los tres casos, se logró la cuantificación en agua de mar artificial con un límite de detección (LoD) y un límite de cuantificación (LoQ) en el rango de mg/L. Dichos LoD y LoQ están lejos de los valores deseados, ya que, basándose en las concentraciones esperadas de NPMs de plata en agua superficiales, el rango de relevancia medioambiental está en el orden de los ng/L. Por tanto, para mejorar el LoD y el LoQ así como la portabilidad de la plataforma sensórica, se diseñaron y fabricaron cartuchos de microfluídicas donde se integraron los sustratos SERS llegando a LoDs y LoQs en el rango de ng/L. En este caso, se evaluó el desempeño de la plataforma sensórica en agua de mar que contiene materia orgánica, es decir, agua de mar usada para cultivar mejillones en tanques) y se estudió el impacto de la sulfidación de las NPs de Ag en el sistema sensórico desarrollado.

Acknowledgments

I would like to express my deepest gratitude to my advisor Dr. Laura Rodríguez Lorenzo and to Dr. Begoña Espiña, for their support, guidance, and encouragement throughout this journey. Thank you for your patience, understanding and, above all for your time, especially during challenging times.

My sincere thanks go to Prof. Miguel A. Correa-Duarte from the University of Vigo, for his availability even at distance, and to Professor Antonio Moreda Piñeiro for receiving me during my stay at the University of Santiago de Compostela.

A special thanks go to INL microscopy facility, in particular to Dr. Alec La Grow for trusting, guiding and helping me with my tons of not-beam friendly samples.

I would like to thank INL and especially my colleagues from the Water Quality group for their support and friendship during these years. No matter how grey the day was, you were always there to cheer me up and to make all the burnt coffees taste sweeter!

Also, Obrigada a:

All INLers and not that cross my path during these years, you made Braga a less rainy city.

The Italian Chicchi, for all the “podes trazer tremoços, por favor?”, to make me feel at home even miles away and to be there when only your native language could fully express yourself.

To you, well, you already know. But a big thank you for being there, for your patience, which with me is never enough, and to support me on the very bad days.

To the friends of a lifetime who continue to walk beside me.

To Noemi, the constant proof that distance does not exist.

And to my family, mamma, papà e Peppe, for their unconditional love, support, and encouragement through my life and career. I dedicate this work to you.

All those I have not mentioned, but who know to occupy a special place in my heart..GRAZIE!

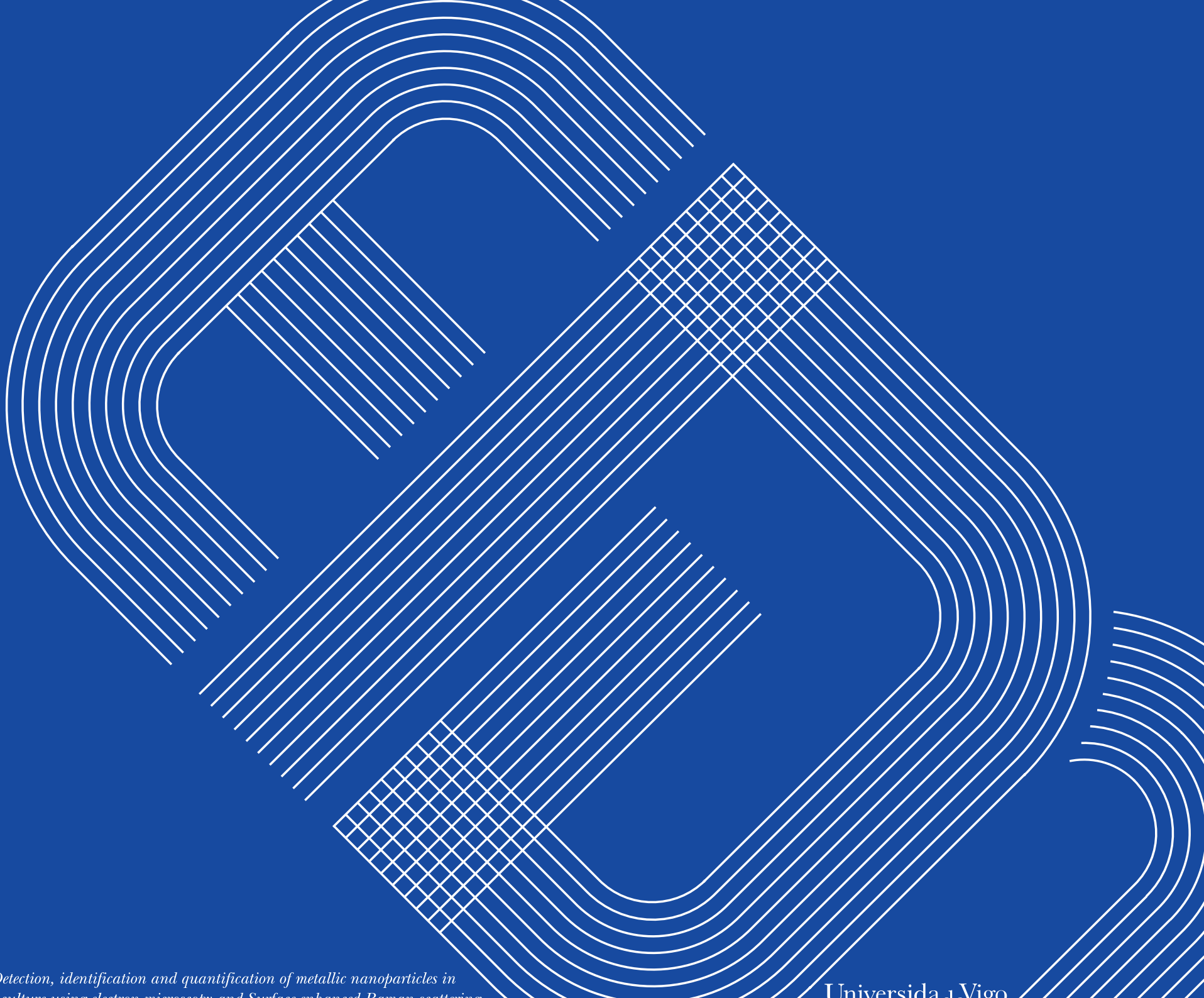

Universidade Vigo

Detection, identification and quantification of metallic nanoparticles in

Universidade Vigo